Università degli Studi di Catania
Dottorato di Ricerca in Geodinamica e Sismotettonica
XXV Ciclo

GEOCHRONOLOGY OF TERRACED COASTAL DEPOSITS IN CALABRIA AND EASTERN SICILY: TECTONIC IMPLICATIONS

Dottoressa
Gloria Maria Ristuccia

Tutor: Prof. C. Monaco
Co-tutors: Prof. S.O. Troja
Prof.ssa A.M. Gueli

A. A. 2011 - 2012

"Non ho particolari doti.

Sono solo appassionatamente curioso"!!

(Albert Einstein)

ABSTRACT

Calabrian Arc and Eastern Sicily (Southern Italy) are characterized by flights of coastal terraces occurring in various geological domains. These features are formed by interaction between the glacio-eustatic sea level changes and Late Quaternary uplift. Indeed, since Middle Pleistocene times this region of the central Mediterranean has been mostly affected by extensional and transcurrent tectonics that have been coupled with a strong regional uplift with values of ~1 mm/yr along the Tyrrhenian and Ionian coasts. Thus, by combining ages and elevations of inner edges with the OIT stages of high sea-level stands, it is possible to accurately evaluate the uplift rates of coastal areas and to discriminate, where possible, the regional and local components of uplift. At this purpose, in this thesis the Optically Stimulated Luminescence (OSL) method has been used, mainly for its applicability to the detrital minerals of the terraced sediment (i.e. quartz) and for its accuracy.

The research project is based on interdisciplinary study that involved the PH3DRA (Physics for Dating Diagnostic Dosimetry Research and Applications) laboratories of the Department of Physics and Astronomy of the Catania University, where preparation of geological samples, measurements and analysis of results were carried out, in order to optimize the dating procedure and to obtain OSL age of samples collected from the studied terraced deposits. For each sites the structural and geomorphological issues have been dealt with and then samples of sands have been collected from the studied areas. Four key sites, characterized by different tectonic setting, have been chosen: Amendolara (north-eastern Calabria), Capo Vaticano peninsula (western Calabria), Sant'Agata di Militello (north-eastern Sicily), Terreforti Hills (eastern Sicily). For the first site, the OSL dating methodology on quartz grains failed.

Quaternary terraced deposits outcropping on the Capo Vaticano peninsula have been investigated in order to obtain new chronological estimates. OSL age

determinations correlated with geological and morphological evidences have provided new constraints for correlating the distinct orders of marine terraces with the last seven interglacial stages of the eustatic curve. This correlation indicates that in the Middle-Late Pleistocene this portion of the southern Calabrian Arc was affected by a vigorous uplift characterized by rates up to ~2 mm/yr, accompanied by faulting and tilting of the peninsula towards the northeast.

Along the coastal sector of Sant'Agata di Militello the geomorphological survey and the analysis of stereo-pairs of aerial photographs allowed to recognize at least five main orders of well-preserved Quaternary surfaces and relative deposits. They are mostly located on the hanging-wall and on the footwall of the Pleistocene northwest-dipping Capo d'Orlando normal fault, which controlled the geomorphological evolution of the coastal area. In order to better define the whole terrace chronology, deposit samples were analysed by OSL methodology, a conventional single-aliquot regenerative-dose (SAR) protocol used with sand-sized quartz. New dating, together with the detailed morphostructural analysis, allow to relate the 2^{nd} and 4^{th} order terraces to MIS 5.5 and 8.5, respectively, and to reconstruct the tectonic evolution of this coastal area, constraining the activity of the Capo d'Orlando fault.

Coastal-alluvial terraces outcropping in the area between Mt. Etna volcano and the Catania Plain, known as the "Terreforti Hills", at the front of the Sicilian fold and thrust system, were analyzed. The obtained OSL ages were consistent with the normal evolutionary model of a terraced sequence, moving from the highest to the lowest elevations and the new data allowed us to determine a mean uplift rate of 1.2 mm/yr during the last 330 ka, mostly related to regional uplift processes coeval to Quaternary sea-level changes. Moreover, the two highest order terraces are folded, forming the large Terreforti anticline. According to our analysis, this anticline represent a thrust propagation fold developed at the front of the Sicilian chain between 236 and 197 ka ago.

INDEX

INTRODUCTION

Calabrian Arc and Eastern Sicily (Southern Italy) are regions of the central Mediterranean where the effects of Quaternary tectonic events are well preserved.

Since Middle Pleistocene times, tectonic processes have been coupled with a strong regional uplift with values of ~1 mm/yr along the Tyrrhenian and Ionian coasts (Westaway, 1993; Bordoni and Valensise, 1999; Bianca et al., 1999; Catalano et al., 2003). Late Quaternary uplift, associated with the glacio-eustatic sea level changes, described by the global eustatic curve of Waelbroeck et al. (2002), caused the development of prominent flights of coastal terraces that represent a peculiar morphological feature of this area (Valensise and Pantosti, 1992; Westaway, 1993; Bianca et al., 1999; Catalano and De Guidi, 2003; Catalano et al., 2003; Tortorici et al., 2003). Coastal terraces originated from vertical displacement above sea level (a.s.l.) of erosional or depositional surfaces formed during a relative sea-level stand with their inner edges (i.e. a palaeoshoreline). They mostly represent the morphological record of one of the relative maximum high-stands reached by the sea level during a main interglacial stage (Bloom et al., 1974). Considering ~130 m of utmost Pleistocene-Holocene eustatic oscillations (Shackleton and Opdyke, 1973; Chappell and Shackleton, 1986; Lajoie, 1986; Pirazzoli, 1991; Westaway, 1993) and that the present-day sea level is very close to the Quaternary maximum (Chappell and Shackleton, 1986; Pirazzoli and Suter, 1986; Muhs, 1992; Westaway, 1993), the presence of coastal terraces several hundred metres above sea level indicates tectonic uplift. Thus, the reconstruction of the elevation changes of a raised palaeoshoreline is helpful in evaluating the amount of tectonic deformation of a region. Moreover, the elevation of terraces and their offset across the main faults could be used to establish the relative contribution of regional and fault-related

sources to uplift. Hence the chronological datum of terrace formation appears of primary importance, because their dating should provide an understanding of past sea level fluctuations, which are interlinked with global climate changes and/or local tectonic movements. As regards the geochronology, there are a few direct dating methods which can establish the time of deposition of sediments. These methods (e.g. radiocarbon, U-series, Electron Spin Resonance, Amino-Acid Racemization, ...) are all applied to fossil shells and restricted to fossiliferous marine terraces. Their accuracy may be hampered by the poor preservation of the marine fauna (molluscs and corals) or the presence of untraceable reworked shells. These difficulties will be overcome by the use of an independent dating technique, such as the Optically Stimulated Luminescence (OSL) method (Huntley et al., 1985; Aitken, 1998), whose applicability is turned to detrital minerals of the terraced sediment itself (i.e. quartz and feldspars).

In this thesis, an interdisciplinary study has been carried out in order to accurately date flights of Quaternary terraces located in key areas of the Calabrian Arc and eastern Sicily (Fig. 1) and evaluate the vertical deformation rates, both local and regional, of the coastal areas where they are located. In fact, the research project involved the PH3DRA (Physics for Dating Diagnostic Dosimetry Research and Applications) laboratories of the Department of Physics and Astronomy of the Catania University, where preparation of geological samples (based on mineralogical composition), measurements (based on physical behaviour of mineral) and analysis of results (based on the dating model) were carried out, in order to obtain OSL dating of samples collected from the studied terraced sequences.

The thesis starts (Chapter 1) with the description of the geological setting of the studied areas and of the coastal terraces as a tool for determining vertical

deformation. In fact, comparing the altitude distribution of inner edge of coastal terraces with available absolute dating results, the pattern of the regional signal of uplift can be reconstructed.

Chapter 2 treats the basic principles of the OSL methodology, the hypothesis of applicability, and some tests that minimize all the issues regarding the geological dating of samples. The application of modified single-aliquot regeneration dose (SAR) protocol (Murray and Wintle, 2000, 2003) to sand grained quartz, both to the small aliquot and single grain, to determinate the equivalent dose (D_e), are then investigated.

In Chapter 3 the Quaternary terraced deposits exposed on the Capo Vaticano peninsula (western Calabria) are investigated in order to calculate the regional uplift, eventually identifying differently uplifted sections, and to recognise the interaction with possible local fault-related deformations. Six samples collected from unconsolidated sediments associated with the major coastal terraces are analysed by OSL to obtain new chronological estimates.

In Chapter 4 the coastal sector of Sant'Agata di Militello (north-eastern Sicily) is examined. This area is characterized by a flight of raised Middle-Upper Pleistocene coastal terraces occurring at different heights with respect to the present sea level. New OSL dating of Pleistocene terraced deposits, together with detailed geomorphological survey and the analysis of stereo-pairs of aerial photographs, allow the reconstruction of the tectonic evolution of this coastal area and to constrain the relationships between coastal terracing and normal faulting in a precise time range.

In Chapter 5 the "Terreforti Hills" site (southern-east Sicily) is studied. In order to understand the local tectonic processes, related to the migration of the front of the Sicilian chain, five samples belonging to a flight of coastal-alluvial terraces have been collected to date the deposits using the OSL method. Here, unlike the other sites, the modified SAR protocol on single grains (Murray and Roberts, 1998; Roberts, 1997; Roberts et al., 1998, 1999; Olley et al., 1999) is applied rather than on small aliquots where the large number of D_e values obtained for each sample. This permits the rejection of data from individual grains that can adversely influence the dose distributions of a sample and to optimize the calculation of D_e used in the age equation and then the chronological attribution of the studied terraces.

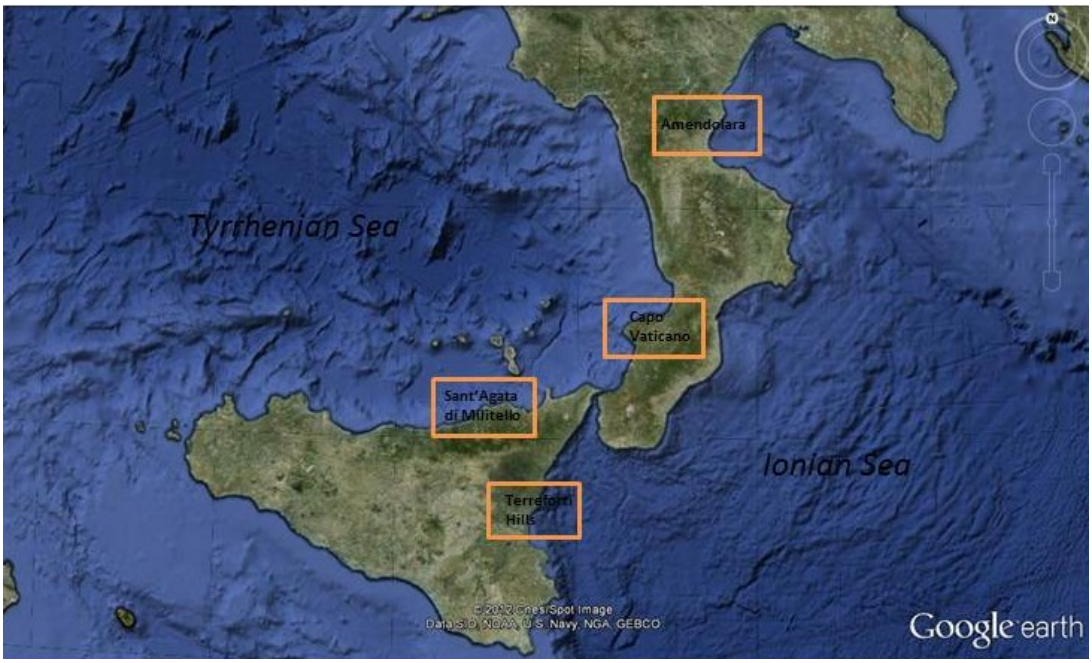

Fig. 1 - Investigated sites in current thesis.

Chapter 1

TECTONIC FRAMEWORK

1.1 GEOLOGICAL SETTING

Eastern Sicily and Calabria (see Fig. l) represent key areas for understanding the tectonic processes that since Plio-Pleistocene time have interested the Southern Italy. In particular, the Calabro-Peloritan Arc (or simply Calabrian Arc) developed during the Neogene-Quaternary NNW-SSE convergence between African and Eurasian plates and coupled to the subduction of the oceanic or transitional Ionian slab lithosphere beneath the Sardinia-Corsica block to the NW (Malinverno and Ryan, 1986; Doglioni, 1991; Faccenna et al., 2007). These processes have accompanied the growth of the Tyrrhenian back-arc basin in the wake of the progressive SE migration of the subduction hinge and slab roll-back.

Despite plate convergence occurred at a rate of 1-2 cm/yr since the last 5-6 Ma, the Calabrian Arc experienced rapid E to SE motion at a rate of 5-6 cm/yr (Malinverno & Ryan, 1986). Motion was related to roll-back of the subjacent Ionian transitional to oceanic crust and back-arc extension in the Tyrrhenian Sea back-arc basin behind (Gueguen et al., 1998; Faccenna et al., 2007; Rosenbaum and Lister, 2004), even if during the Middle-Late Pleistocene, roll-back and subduction slowed to less than 1 cm/yr (Faccenna et al., 2001).

The location and geometry of the slab are well established by deep earthquakes and seismic tomographic images down to 500 km beneath the southern Tyrrhenian Sea (Giardini and Velonà, 1991; Amato et al., 1993; Selvaggi and Chiarabba, 1995; Wortel and Spakman, 2000; Faccenna et al., 2001; 2007; Chiarabba et al., 2008). Recent studies (Neri et al., 2009) have highlighted that a slab detachment might have occurred in the northern and southern parts of the Arc beneath northern

Calabria and north-eastern Sicily. This event might have been prompted by a reorganization of the plate kinematic framework of the central Mediterranean that, according to Goes et al. (2004) and Jenny et al. (2006), occurred in the Middle Pleistocene.

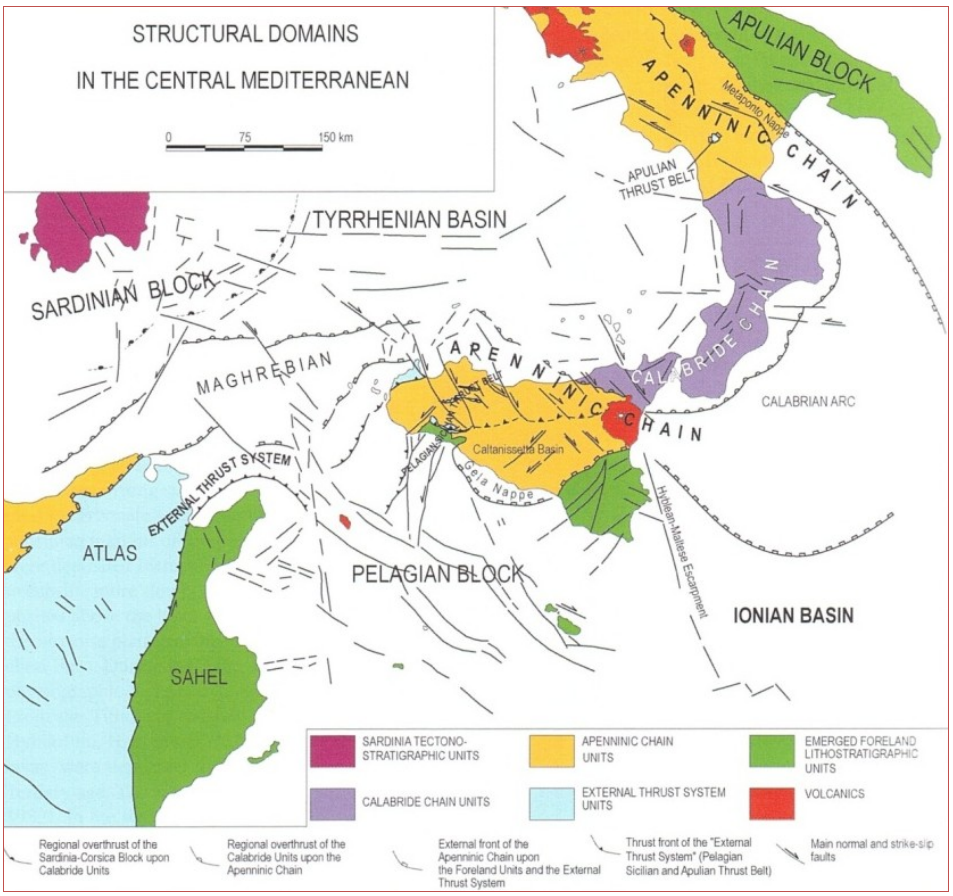

Fig. 1 - Structural domains in the central Mediterranean Sea (Finetti et al., 2005).

Since the Middle Pleistocene, the region has been affected by strong uplift, which caused to the development of spectacular flights of marine terraces along coastal areas and, on land, a deep entrenchment of rivers with the consequent

deposition of alluvial and/or transitional coarse grained sediments along the major depressions on top of pelagic sequences (Dumas et al., 1982; Ghisetti, 1992; Valensise and Pantosti, 1992; Westaway, 1993; Miyauchi et al., 1994; Bianca et al., 1999; Catalano and De Guidi, 2003; Tortorici et al., 2003; Ferranti et al., 2009; Caputo et al., 2010). The formation and the preservation of terraces were the result of the interaction between uplift and Quaternary cyclic sea-level changes (Bosi et al., 1996; Carobene and Dai Pra, 1991; Westaway, 1993). Uplift has been interpreted as a response to asthenospheric flow into the gap resulting from slab detachment (Westaway, 1993; Wortel and Spakman, 2000; Goes et al., 2004), or as being supported by asthenosphere wedging beneath the decoupled crust (Hirn et al., 1997; Doglioni et al., 2001; Gvirtzman and Nur, 1999), or as due to visco-elastic response to sedimentary flux from land to sea triggered by enhanced erosion following onset of glacial-interglacial cycles (Westaway and Bridgland, 2007).

The Pliocene-Quaternary evolution of the Calabrian Arc has witnessed the coexistence of two different deformation regimes at crustal levels. Whereas the western (Tyrrhenian) and axial sectors of Calabria and Ionian shore of Sicily were dominated by Quaternary extension tectonic regime, still active today (Monaco and Tortorici, 2000), the NE and SW boundaries, and large part of the eastern (Ionian) margin were involved by Quaternary strike-slip and contractional deformation. As a matter of fact, a NW-trending system of right-oblique faults (Aeolian-Tindari-Letojanni Fault, ATLF) with transtensional or transpressional features runs between the Ionian side of NE Sicily and the eastern Aeolian archipelago (Fig. 2), and currently separates extension in the east and contraction in the west (Pepe et al., 2003; Billi et al., 2006; 2007; Argnani et al., 2007; Mattia et al., 2008). This system has been interpreted like a transform fault, permitting the SSE-ward migration of the Arc front, at the expense of the oceanic Ionian Basin (see Palano et al., 2012 and

reference therein). To the north, along the Ionian side of central-northern Calabria and Basilicata region, transpressional regime and shortening are documented by the deformation of coastal terraces and folding of the sea-floor (Ferranti et al., 2011), although the area lacks a seismic signature (Ferranti et al., 2009; Santoro et al., 2009; Caputo et al., 2010).

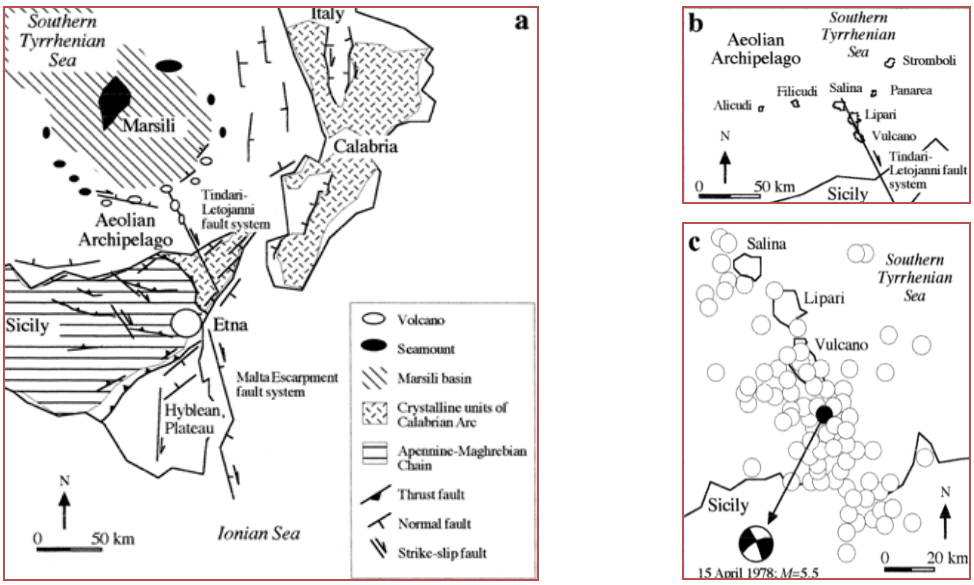

Fig. 2 - a), b) Location and structural sketch map of Southern Tyrrhenian Sea, Aeolian Islands and Sicily modified from C.N.R., 1991. c) Epicenters of shallow -25 km. earthquakes in the Lipari-Vulcano sector of the "Tindari-Letojanni" fault system data from Neri et al., 1991, 1996. The epicenter and the focal mechanism of the 15 April 1978, Ms 5.5 earthquake is also reported data from Gasparini et al., 1985 (Ventura et al., 1999).

The western and northern boundaries of the Arc have acted as distributed railways for SE migration of the Arc (Fig. 1; Malinverno and Ryan, 1986; Van Dijk et al., 2000; Tansi et al., 2005), and are thought to be tear faults in the underlying Ionian slab (Nicolich et al., 2000; Doglioni et al., 2001; Faccenna et al., 2007; Chiarabba et al., 2008; Rosenbaum et al., 2004). The Neogene-Quaternary frontal wedges are emplaced upon the Ionian abyssal plain or upon the flexed sectors of the

Hyblean and Apulia foreland, which are in turn involved in deep contraction, forming a thrust and fold system. Plio-Pleistocene foredeep basins (Gela-Catania and Bradano basin in Sicily and southern Apennines, respectively) have developed between the chain front and the foreland. The frontal belt in eastern Sicily is characterized by thrust propagation folds (Labaume et al., 1990; Monaco et al., 2002), and compression seems responsible for crustal seismicity (Cocina et al., 1997; Lavecchia et al., 2007).

Starting from Late Pliocene, and more markedly in the Quaternary, concurrently with back-arc extension in the Tyrrhenian Sea, the inner side of the Arc, has experienced extensional deformation accommodated by NE-SW, NNE-SSW, and N-S striking normal fault systems (Bousquet et al., 1980; Ghisetti, 1984, 1992; Tortorici et al., 1995; Valensise and Pantosti, 1992). Extensional tectonics along the inner side of the Arc accompanied the Quaternary uplift. The main regional feature is represented by a prominent normal fault belt (Fig. 3) that runs more or less continuously along the Tyrrhenian side of Calabrian, as far as the Straits of Messina area where it crosses the chain, joining to the Malta Escarpment fault system along the Ionian coast of Sicily as far as the eastern boundary of the Hyblean Plateau (Palano et al., 2012). Extension along this fault system has a WNW-ESE azimuth, as documented by structural (Tortorici et al., 1995; Monaco et al., 1997; Jacques et al., 2001), seismological (CMT and RCMT catalogues) and GNSS velocity field (D'Agostino and Selvaggi, 2004; Goes et al., 2004; Mattia et al., 2009) investigations.

Extension is spatially correlated with a strong crustal seismicity, whose distribution (CPTI Working Group, 2004) coincides with the down-thrown part of the Arc in the hanging-wall of normal faults. The distinct fault segments are characterized by very young morphology and control both the major mountain

fronts of the region (Catena Costiera, Sila, Serre, Aspromonte, Peloritani, Hyblean Plateau) and the coastline of southern Calabria (Capo Vaticano, Palmi high and Messina Straits). In eastern Sicily (Fig. 3) the fault system is mostly located offshore and controls the Ionian coast from Messina to Taormina joining to the system of the Malta Escarpment from the eastern lower slope of Mt. Etna to the south (Valensise and Pantosti, 1992; Westaway, 1993; Tortorici et al., 1995; Stewart et al., 1997; Bianca et al., 1999; Monaco and Tortorici, 2000, 2007; Jacques et al., 2001; Neri et al., 2006).

So, the Late Quaternary tectonics of the Calabrian Arc reflects the interplay of different processes (Westaway, 1993). This may be reflected by the existence, within the deformation profile of the flights of coastal terraces, of both a long- and a short-wavelength signal, the former related to lower- or sub-crustal processes and the second arising from upper crustal displacements. According to Westaway (1993), 1.7 mm/yr of post-Middle Pleistocene uplift of southern Calabria is subdivided into 1 mm/yr regional (or deep) processes and the residual to distributed displacement on major faults, and mostly results in footwall uplift. Minor (~0.5 mm/yr) cumulative Quaternary uplift rates have been found in SE Sicily, suggesting a decrease of either, or both, the regional and local magnitudes of displacement (Bianca et al., 1999; Scicchitano et al., 2008; Dutton et al., 2009).

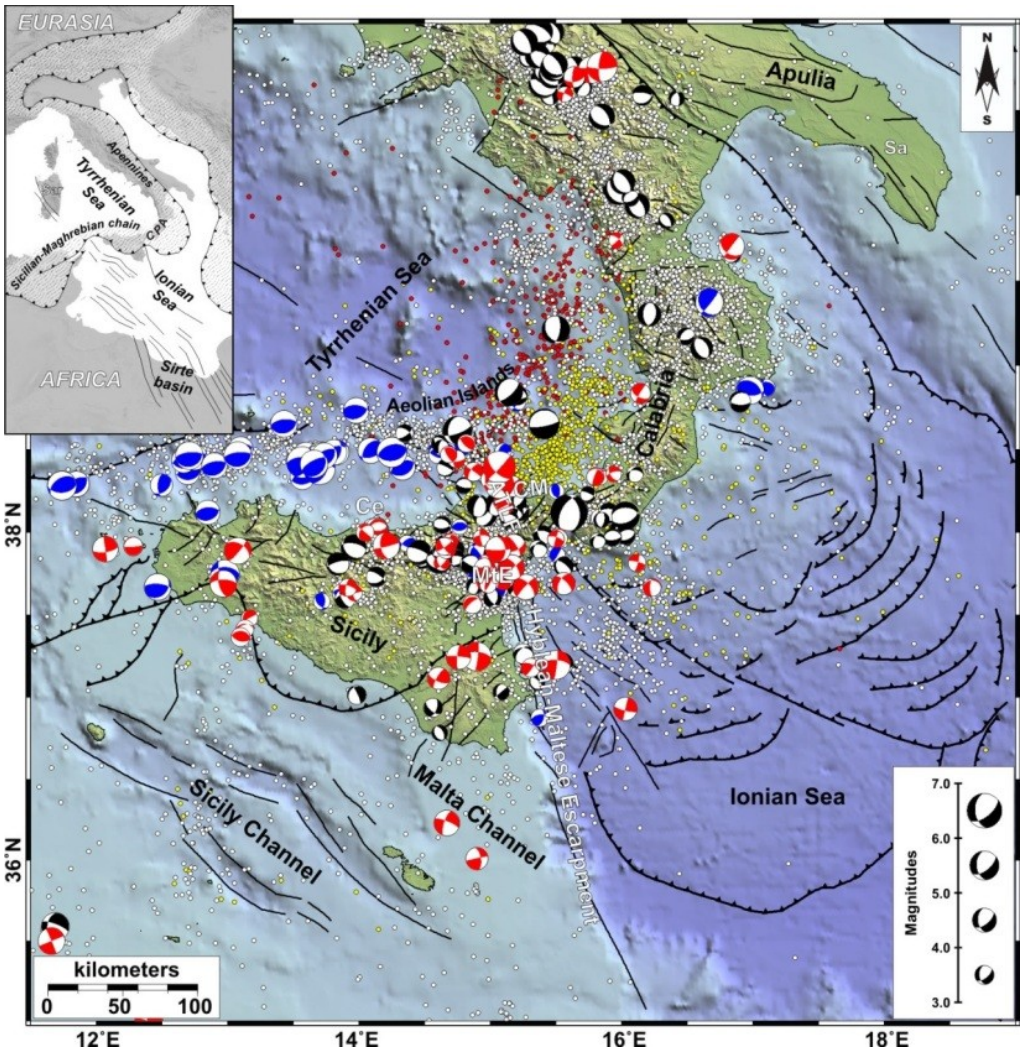

Fig. 3 - Simplified tectonic map of the Sicilian-Calabrian area. Tectonic structures in the Ionian Sea redrawn from Polonia et al. (2011). Instrumental seismicity since 1983 with magnitude ≥2.5 (http://iside.rm.ingv.it): white for events occurring at depth h <30 km; yellow for those occurring at depth ranging between 30 and 200 km; red for those at depth >200 km. Focal mechanisms (FM) of events with magnitude >3.0 are also reported according to the faulting styles based on definitions by Zoback (1992): red for strike-slip, blue for thrust faulting and black for normal faulting. Abbreviations are as follows: ATLF, Aeolian-Tindari-Letojanni fault system; Ce, Cefalù, MtE, Mount Etna; CM, Capo Milazzo; Sa, Salina Island, Vu, Vulcano Island, Us, Ustica Island; HP, Hyblean Plateau. The Africa-Eurasia plate configuration is shown in the inset; CPA, Calabro-Peloritan Arc; Sar, Sardinia (Palano et al., 2012).

1.2 COASTAL TERRACES AS A TOOL FOR DETERMINING VERTICAL DEFORMATION

Coastal terraces symbolize useful markers to evaluate uplift movements occurring in tectonically active regions. In a coastal region, the occurrence of a flight of coastal terraces represents the result of the interaction between long-term tectonic uplift and Quaternary cyclic sea-level changes (Lajoie, 1986; Westaway, 1993; Carobene and Dai Prà, 1991; Cinque et al., 1995; Bosi et al., 1996; Armijo et al., 1996; Bianca et al., 1999) which are represented in the global eustatic curve derived from the Oxygen Isotope Time (OIT) scale. This curve (Shackleton and Opdyke, 1973; Imbrie et al., 1984; Chappel and Shackleton, 1986; Martinson et al., 1987; Bassinot et al., 1994; Chappel et al., 1996; Waelbroeck et al., 2002) shows a cyclic trend characterized by peaks corresponding to distinct coastal interglacial high-stands, represented by the odd-numbered Marine Isotope Stages (MIS) and marine glacial low-stands, indicated by the even-numbered MIS. The absolute sea-level changes range from about 130 m below the present sea-level, during the last glacial maximum, up to 6 m above the present sea-level during the Eutyrrhenian interglacial period (MIS 5.5, 124 ka).

The inner edge of terraced surfaces and the alignments of marine caves and notches carved in the coastal cliffs represent a remarkable record of the palaeo-shorelines formed at sea level during a marine still-stand. More usually the inner edges of the terrace surfaces represent the palaeo-shorelines corresponding to the main eustatic high-stands of the reference global eustatic curve, related to the interglacial periods (Bloom et al., 1974; Lajoie, 1986; Bosi et al., 1996; Caputo, 2007). Taking into account that present-day sea level is very close to the Quaternary maximum, the presence of coastal terraces at several tens or hundred metres a.s.l. indicates tectonic uplift. This implies that strands of terraces and palaeo-shorelines

are visible only in uplifted regions with the number of orders rising with the increasing of the uplift rate. By combining ages and elevations of palaeo-shorelines with OIT stages of high sea-level stands and absolute sea-level variations it is thus possible to accurately evaluate the uplift rates of rising regions (Westaway 1993; Armijo et al. 1996; Bosi et al. 1996).

In order to evaluate the Quaternary uplift of the studied areas, we detailed the distribution of coastal terraces. The coastal terrace surfaces with their relative inner and outer edges have been mapped over the whole area using the 1:25.000 scale topographic maps of the Istituto Geografico Militare, SPOT satellite images and 1:33.000 and 1:10.000 scale aerial photographs. This was coupled with detailed field observations that in the most important areas have been traced on 1:10.000 scale topographic maps. Inner edges which have been mapped with an error margin in the elevation of ±5 m. However, this margin basically depends on erosion and depositional processes following the emergence of the terraces and is negligible in estimating the long-term Quaternary uplift rates involving time spans of tens to hundreds of thousands of years. This implies that the elevations of the palaeo-shorelines reported in this paper are to be considered as mean values, useful for estimating the long-term uplifting during the Late Quaternary.

The uplift rates are estimated by subtracting the altimetry value of each terrace from the sea level of the interglacial maximum assigned and then dividing this value by the age assigned to the terrace (MIS odd number). For example, if a 125 ka terrace is presently 131 m a.s.l. (this is its relative sea-level position), it can be assumed to have formed during the last interglacial maximum sea level of +6 m.

The tectonic uplift is consequently 125 m (131 - 6 m), and the average uplift rate is 1 mm/yr.

Chapter 2
OSL METHODOLOGY

The Quaternary was, and is, arguably one of the most important periods in Earth's history, in which it has been a time of extreme climatic fluctuations. This significant period has, however, been difficult to put into an absolute temporal context, despite the application of several dating techniques. This is because most techniques require the presence of a specific material, often uncommon, that has to occur in the relevant context. Moreover, many dating methods are only useful over short time scales, the calculated age does not directly date the desired event, and/or complex age calibration may be necessary which can significantly increase the uncertainty in the final result. Chronological control, thus, remains critical to the interpretation of environmental changes and to establishing long-term rates of geomorphological processes.

Luminescence dating is now an important element in the set of Quaternary geochronological methods. In particular, the Optically Stimulated Luminescence (OSL) dating has been developed over the last 30 years (see Huntley et al., 1985; Aitken, 1998), where the improvement has been its application to Quaternary sediments. The method uses as radiation dosimeters detrital grains, e.g. quartz and feldspars, providing an absolute age for the last exposure of the minerals to daylight, becoming thus a great tool to determine the burial age of the same.

The upper and lower limits of the age that can be measured are dependent on sample type, physical behaviour of mineral and used techniques (Aitken, 1998).

OSL methodology is key share of this work, in which the discussion, even if brief, isn't limited to the aspects exclusively related to those one needed for my geological thesis development. In this chapter the physical principles of OSL

methodology and its applications will be treated, in order to demonstrate the complexity of physical-chemistry interactions and to highlight the difficulty to use it like dating method. This last requires exhaustive studies for which the answers are partial or still open. These results represent a limit that influence on the accuracy of the measures and, in turn, on their reliability. For other research materials about OSL it is possible refer to the existent wide bibliography.

2.1 OSL DATING: *HYPOTHESIS*

OSL dating is based on the assumption that the quartz and feldspars inclusions present in many natural samples are able to accumulate, in trap energy levels with a long mean-life, electrons that have acquired sufficient energy from α, β and γ radiations emitted by natural radionuclides belonging to the ^{235}U, ^{238}U, ^{232}Th decay chains, ^{40}K, ^{87}Rb and from cosmic radiation. It is admissible to consider that the number of electrons trapped is proportional to the total absorbed dose (the energy absorbed per mass unit measured in Gray) and, consequently, the crystals are capable to store information related to these quantity. Optical stimulation induces the rapid emptying of the trap states with the emission of photons in a number proportional to the electrons released from the traps, and therefore, indirectly, to the total energy which determined the entrapment.

The luminescence emitted by crystals which have never been exposed to light is correlated to the total dose absorbed since their geological formation. In crystals that have been subjected to solar exposition this event empties the electron traps and zeroes the internal luminescence clock (*bleaching event*). The crystals therefore lose the information related to the dose accumulated over geological time (Fig. 1).

In our case, the zeroing of signal take place during the transportation of the grains by wind, water or gravity. The bleaching is strongly linked to the transport

mechanism, with parameters like water depth, transport distance and sediment load regulating the efficiency of sunlight exposure (Murray et al., 1995; Jain et al., 2004). After the coverage by other sediment, as a result of the radioelements normally present in the natural environment, the crystals once again begin to accumulate a dose of radiation, known as the *paleodose*. This is accumulated with an annual rate characteristic of the sample itself as well as of the environment in which the sample is buried. Our hypothesis is that these conditions remain unvaried over time, and the annual dose will be considered constant.

Under these conditions, therefore, the paleodose is proportional to the age of the sample. The crystals contained in such samples thus provide information regarding the time which has passed since their last exposure, in accordance with the age (ka) equation: Age = *Paleodose*/*Dose rate*, where the paleodose is the absorbed dose by crystals (expressed in Gy) and the dose rate is mean annual dose (expressed in Gy/ka). Often the term "equivalent dose" (*ED*, or D_e - the laboratory dose of nuclear radiation needed to induce luminescence equal to that acquired subsequent to the most recent bleaching event) is used instead of paleodose. It is obtained by comparing the natural optical signal with the signals obtained from portions to which known doses of nuclear radiation have been administered from a calibrated radioisotope source, and are strictly related to the properties of the crystals.

The possibility of applying OSL dating methodologies to sediments is, therefore conditioned by the possibility of measuring the total dose absorbed by the crystals.

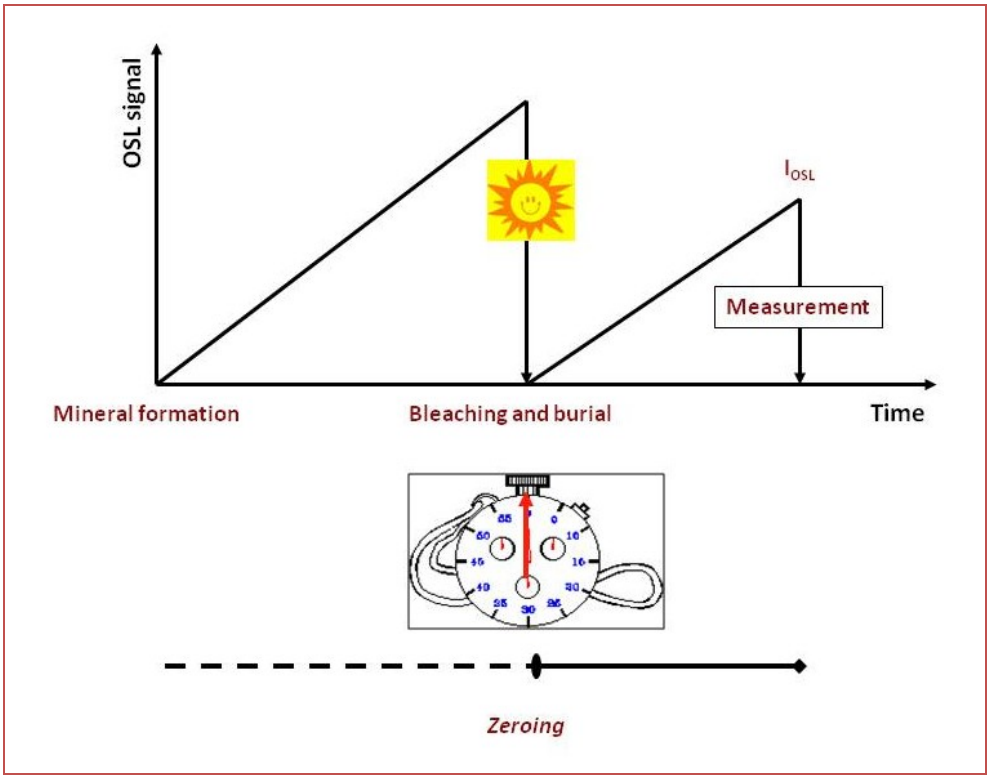

Fig. 1 - The event dated in optical dating is the setting to zero of the latent luminescence acquired at some time in the past. With sediment this zeroing occurs through exposure to sunlight or daylight (*bleaching*) during erosion, transport, and deposition until cover from other sediments. Subsequently the latent signal builds up again through exposure to the natural flux of nuclear radiation.

This is closely linked to the opportunity of performing experimental measurements to determine the dose yielded by the environment in the immediate vicinity of the sampling point, as well as the internal dose of the sediment sample itself. The homogeneity and uniformity in space and time of the exposition to natural radiation determines the effective prospect of dating each sediment. It is for this reason that the sediment buried for a long time in unchanging environments electively lend themselves to dating.

The *dose rate* (or annual dose - *AD*) represents the rate at which energy is absorbed from the flux of nuclear radiation; it is associated with the natural

radiation coming from different contributions and it is therefore necessary to determine each single component. Thus, in general, the dose rate:

$$Dose\ rate = D_\alpha + D_\beta + D_\gamma + D_{cosm} \quad \text{(eqn. 1.1)}$$

where D_α is the total α dose-rate component, D_β the β dose-rate component, D_γ the γ component and D_{cosm} cosmic dose-rate contribution. Each of these is therefore, in turn, the sum of single α, β and γ contributions due to the crystal itself and surrounding environment.

2.2 PRINCIPLE OSL

Luminescence refers to the light emitted by some materials in response to some external stimulus, such as heat (resulting in thermoluminescence, TL), pressure (triboluminescence), a chemical reaction (chemiluminescence), electromagnetic radiation (radioluminescence), or ionising radiation (photoluminescence). In the latter case, the term "optical dating" is used when the stimulation is either by visible light (commonly referred to as optically stimulated luminescence, OSL) or near-infrared radiation (infrared stimulated luminescence, IRSL).

Although the mechanisms responsible for luminescence are much more complex, it is convenient to use a simplified model for explaining the behaviour of luminescent crystals in the context of the dating method. In this model (see section 2.2.1), an ideal insulating crystal is characterized by an occupied valence band and an empty conduction band, with an energetically forbidden zone in between.

Natural crystals, however, are not perfect and have structural defects and chemical impurities (such as vacancies, dislocations and substitutional impurities),

some of which can act as traps for unbound (free) electrons, leading them to localized energy levels within the forbidden zone.

The first step in the luminescence process is the creation of electrons and holes due to the interaction of ionizing radiation with the mineral lattice (Fig. 2). Free electrons are produced when the mineral grains of interest are exposed to ionising radiation: alpha and beta particles, and gamma rays, emitted by the decay of radioactive elements within the minerals and their immediate surroundings, and from cosmic rays originating from unknown sources in the universe.

These electrons and holes subsequently can get "trapped" at defects T and L, respectively in the forbidden zone (Fig. 2).

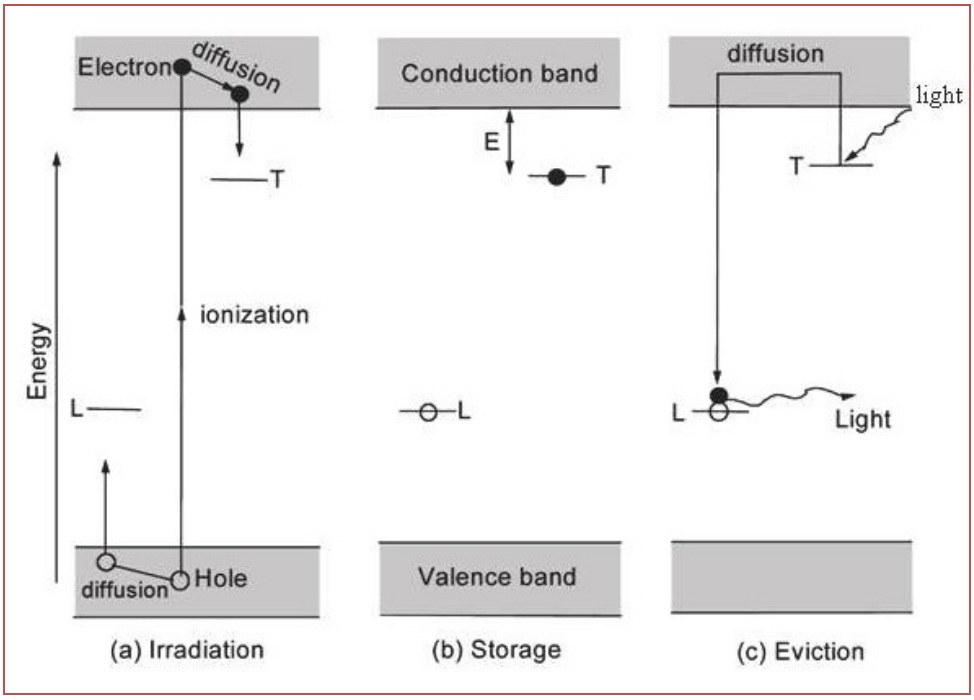

Fig. 2 - Energy-level diagram of OSL process (based on Aitken, 1998): a) ionization due to exposure to nuclear radiation with trapping of electrons and holes at crystal defects; b) storage during time; c) the electron is evicted from its trap by shining light and recombines with a luminescence center under emission of OSL signal.

The longer the mineral is exposed to ionizing radiation, the more charges are accumulating in the traps. Moreover, at room temperature (~20 °C), some traps are only able to hold electrons for a few days or less, while others can hold electrons for millions of years or more. The latter types of trap are referred to as deep traps, and these have thermal lifetimes that are sufficiently long for Quaternary dating.

The trapped electrons can become free once again if the crystal is exposed to light of a specific wavelength (Fig. 2). Luminescence finally occurs if the released electrons recombine with hole centers with energy corresponding with light emission, also called luminescence centers.

The electrons were accumulated in traps, characterized by their depth E below the conduction band (Fig. 2), proportionally to amount of absorbed energy.

The luminescence emitted is, then, proportional to the total absorbed radiation dose (ignoring the effects of signal saturation) during burial. This is the fundamental basis of OSL dating.

2.2.1 SIMPLEST MODEL: ONE TRAP/ONE CENTER

In order to explain the trend OSL signal in function of time, it is possible to consider the simplest model (McKeever and Chen, 1997) by which OSL can be produced (see Fig. 2). Here light stimulates trapped electrons, concentration n, into the conduction band at rate f, followed by recombination with trapped holes, concentration m, to produce OSL of intensity I_{OSL}. With the usual definitions, the rate equation describing the charge flow is:

$$\frac{dn_c}{dt} = -\frac{dn}{dt} + \frac{dm}{dt} \qquad \text{(eqn. 1.2)}$$

Where n_c is the concentration of free electrons in the conduction band. Which can be derived from the charge neutrality condition:

$$n_c + \quad = \quad n \qquad \text{(eqn. 1.3)}$$

With the assumptions of quasi-equilibrium ($\frac{dn_c}{dt} << \frac{dn}{dt}, \frac{dm}{dt}$ *and* $n_c << , m$) and negligible re-trapping we have :

$$I_{OSL} = - \frac{dm}{dt} = - \frac{dn}{dt} = f \qquad \text{(eqn. 1.4)}$$

the solution of which is:

$$I_{OSL} = n_0 f \exp - tf = I_0 \exp\left(- \frac{t}{\tau} \right) \qquad \text{(eqn. 1.5)}$$

Here, n_0 is the initial population of trapped electrons at time t = 0, I_0 is the initial luminescence intensity at t = 0, and $\tau = 1/f$ is the decay constant.

The excitation rate is given by the product of the excitation intensity φ and the photoionization cross-section (f = φσ).

One can observe a straightforward relationship in which the initial intensity is directly proportional to the excitation rate and the decay of the OSL with time is a simple exponential.

2.3 OSL DECAY CURVE

The optical excitation used in this thesis is continuous wave (CW), operating with infrared (875 nm) LEDs, blue (470 nm) LEDs or a green (532 nm) laser. The luminescence is monitored continuously while the excitation source is on, and

narrow band and/or cut-off filters (Hoya U-340) are used in order to discriminate between the excitation light and the emission light, and to prevent scattered excitation light from entering the detector (see appendix A). Overall, the decay shape and the intensity OSL are dependent on the type of mineral, on the absorbed dose and on the illumination intensity.

Smith and Rhodes (1994) deduced that a shine-down curve for quartz consists of three main components (see also Bailey et al., 1997; Bulur et al., 2000; Jain et al., 2003), commonly referred to as "fast", "medium" and "slow" in decreasing order of sensitivity to illumination, that having different detrapping probabilities or photo-ionization cross-sections (Smith and Rhodes, 1994; Huntley et al., 1996; Bailey et al., 1997). In order to examine how different components contribute to the OSL signals, the CW OSL curve is deconvoluted (Bailey et al., 1997; Bulur et al., 2000; Choi et al., 2003; Jain et al., 2003; Murray and Olley, 2002; Murray and Wintle, 2000, 2003) into three components using first-order exponential equations (see in eqn 1.5). In optical dating, the fast component is primarily of interest, because contributes above 90% of the total signal in the initial time, it can be bleached quickly and completely by sunlight, it is stable on geological timescale and less susceptible to thermal transfer of charge (Wintle and Murray, 2006). In fact, the initial part of the CW-OSL curve, with subtraction of both the background and the slow component, for D_e determination is usually used.

The presence of the medium component in the initial part of OSL signals may interfere with the fast component and may yield problematic results in D_e determination. Choi et al. (2003) reported a significant underestimation of D_e values using the simple integration of initial OSL signals where a large proportion of medium component contributed to the initial signal. Similar results are also found in other studies (e.g. Tsukamoto et al., 2003).

A simple and useful method for checking the influence of the medium component is to use a D_e(t) plot. The form of the D_e(t) plot is affected by the composition of the OSL signals; thus the shape of the D_e(t) curve could be an effective tool for assessing the bleaching history of sediment samples (e.g. Aitken, 1998; Bailey, 2000; Bailey et al., 2003). For well-bleached samples, the D_e should be independent of the illumination time. If the samples are partially-bleached before burial and more relatively slower components remained, the D_e value will increase with illumination time. This method was successfully applied for assessing the bleaching history of modern samples and young samples (Bailey et al., 2003; Singarayer et al., 2003). For older samples, other factors (see section 2.8.1) may contribute potentially to the shape of D_e(t) plot. The relative contributions as a function of illumination time of different components to the total signal are shown in Fig. 3. Standard practice for selection of integration time intervals follows Banerjee et al. (2000), with an initial integral of the decay curve (e.g. 0-0.8 s) usually taken as indicative of the fast-component signal, once a late background (e.g. 36-40 s) is subtracted. Using the last few seconds of the decay as background adequately removes photomultiplier dark noise and stimulation light leakage from the signal, and also subtracts the majority of the slow component.

The method in which the background integral is taken from the last few second of OSL curve, known as “late-background” (LBG) approach, is contrasted to the “early-background” (EBG) approach, where the background integral immediately follows the initial signal. This last is applied above all to young samples (Cunningham and Wallinga, 2010).

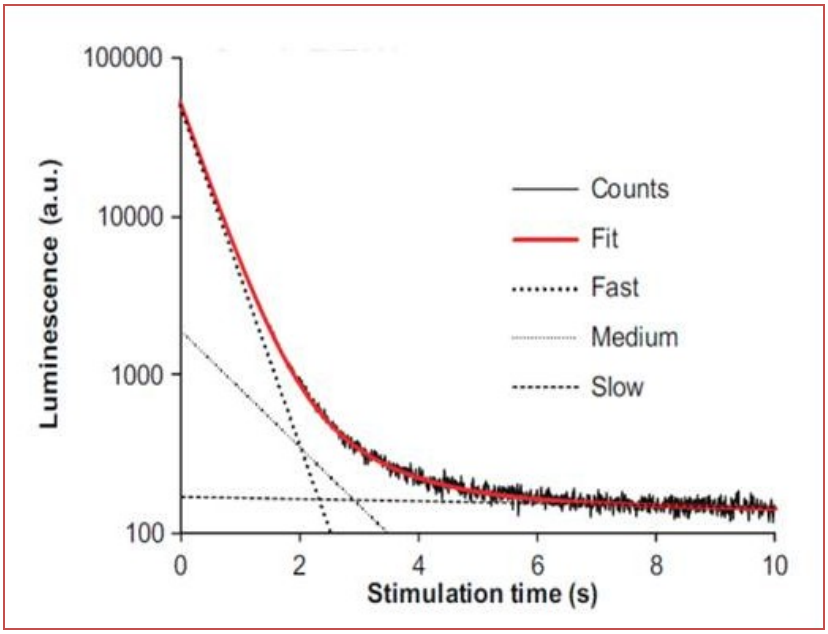

Fig. 3 - Representative example of a laboratory regenerative OSL decay curve stopped at 10 s to underline the OSL components. Using curve fitting, the data is well-described by the sum of three exponential decays termed the fast, medium and slow components, with the fast component being dominant (forming 90% of total luminescence in the 0-0.8 s of the OSL decay) (Pawley et al., 2010).

2.4 NATURAL RADIOACTIVITY

The annual radiation dose in luminescence dating originates from the ionizing radiation (α, β and γ radiations) of naturally occurring, long-lived primordial radionuclides (^{235}U, ^{238}U, ^{232}Th, ^{40}K and ^{87}Rb) present in the sample and its immediate surroundings and from cosmic radiation.

When nuclei of ^{40}K with a natural atomic abundance of 0.0117% undergo radioactive decay, beta particles and a gamma ray are emitted. For ^{87}Rb, there is emission of β-particles only. The radioactive decay schemes of ^{40}K and ^{87}Rb are shown in Figs. 4a-4b. Natural uranium and thorium consist of three radioactive decay series headed by ^{235}U, ^{238}U and ^{232}Th and ending in ^{207}Pb, ^{206}Pb and ^{208}Pb, respectively (Figs. 4c-4d-4e).

Grains are irradiated by all four types of radiation, alpha, beta, gamma and cosmic, but, because of their short range, alpha particles penetrate only the outer rind of sand-size grains (Fig. 5).

Beta particles from K and Rb are emitted within a K-feldspar grain and these deposit some of their dose within the grain before escaping. Whereas the effect of alpha particles, in minerals such as quartz and feldspars, is highly localized to within the order of 25 μm of the emitting nucleus, the upper limit to the range of the beta particles is a few millimeters (Aitken, 1985).

Considering a sphere of sediment of ~30 cm, with density of ~2 g/cm^3, about 95% of the gamma radiation will be attenuate. Cosmic radiation is the most penetrating of all, attenuating by only about 14% in a meter of sediment of widespread density.

In the radioactive decay chains, as shown above, each parent decays into a daughter nucleus which itself is radioactive, until the chain ends with a stable lead isotope. If the system is closed, a radioactive equilibrium or secular equilibrium is reached in which $\lambda_1 N_1 = \lambda_2 N_2 = \lambda_i N_i$, where $\lambda = (\ln 2)/T_{½}$ is the decay constant, N is the number of nuclei and λN is the activity. Secular equilibrium in the decay chains through time and "closed system" behaviour (i.e. physical-chemistry stability) are assumed in most luminescence dating applications, assuming that geological processes have not altered the radioactive concentrations during the entire burial period. In case of branched decay, a multiplication has to be done with the branching factor. It is important to note that, if the half-life of the parent radionuclide is much longer than that of the daughter, the latter determines the time after which equilibrium is reached. Indeed, beyond about 10 half-lives of the daughter radionuclide it decays at the same rate as it is produced - a state called secular equilibrium.

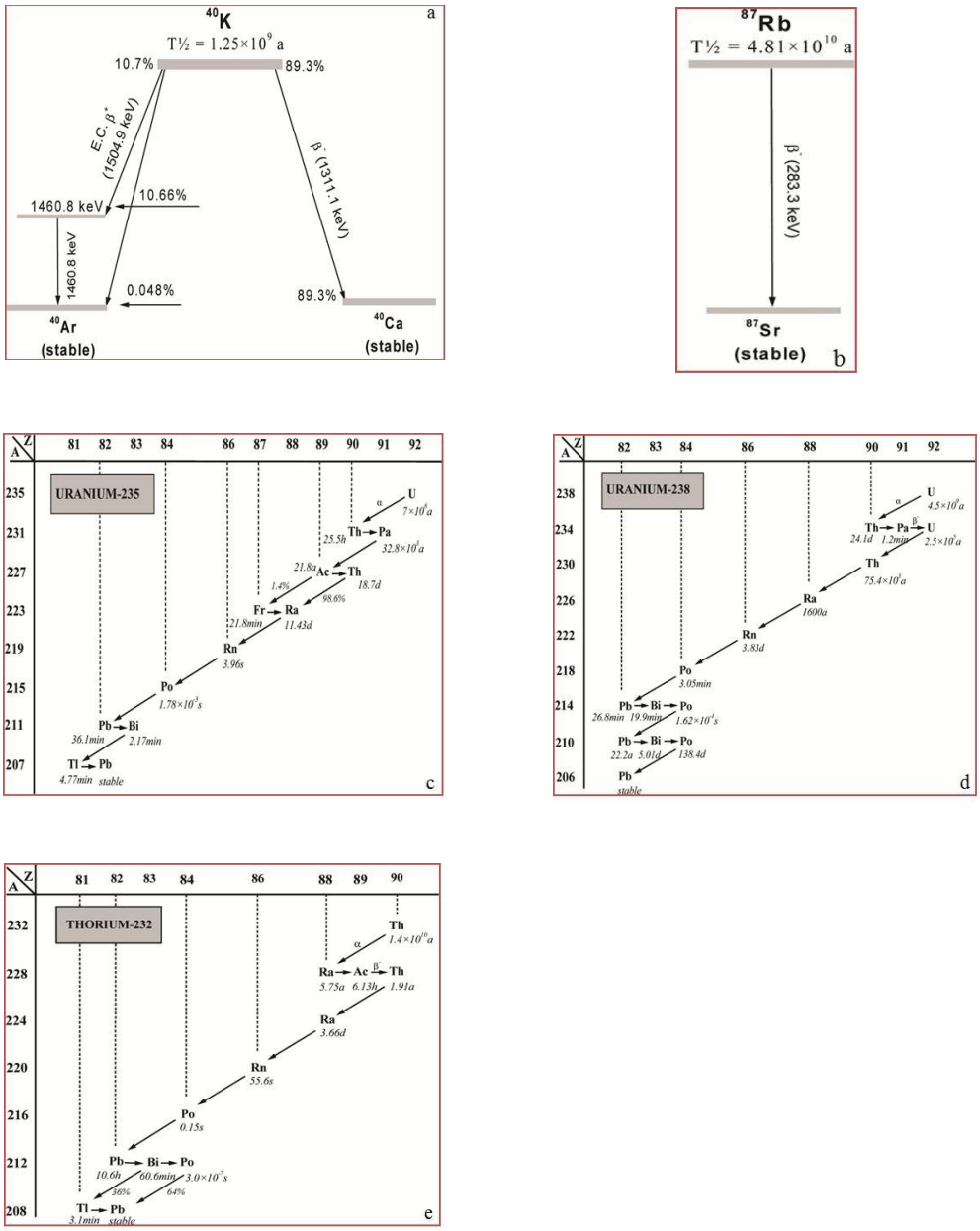

Fig. 4 - a, b) Decay schemes of ^{40}K and ^{87}Rb. c) Decay scheme for the ^{235}U; d) ^{238}U; e) ^{232}Th. Data are from Lorenz (1983). A long arrow indicates alpha decay and a short one beta decay. Branching is shown except when the branching involved is less than 1%. Linking the start and end of the chains there are several radioactive daughters of ^{235}U, ^{238}U and ^{232}Th that are significant since they emit a variety of α, β and γ radiations. E.g. when the nucleus of ^{235}U undergoes radioactive decay, with emission of an α particle, the daughter nucleus formed, ^{231}Th, is also radioactive. This process continues through radioactive daughters until the stable ^{207}Pb isotope is reached.

A relevant example is the mother-daughter pair ^{226}Ra ($T_{½}$ = 1600 a) which decays to ^{222}Rn (3.83 days), for which equilibrium is thus reached after about one month.

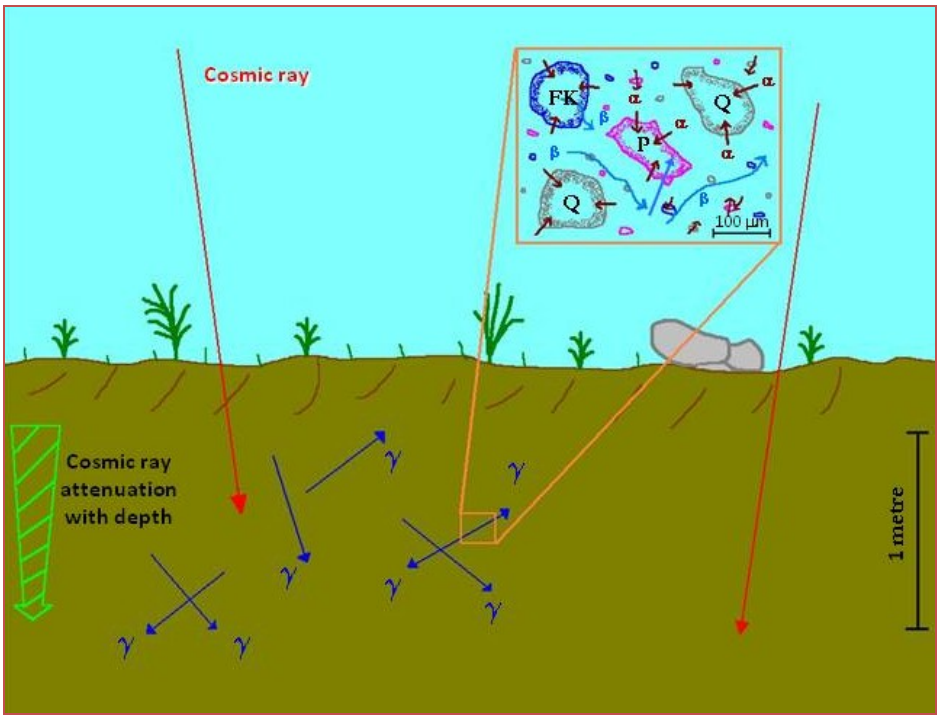

Fig. 5 - Schematic representation of some relevant aspects of natural radioactivity (Aitken, 1998).

METHODOLOGY

At first the sample of any geological context is drawn, and then is prudent to be certain that the sample has a relationship to the stratigraphic and/or geomorphology of the site. In Fig. 6 is possible to see the overall scheme of practical steps and procedures used for obtaining an OSL date.

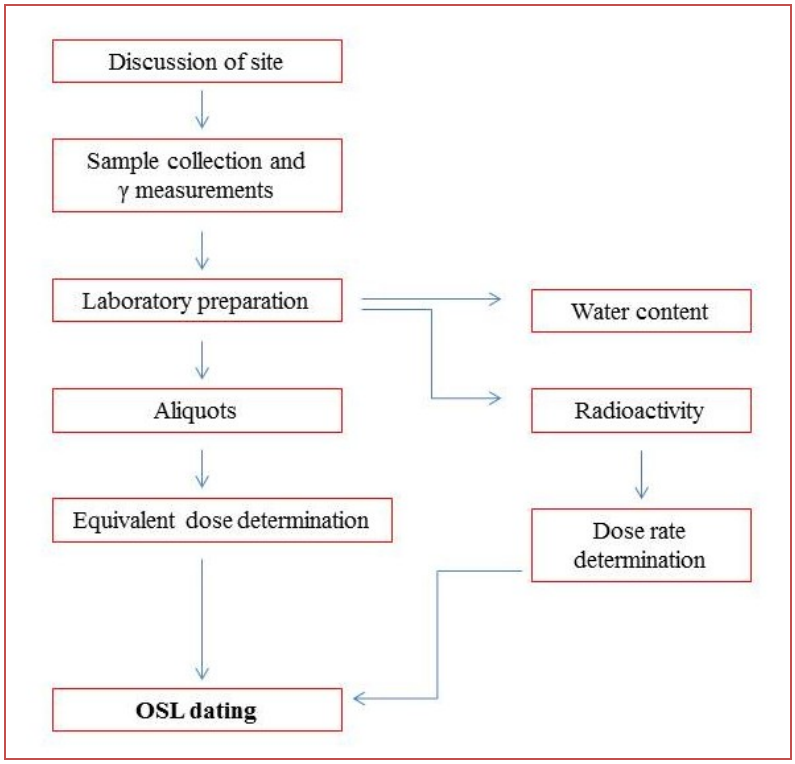

Fig. 6 - General scheme of practical steps.

2.5 SAMPLING COLLECTION

It is of critical importance that the grains of the sample are not exposed to daylight; a few seconds of this is liable to reduce the dating signal very substantially, and hence also the final age. One approach is to collect at night, first of all scraping off the surface layer and then putting the sediment in an opaque black plastic bag for transportation.

A more generally applicable approach is to push, or hammer, a steel or opaque PVC cylinder into a vertical section of the sediment. A convenient size of cylinder with a diameter of 10 cm and length of 60 cm (see Fig. 7).

Fig. 7 - Particular of PVC cylinder into a vertical section of the sediment.

Immediately after coring, the sampling tubes are sealed at both ends and stored so as to avoid any accidental light exposure and possible mixing of collected materials.

2.6 SAMPLE PREPARATION FOR OSL MEASUREMENTS

Under controlled lighting to avoid any natural luminescence signal loss, aliquots of coarse grained fraction are obtained following protocol after described.

In the laboratory, the outer few centimeters should be discarded as far as paleodose evaluation is concerned, even if this material can be retained for radioactivity measurements and also for the water content determination.

After drying and sieving (see Fig. 8), the sample is treated with hydrochloric acid (10% HCl) to dissolve carbonates and then hydrogen peroxide (35% H_2O_2) to remove organic material.

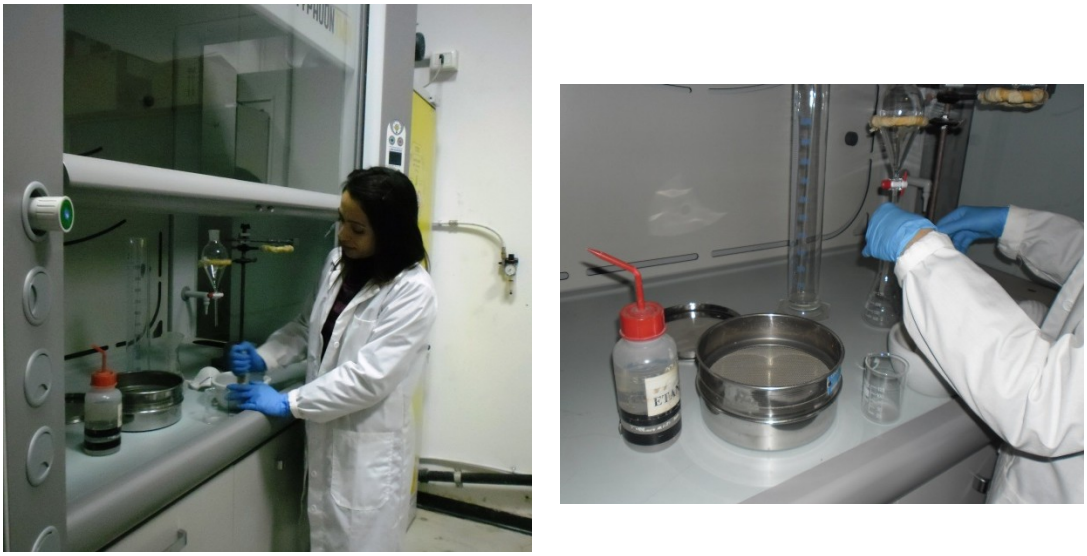

Fig. 8 - Example of particular step of sample preparation.

To separate the quartz fraction from both heavy minerals (>2.70 g/cm^3) and feldspars (<2.62 g/cm^3), solutions of sodium polytungstate of variable density are used (Mejdahl, 1985). In order to remove the outer α-irradiated layer (Aitken, 1985, 1998) and dissolve the remaining feldspars as inclusions in the quartz (Reimann et al., 2010), separated fractions are etched with hydrofluoric acid (40% HF). Finally, to eliminate any fluorides eventually produced is used hydrochloric acid (10% HCl).

Considering the different penetrating powers of radiations involved (see section 2.4), the α-ray contribution from radioactivity external to the grains is eliminated as just indicated, and dose rate equation for *coarse-grain* dating becomes:

$$Dose\ rate = f\,D_{\beta} + D_{\gamma} + D_{cosm} \qquad \text{(eqn. 1.6)}$$

The energy derived from the β rays is attenuated by the factor f, related to the attenuation of β rays in dependency of grain size (Aitken, 1985).

The luminescence measurements are performed on small aliquots of diameter equal to 9.7 mm (Duller, 2008), composed of quartz grains within the selected size range, deposited in a monolayer onto stainless-steel discs, coated with silicon oil; in alternatively the single grains quartz are mounted on discs drilled with a 10×10 array (300 μm wide and 300 μm deep).

2.7 QUARTZ AS DOSIMETERS

Various are the reasons because the OSL signals by quartz, instead of feldspars, are considered in this thesis.

The use of feldspars implicates the presence of internal ^{40}K and some malign properties, e.g. the "anomalous fading". This is referred to the loss of electrons from traps that are thermally stable at room temperature over geological time that could cause underestimated age. No evidence has been found to indicate that quartz OSL suffers from anomalous fading, and quartz signals are bleached more readily in daylight than feldspars OSL signals (Godfrey-Smith et al., 1988).

For these explanations it is usually necessary to separate quartz and feldspars OSL signals to obtain useful quartz dose estimates.

Moreover, it is essential to ensure the absence of the feldspars, because they could involve a change of the shape of the curve decay OSL, and finally on the OSL age value. The purity of the quartz is tested (see Table 1; Henshilwood et al., 2002 and Duller, 2003) by monitoring the presence of feldspar through measuring the IRSL signals at RT and using the approach of the $(L_{post\text{-}IR\ OSL}/T_2)/(L_{OSL}/T_1)$ (denoted here as post-IR OSL/OSL). This test assumes that an IRSL signal at RT is emitted by feldspars. Thus, the ratio is at unity if no feldspar component is present (see Fig. 9) and it is < 1 in the case of contamination.

Table 1 - Feldspar contamination test (Henshilwood et al.,2002; Duller, 2003).

Step	Treatment	Observed
1	Give dose, D_i	-
2	Preheat@160-300°C for 10 s	-
3	Stimulate with blue LEDS@125 °C for 40 s	L_{OSL}
4	Give test dose, D_t	-
5	Cut-heat < T_{PH} in step 2	-
6	Stimulate with blue LEDS@125 °C for 40 s	T_1
7	Give dose, D_t	-
8	Preheat@160-300°C for 10 s	-
9	Stimulate with IR LEDS@50 °C for 100 s	-
10	Stimulate with blue LEDS@125 °C for 40 s	$L_{post\text{-}IR\ OSL}$
11	Give test dose, D_t	-
12	Cut-heat < T_{PH} in step 2	-
13	Stimulate with blue LEDS@125 °C for 40 s	T_2

For the natural sample, I = 0 and D_0 = 0 Gy.

L_i and T_i are derived from the initial OSL signal minus a background estimated from the last part of the stimulation curve.

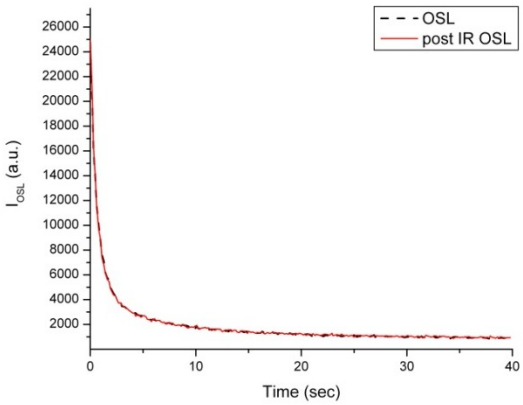

Fig. 9 - Results from feldspar contamination test. The OSL and post-IR OSL curves overlap, because etching treatment (40% HF for 10 min) has removed the feldspar content.

2.8 OSL MEASUREMENTS

All luminescence measurements are made using a semi-automated Risø reader TL-DA-15 (for instrumental parameters see Appendix A) carried out by PH3DRA (Physics for Dating Diagnostic Dosimetry Research and Applications) laboratory, at Department of Physics and Astronomy of Catania (Italy).

The modified single-aliquot regenerative-dose (SAR) protocol (for details see following section) of Murray and Wintle (2000, 2003) proposed to determinate the equivalent dose (D_e) of coarse grained quartz, incorporates several test that attempt to simulate natural bleaching and to check on the luminescence behaviour of the minerals and hence the suitability of the measurement procedure. The natural OSL

signal is measured and in the process light-sensitive traps are emptied of trapped charge. A laboratory dose D_i is then given to the sample and a regenerated OSL signal measured. This procedure can be repeated any number of times and by varying the regeneration doses, a dose response curve (also known as a growth curve) showing how the OSL signal grows with radiation dose can be constructed. Interpolating the natural OSL signal onto this growth curve gives the laboratory dose (the equivalent dose) required to induce an OSL signal equivalent to the natural OSL signal.

However, dose estimation is complicated by the fact that the sample needs to be preheated prior to OSL measurement. Franklin et al. (1995) concluded that the quartz TL peaks located at 110°, 180°, 220° and 325 °C all use the same luminescence centre, which is accessed via the conduction band. Thus, in order to be able to compare natural and regenerated signals the unstable contributions to the observed OSL signal (probably originating from the 110°, 180° and 220 °C TL traps) must be removed. One way of doing this is by preheating the sample, i.e. to heat the sample prior to OSL measurement. Unfortunately, the major luminescence sensitivity change usually seems to occur when the sample is first heated. The first true SAR protocol able to overcome the problem of sensitivity changes in quartz was described by Murray and Roberts (1998) and improved by Murray and Wintle (2000). In the SAR protocol sensitivity changes are explicitly monitored and corrected by the insertion of a test dose. All OSL measurements are carried out at 125 °C in order to prevent re-trapping of charges from the shallow trap corresponding to the 110 °C TL peak (Murray and Wintle, 1998).

There are many published descriptions of the SAR protocol and its applications (e.g. Murray and Olley, 1999; Bailey et al., 1997; Stokes et al., 2001). In the

following a brief description of the modified SAR (Murray and Wintle, 2003) protocol is presented and a generalised measurement sequence is shown in Table 2.

Table 2 - Experimental parameters of modified SAR protocol used for D_e determination (after Murray and Wintle 2003).

Step	Treatment	Observed	Note
1	Give dose, D_i	-	For natural samples, $D_i = 0$ Gy
2	Preheat@160-300°C for 10 s	-	Remove the charge from light-sensitive, thermally unstable traps
3	Stimulate with blue LEDS @ 125 °C for 40 s	L_i[a]	Bleach OSL signals
4	Give test dose, D_t	-	Monitor the luminescence sensitivity
5	Cut-heat < T_{PH} in step 2	-	
6	Stimulate with blue LEDS @ 125 °C for 40 s	T_1	Measure the test dose OSL response
7	Stimulate with blue LEDS @ 280 °C for 40 s[b]	-	Remove remaining Re-OSL
8	Return from step 1 to 7	-	

[a] L_i and T_i are derived from the initial OSL signal minus a background estimated from the last part of the stimulation curve.
[b] R is recuperation (to minimize the thermal transfer of charges possible; Choi et al., 2003; Murray and Wintle, 2003; Wintle and Murray, 2006).

2.8.1 SINGLE-ALIQUOT REGENERATIVE-DOSE (SAR) PROTOCOL

Since the last event of bleaching, to mineral is given a dose D_n before sampling. In the laboratory the sample is, at first, preheated to a temperature T_{PH} (usually between 160° and 300°C and held for 10 s). The natural OSL signal L_n is then measured by optical stimulation until the signal has decayed to a negligible level (i.e. until the OSL traps are empty). A small test dose D_t (usually ~10% of the natural dose D_n) is then administered to the sample. The sample is subsequently heated to a temperature T_{CH} (typically 160°C to empty the 110°C TL trap), cooled immediately and the OSL signal T_n induced by the test dose measured. The second measurement cycle in the SAR protocol is initiated by giving the first regenerative dose D_1 to the sample. After irradiation the sample is heated to the same preheat

temperature T_{PH} as in the first measurement cycle and the regenerated signal L_1 measured. The sample is then given another test dose D_t (same as in the first cycle), heated to T_{CH} and the induced OSL signal T_1 measured.

In order to build a growth curve the second regenerative cycle is repeated, but increasing the size of the regenerative dose D_i (see Fig. 10).

It is the OSL response to the fixed test dose D_t that is used to monitor sensitivity changes occurring in the measurement protocol. If no sensitivity changes took place all values of T_i would be identical. By dividing the natural and regenerated OSL signals with the subsequent test dose signals (i.e. $L_n = T_n$ and $L_i = T_i$ respectively) a sensitivity-corrected measure of the OSL signal is obtained. The regeneration doses are typically chosen such that the sensitivity corrected values $R_i = (L_i/T_i)$ encompass the natural sensitivity corrected value $R_n = (L_n/T_n)$, i.e. 1) $R_1 < R_n$; 2) $R_2 \sim R_n$ and 3) $R_3 > R_n$. A sensitivity-corrected growth curve is constructed by plotting values of R as a function of D. The natural dose D_n is then estimated by interpolation of the ratio R_n onto the sensitivity corrected growth curve (see Fig. 11).

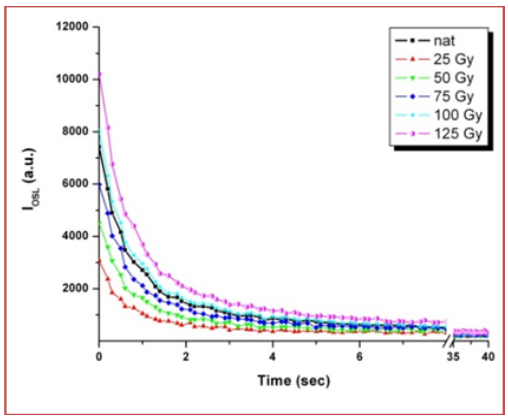

Fig. 10 - Graphical presentation of regenerative curves together to natural OSL signal.

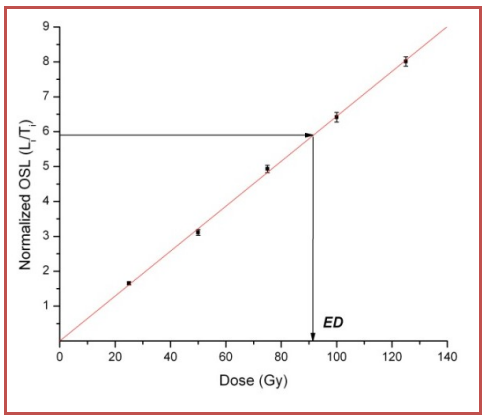

Fig. 11 - The equivalent dose (D_e) is obtained by projection of the sensitivity-corrected natural value onto the sensitivity-corrected dose response curve.

If the correction for sensitivity change works properly the corrected OSL ratio R_i should remain constant throughout the measurement cycle for a fixed D_i, i.e. it should be independent of prior dose and thermal treatment. This is tested in the SAR protocol by repeating one of the regeneration cycles, usually the 6th cycle is a repetition of the 2nd cycle, i.e. $D_5 = D_1$.

The ratio $R_5 = R_1$ is called the recycling ratio and if the protocol corrects for sensitivity change, should ideally be equal to unity, then $R_5 = R_1 = 1$.

If no dose (D = 0 Gy) is administered to a sample, no detectable OSL signal should be observed. In practice, however, a detectable recuperated OSL signal is seen (Aitken and Smith, 1988). In the SAR protocol the recuperation is estimated by inserting a measurement cycle with D_i = 0 Gy (usually i = 4). The ratio R_4 should ideally be zero, but is in practice finite. One of the prime reasons for preheating is to prevent contamination of the regenerated signals by contributions from thermally unstable but light-sensitive traps. However, preheating can also result in recuperation of the OSL signal after the OSL traps have been emptied optically.

Murray and Wintle (2000) suggested that the recuperated signal (at least in part) arises from charge inserted by the test dose into thermally shallow but light-insensitive traps, which are not emptied by heating to T_{CH} (usually 160°C), but are emptied by heating to T_{PH} (usually 280°C) and partly re-trapped by the OSL trap. In fact at the end of each run the aliquots or single grains are optically stimulated at 280°C for 40 s to bleach the remaining OSL signal as much as possible to minimize the thermal transfer of charges (Choi et al., 2003; Murray and Wintle, 2003; Wintle and Murray, 2006) and to prevent signal carry over to the next cycle. This value should not exceed 5% of the sensitivity corrected natural signal Murray and Wintle (2000). In general, the growth curve will often appear linear at low dose levels, but at higher dose levels the luminescence signal saturates, because of a finite number

of available charge traps. The growth curve is usually fitted adequately by a single saturating exponential (Thomsen, 2004).

2.8.2 REJECTION CRITERIA

In order to check whether the first sensitivity measurement (T_n) is appropriate to the natural signal (L_n), to assess the reliability of D_e interpolation in the SAR protocol and to confirm that pre-heating has not induced a significant difference in luminescence sensitivity between the natural and regenerated measurements, it is suggested a test, called dose recovery (Roberts et al,. 1999; Murray and Wintle, 2003). This is carried out on unheated portions that have given a laboratory dose, approximately equal to their D_e estimates, following removal of naturally trapped charge by optical stimulation. The aim of these studies is to simulate the OSL signal using the same process as in nature. Since a known dose is given, the ability of the chosen SAR protocol to measure this dose accurately is tested directly.

The ratio of the measured dose to the known dose is calculated, and if the SAR protocol is working correctly, then this ratio will be unity. The dose recovery test also provides information on the maximum precision that can be achieved in the absence of natural variations in dose rate resulting from inhomogeneity of the bulk sample and variations in the degree of bleaching from grain to grain.

2.9 DISCUSSION OF DATING RESULTS: ANALYSIS OF D_E DISTRIBUTION AND STATISTICAL MODELS

For the aliquots/grains that passed the stringent rejection criteria (e.g. recycling ratios within 10% of unity and low recuperation), the obtained D_e values are plotted, at first, as standard frequency distribution, also called *histogram*, getting an un-weighted mean D_e values. These distributions are classified, principally, in two

types and their characteristic shapes are related to the degree of bleaching during transport of mineral grains, following Arnold et al. (2007). Distribution type 1 is an example of an well-bleached sample, with a near-normal distribution (Fig. 12), whereas type 2 is positively skewed and has a characteristic tail of larger equivalent doses, representing a classic partially-bleached distribution (Fig. 13).

However, these diagrams do not take into account errors of the equivalent doses, the maximum of the histogram may therefore not coincide with the "true" geological dose, unless the errors are more or less uniform. Distortions of the shape of a histogram can occur by bright, but poorly bleached grains. Despite disadvantages, histograms offer easy visual information on how far a population of grains is bleached. This diagrams establishes, thus, a useful tool for visual inspection of data, but does not permit an quantitative statistical dose assessment (Goedicke, 2003).

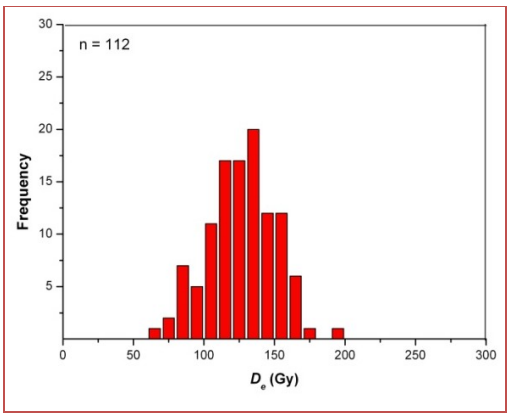

Fig. 12 - Distribution type 1: example of an well-bleached sample. Frequency distribution (histogram) of the equivalent doses obtained from 112 single grains of sand-sized quartz.

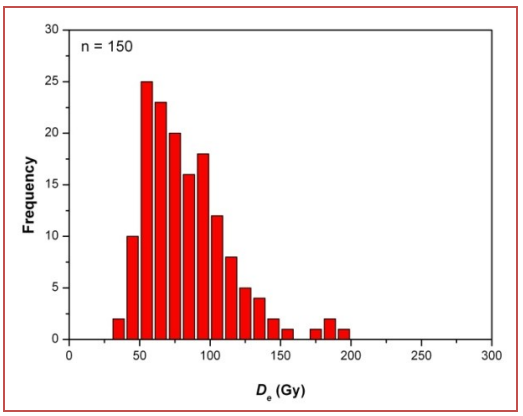

Fig. 13 - Distribution type 2: example of a classic partially-bleached distribution. Frequency distribution (histogram) of the equivalent doses obtained from 150 single grains of sand-sized quartz.

To circumvent the doubts inherent in histograms, Galbraith et al. (1988, 1999) promoted the *radial plot* (see Fig. 14) for the presentation of single-aliquot and single-grain data. The radial plot displays not only the D_e value for an aliquot/grain (found by drawing a line from the y-axis ("standardized estimate") origin through the dose point of interest until it intersects the radial axis, at the value of the equivalent dose, on the right-hand side), but also its measurement uncertainty (expressed as the standard error, found by extending a line vertically to intersect the x-axis). The latter is displayed as both "relative error" and as its reciprocal ("precision"), so that the dose estimates measured with the highest precision plot farthest to the right. These display both the individual D_e values and the related precision on a plot that also enables visual evaluation of whether a sample is dominated by one population of D_e values, or is more complex.

Though not designed as an analytical tool, radial plots may serve to filter out data from a group that are placed within an area of ±2σ relative to an arbitrary central value (Galbraith et al., 1990, 1999). Assuming that the "true" geological dose is found within the low dose region of a distribution, a possible approach of finding this dose may consist in selecting data points by moving the 2σ area over the distribution so that the data with the lowest doses are included in the 2σ-band. The advantage of this evaluation over the evaluation of histograms is that errors are properly accounted for. An estimate for the equivalent dose is then calculated as the weighted mean of the data within the ±2σ band. It must be emphasized that the selection of data is based on a 2σ level, the final weighted mean, however, is quoted with a 1σ error.

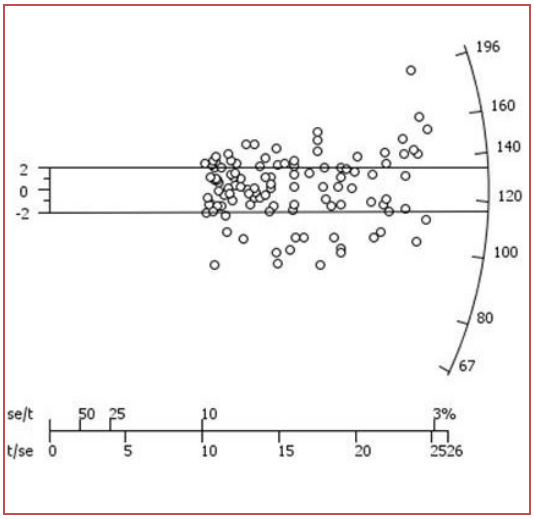

Fig. 14 - Radial plot of the measured doses following Galbraith et al. (1990, 1999).

Despite these improvements to the analysis and display of single-aliquot and single-grain data, a most pressing challenge remains that of understanding the nature of the distribution of equivalent doses that often occurs in a single sample, and how to determine an accurate age from an equivalent dose distribution. This problem is addressed by Bailey and Arnold (2006). They model the response of the quartz OSL to various irradiation and bleaching conditions to test the fidelity of current techniques used to extract the "true" equivalent dose (and age) from a sample composed of grain populations, each with a different equivalent dose. The main finding of their study is that no single method of analysis is applicable to all samples (depositional environments), but that it is possible to choose the most appropriate model on the basis of the shape of the equivalent dose distribution.

The "Central Age Model" (CAM) works best at estimating the true D_e for type 1 distributions (Fig. 12). The "Minimum Age Model" (MAM) works best at estimating the true for type 2 distributions (Fig. 13).

In particular, the CAM (Galbraith et al., 1999) assumes that the logarithmic distribution of D_e values is normal (follows the Gaussian function) but that they are not consistent with a single value of D_e; instead they are randomly spread around a central D_e value with a standard deviation that is too wide to be accounted for by measurement uncertainties alone. This model calculates the weighted-mean D_e for a set of single-aliquot or single-grain estimates, taking into account the extra spread above and beyond that associated with the measurement uncertainties.

If there are grains with different bleaching and/or irradiation histories, the MAM (Galbraith et al., 1999; Olley et al., 2004) can be used. With this model, some estimate of the underlying overdispersion should also be taken into consideration, preferably from a sample of well-bleached grains derived from the same source (Galbraith, 2005). The most appropriate D_e would therefore relate to the lowest range of D_e's, i.e. those that represent the bleached grains. It is to remember well that statistical models should, of course, be applied with consideration of sedimentary process and other lines of evidence about the bleaching and burial history of the deposit. For other statistical models it is possible refer to the current bibliography (e.g. Jacobs et al., 2003, 2006; Lepper and McKeever, 2002; Olley et al., 1998, 2006; Roberts et al., 1998; Rodnight et al., 2005; Sivia et al., 2004; Stokes et al., 2001).

2.10 DOSE RATE DETERMINATION

In order to calculate the rate at which ionizing radiation energy is absorbed by the mineral grains of interest, a subsample of the sediment is used to determine the concentrations of radioactive elements involved, i.e. U, Th, K and Rb, together with an estimate of the cosmic ray intensity at the sampling site.

A number of factors can complicate this assessment, such as the need to estimate the average water content over the entire period of sample burial, and to establish whether or not, at any time since this event, the U-series decay chain has been in a state of disequilibrium, e.g. due of leakage of radon present in chain (Key et al., 1979). Fortunately it is possible to calculate the dose-rate in buried sediment without going into the intricacies of the interactions by which energy is absorbed from the nuclear radiations. There are many analytical methods that have been adopted in the past for determining the annual radiation dose.

Considering the assumption of infinite matrix (Adamiec and Aitken, 1998), within a volume having dimensions greater than the ranges of the radiations, the overall rate of energy absorption is equal to the rate of energy emission. Further, to the extent that homogeneity can be assumed both in radioactive content and in absorption coefficient, the absorption per unit mass is equal to the emission per unit mass; the latter is available from complex nuclear data tables. Thus by determining the concentrations of the radioelements in a sediment, the dose-rate can be calculated; however, there are other routes based on direct measurement of the radiations which are less difficult and which are essential if there is the possibility of radioactive disequilibrium.

The radionuclide concentrations calculated by measuring the radionuclide concentrations (inductively coupled plasma mass spectrometry, ICP-MS) (Preusser and Kasper, 2001), are converted to total beta and gamma dose rates using the conversion factors of Adamiec and Aitken, 1998. This method provides, next to K, only the U and Th parent nuclide concentrations, and they are therefore only reliable on condition that the U and Th decay series are in equilibrium.

Beta dose rate is, also, weighted by attenuation factors depending on grain size (Mejdahl, 1979). Cosmic ray contributions are estimated for each sample from the

altitude and latitude of the section as well as the thickness and density of the overburden (Prescott and Hutton, 1988; 1994). The gamma dose rate by radioisotope concentrations is compared with *in situ* gamma-measurements. In our case the used methodology is gamma spectrometry, performed with a probe inside the hole of sampling (by Canberra InSpector 1000 spectrometer), to show if there is a good agreement. The values of moisture-corrected dose-rates are obtained considering the water content at the moment of sampling using the attenuation factors given by Zimmerman and Huxtable (1971).

Water in the interstices of sediment absorbs part of the radiation that would otherwise reach the grains on which OSL measurement is made; hence the dose-rate in sediment containing moisture is less than that in the same sediment when it is dry, and if the effect is ignored there may be appreciable underestimation of the age.

Although the degree of wetness in the sediment "as-found" can be measured, and appropriate correction (Aitken, 1985; 1998) made, it is the average wetness over the whole burial span of the sediment that is relevant; uncertainty about this is usually a fundamental limitation in reducing error limits on the age to below the level of about 5%. Of course for arid environments that have always been arid there is no problem; similarly when there is certainty of continual saturation. Other-wise an estimate has to be made taking into account the wetness as-found and whatever indications are available about past variations; however, the effect is limited by the porosity.

2.10.1 RADIOACTIVE DISEQUILIBRIUM

Disequilibrium is the condition, thus, where the activity concentrations of the parent and daughter nuclides are not equal. This process results from geochemical sorting, whereby a process acts to move a parent or daughter into or out of a system at a rate which is significant relative to the half-life of the daughter (Osmond and

Cowart, 1982). The decay chains in deeply buried, unweathered materials are generally in equilibrium (Iyengar, 1990). However, weathering processes that occur at or near the earth's surface operate on a sufficiently short time scale that disequilibrium results.

The main mechanisms by which disequilibria are established in the superficial environment are i) solution and precipitation reactions (because of differing chemistries of the elements in the decay chains), ii) gaseous diffusion of the radon isotopes, and iii) alpha particle recoil. For a detailed discussion of each of these, see Osmond and Cowart (1976, 1982); Gascoyne (1992); Ivanovich and Harmon (1982, 1992); Hossain, (2003). If the system subsequently becomes effectively closed, and if the parent is longer-lived than the daughter, the daughter will either decay or grow into equilibrium with its parent, depending on whether its activity concentration is greater than or less than that of its parent. A state of equilibrium may never be re-attained if the system remains open; in this thesis, this condition has been avoid.

Chapter 3

LUMINESCENCE CHRONOLOGY OF PLEISTOCENE MARINE TERRACES OF CAPO VATICANO PENINSULA (CALABRIA, SOUTHERN ITALY)

Published on Quaternary International (2011), Vol. 232, pp. 114-121 (v. Bianca et al., 2011).

3.1 INTRODUCTION

The Capo Vaticano peninsula is a structural high located along the Tyrrhenian side of the Calabrian arc (Fig. 1). In this area is shown the Late Quaternary tectonics characterized by the occurrence of a major normal fault belt along the western side of Calabria, developed in response to WNW-ESE regional extension (Fig. 1). Since Middle Pleistocene times, extensional tectonics have been coupled with a strong regional uplift which developed spectacular flights of coastal terraces (Miyauchi et al., 1994; Tortorici et al., 2003; Cucci and Tertulliani, 2006).

Chronological proposals for coastal terraces on the Capo Vaticano peninsula are in fact poorly supported by absolute dating (e.g. luminescence, Th/U and amino acid determinations) of Pleistocene sediments, which are themselves only exposed in few scattered sites (Dumas et al., 1987, 1991; Dai Pra et al., 1993; Balescu et al., 1997).

Appropriate age constraints for coastal terraces thus represent a basic tool for accurately evaluating vertical movements of regions affected by Quaternary tectonic uplift. In this work are proposed new absolute OSL age estimates of Pleistocene marine terrace deposits located on the Capo Vaticano peninsula, where a complete series, characterized by both marine and continental deposits, occurs. In order to correlate the sampled deposits with the sequence of coastal terraces, a new detailed mapping of the different Quaternary terrace surfaces has been carried out on the entire Capo Vaticano peninsula (see also Tortorici et al., 2003). Terrace surfaces have been mapped by detailed field mapping on 1:10.000 scale digital topographic

maps integrated with analysis of 1:33.000 scale aerial photographs and LANDSAT satellite images.

3.2 GEOLOGICAL AND GEOMORPHOLOGICAL SETTING

The Capo Vaticano area is a horst structure bounded by two antithetic, NE-SW striking, Tropea and Mileto normal faults (Fig. 1), resulting in a steep coastal morphology. To the northeast, the Briatico area represents the overlap zone between the en-echelon Tropea and Vibo faults. This area, interpreted as a "bridge zone" or "relay ramp" by Tortorici et al. (2003), is characterized by a slightly inclined morphological surface and a well-developed stream-channel pattern. The occurrence of a NE-SW striking, NW-facing normal fault system in the north-western offshore (Fig. 1) has been proved by a SSE-NNW striking single-channel seismic profile (Vp3; Trincardi et al., 1987), showing a prominent normal fault scarp, located at about 10 km from the coastline. Also the bathymetric map constructed by Argnani and Trincardi (1988) shows another ENE-WSW trending fault scarp, located at about 5 km from the coastline (Fig. 1). To the south-west, the promontory is abruptly truncated by two major WNW-ESE striking, SSW-dipping normal faults (Coccorino and Nicotera faults) which separate the Capo Vaticano structural high from the Gioia Tauro Basin. This latter is filled by a thick Upper Pliocene-Quaternary sedimentary succession (Ghisetti and Vezzani, 1982). The isobaths pattern of Fig. 1 strongly suggests the offshore continuation of the Coccorino fault that interrupts the continuity of the NE-SW fault system. Landward, to the south-east, antithetic SE-facing fault segments (Mileto fault) separate the Capo Vaticano horst from the Mesima Basin (Fig. 1), a basin filled by a thick Upper Pliocene-Lower Pleistocene marine succession (Ghisetti and Vezzani, 1982), capped by several marine and fluvial terraces (Fig. 2).

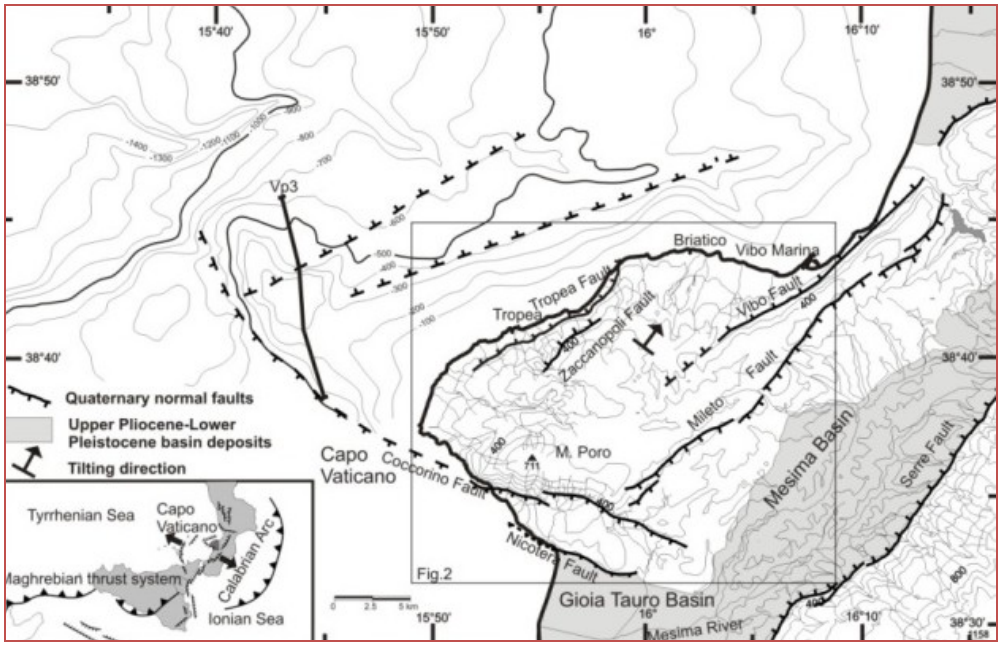

Fig. 1 - Structural map of the Capo Vaticano peninsula and the Tyrrhenian offshore (from Tortorici et al., 2003). Bathymetry from Argnani and Trincardi (1988, modified). The location of the seismic profile VP3 (Trincardi et al., 1987) is also drowned. Inset shows the tectonic setting of the Calabrian Arc and surrounding regions. Lines with triangles indicate the front of the thrust belt, lines with barbs the main Late Quaternary normal faults; black arrows show the maximum extension direction.

The geological backbone of the Capo Vaticano peninsula mainly consists of granites and gneiss of the Palaeozoic basement, covered by discontinuous remnants of Miocene and Pliocene carbonate and terrigenous deposits (Burton, 1971), on top of which eight distinct orders of well-preserved Quaternary erosion surfaces and marine terraces have been recognized. Their number and their distribution are different from those reported in the maps of Miyauchi et al. (1994) and Cucci and Tertulliani (2006), where twelve and eleven marine terraces, respectively, are distinguished even though they are not always evident in the field. A more realistic analysis is drawn by Westaway (1993) who in the same area recognized at least six wave-cut platforms.

On the top of the promontory, a Pleistocene north-eastward tilted summit surface occurs, extending from Mt. Poro to Vibo Valentia at elevations ranging from 710 m down to about 450 m a.s.l. (Fig. 2).

This surface is highly eroded and locally capped by a red to brown soil resting directly on the highly weathered Palaeozoic crystalline basement. In the San Costantino area (Fig. 2) the summit surface is overlain by up to 10 m-thick cross-bedded fossiliferous calcareous sands, containing pumiceous and cineritic layers of calc-alkaline composition (Cello et al., 1982).

Downslope, the coastal terraces consist of a flight of wave-cut surfaces and/or thin-depositional platforms, usually bounded landwards by well-developed inner edges representing the palaeoshorelines related to the main sea level high-stands.

Depositional terraces are generally made up of shell-bearing cross-laminated siliciclastic marine sands and coarse grained sandstones, covered by alluvial silts, sands and conglomerates. Wave-cut surfaces, usually covered by alluvial plain deposits, cut the underlying substratum including the earlier terraced sediments.

They show a good overall morphological continuity and a concentric geometry around the structural high, with elevations increasing regularly to the south-west.

Along steep fault-controlled coastal stretches the coastal palaeo-surfaces disappear (Fig. 2), being represented only by notch alignments obliterated by scarp degradation processes. At the south-western edge of the peninsula, the terraces are abruptly down-dropped towards the Gioia Tauro basin by the south-dipping Coccorino and Nicotera faults. To the northeast (Briatico area), a fine flight of coastal terraces showing wide wave-cut surfaces is developed on a slightly inclined morphological slope. In the following, the distinct terraces will be described from the highest to the lowest. Unlike the summit surface, the other terraces are accompanied by inner edges that have been mapped with an error margin in

elevation of ±5 m depending on erosional and depositional processes following their emergence. This error is negligible in estimating the long-term Quaternary uplift-rates involving time spans of tens to hundreds of thousands of years. However, it implies that the elevations of the palaeoshorelines reported in this paper are to be considered as mean values, useful for estimating long-term Late Quaternary uplift (Table 1).

Terrace I extensively outcrops along the western side of the Mesima Basin, between Nicotera and Mileto, where cross-bedded fossiliferous calcareous sands have been found. In this area, its inner edge runs along palaeo-cliffs developed on the Coccorino and Mileto faults (Fig. 2).

In the Capo Vaticano peninsula it is represented by a discontinuous and narrow mainly erosional surface that around the top of Mt. Poro is bordered by an inner edge extending at elevations of ~575 m a.s.l., that is downthrown at 350 m a.s.l. by the Coccorino fault. In the Zaccanopoli area it is bordered by a discontinuous inner edge located at ~550 m a.s.l.

Terrace II extends around the top of the Capo Vaticano high along the Tyrrhenian margin and the western side of the Mesima Basin (Fig. 2). Landwards it is bounded by a well-defined inner edge ranging in elevation from 250 m to 500 m a.s.l. This surface is mainly erosional and only in a few places (Spilinga) patches of cross-laminated marine sand are found.

Terrace III is represented by remnants of a narrow platform bounded landward by an inner edge occurring at elevations ranging from ~125 m a.s.l. in the Gioia Tauro basin and 150 m a.s.l. in the Vibo Marina area to ~370 m near the village of Coccorino.

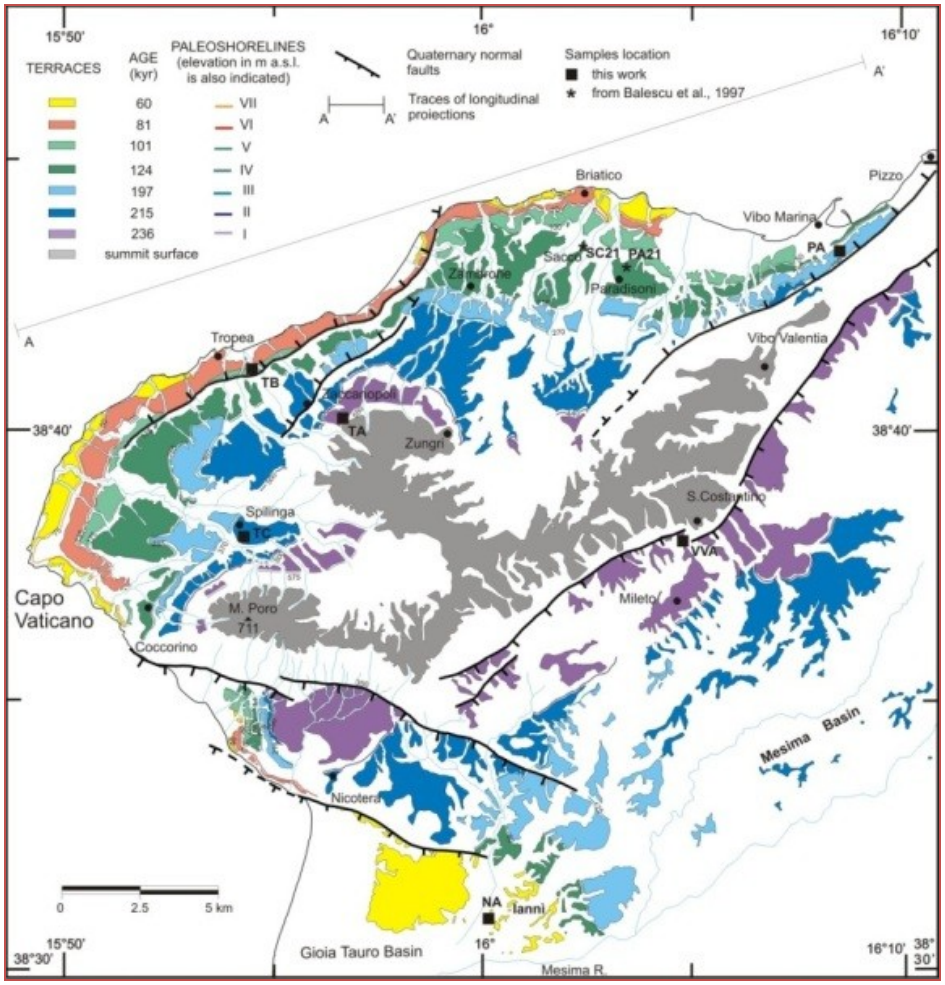

Fig. 2 - Morphotectonic map of the Capo Vaticano peninsula showing the distribution of Quaternary terraces and location of samples.

Terrace IV is one of the most continuous surfaces of the Capo Vaticano peninsula. It is usually represented by a thin depositional platform consisting of littoral sands with lenses of conglomerates bordered by an inner edge that extends continuously from ~75 m a.s.l. in the Vibo Marina area and 90 m a.s.l. in the Gioia Tauro basin up to 285 m near the village of Coccorino. Thermo-luminescence dating of two samples collected from these sediments near Paradisoni and Sacco

yielded two ages of 128±13 ka and 134±13 ka (Balescu et al., 1997). Furthermore, in the Coccorino area conglomerates with sandy matrix cropping out along the inner edge contain Senegalese fauna of Tyrrhenian age (Barrier et al., 1988).

Terrace V is a narrow platform, mainly erosional, which extends discontinuously along the coast of the peninsula ranging in elevation from ~50 m a.s.l. in the Vibo Marina area to ~175 m a.s.l. in the Capo Vaticano area. The continuity of this surface is interrupted between Tropea and Zambrone where its inner edge runs along a palaeocliff developed in the Tropea fault scarp. U/Th dating on Cladocora sp., sampled near Vibo Marina in marine sands containing *Strombus bubonius* and related to this terrace (Dumas et al., 1991; Dai Pra et al., 1993), provided ages of about 125 ka (see below).

Terrace VI shows a morphological continuity following the present coastline rising in elevation from ~45 m a.s.l. in the Briatico area to ~135 m a.s.l. in the Capo Vaticano area. To the South, in the Gioia Tauro basin, Terraces V and VI are not exposed and are overlain by transitional deposits of the lowest terrace surface.

Terrace VII, the youngest and lowest order of the whole flight of coastal platforms, is represented by a discontinuous and narrow surface visible only in the Briatico and Capo Vaticano areas, bordered by an inner edge extending at elevations ranging from ~30 m to ~75 m a.s.l. In the Gioia Tauro basin, the transitional deposits of the lowest terraced surface, constituting coastal dune sands (Bonfiglio et al., 1988), have been ascribed to the Terrace VII on the basis of age determinations (see below).

3.3 OSL MEASUREMENTS

In order to obtain new absolute dating of coastal terraces occurring on the Capo Vaticano peninsula, six samples (for coordinates see Table 2) have been collected

from unconsolidated sandy levels cropping out immediately above the major coastal Pleistocene platforms (for locations see Fig. 2) for OSL age estimates. After preparation (see section 2.6), the luminescence measurements are performed with aliquots composed of ~500 quartz grains deposited onto stainless steel discs coated with silicone oil, using semi-automated Risø reader TL-DA-15 with EMI 9235QA photomultiplier (Bøtter-Jensen, 1997; Bøtter-Jensen et al., 2000), which characteristics are reported in Appendix A.

Before dating measurements, the purity of quartz extracts is checked by IR stimulation; all samples showed IRSL signals of less than 10% of the OSL and then they are used for further experiments (Choi et al., 2009). The D_e of each sample is determined using the single-aliquot regenerative dose (SAR) protocol (Murray and Wintle, 2000) using the parameters shown in Table 3. The cycle of SAR protocol is repeated 5 times from step 1 using regeneration doses D_i increasing from 50 to 150 Gy in 50 Gy intervals for samples VVA, TA, TC and PA and from 25 to 125 Gy in 25 Gy intervals for samples TB and NA. The values of dose test D_t are respectively of 15 Gy for the first group of samples and of 10 Gy for the second one. The integral signal of the first 0.8 s is used as OSL intensity, after subtraction of the background calculated from the last 3.5 s. Uncertainties are quantified on the base of counting statistics of luminescence signals and background signals, and applying error propagation (Taylor, 1990). An example of OSL emission curves, for sample TA, is represented in Fig. 3a. The OSL values versus regenerative doses (L signals) and regeneration cycles at test dose (T signals) are reported in Fig. 3b. The natural dose (or rather its equivalent in the laboratory - the equivalent dose D_e) is then estimated by interpolation of the ratio L_n/T_n, derived from the luminescence natural curve and associated test, onto the sensitivity corrected growth curve (Fig. 4).

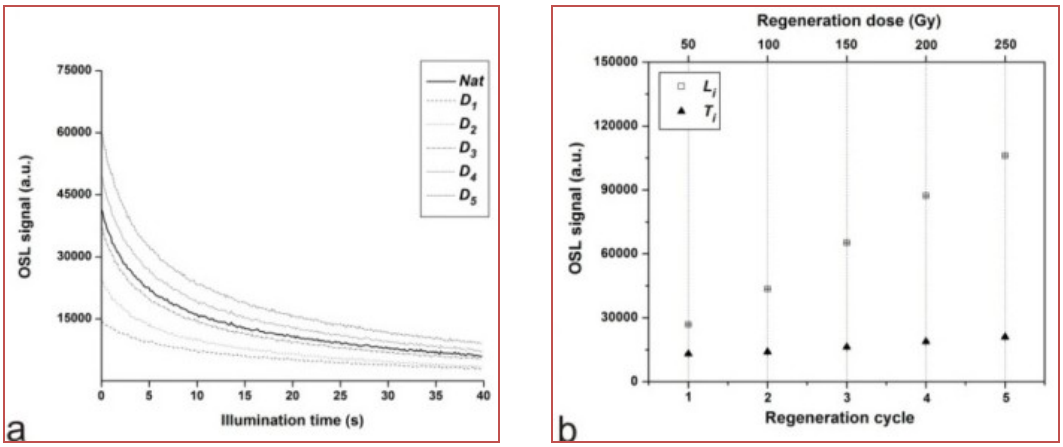

Fig. 3 - a) OSL decay curves from sample TA for different regeneration doses. b) OSL signals vs dose and regeneration cycles.

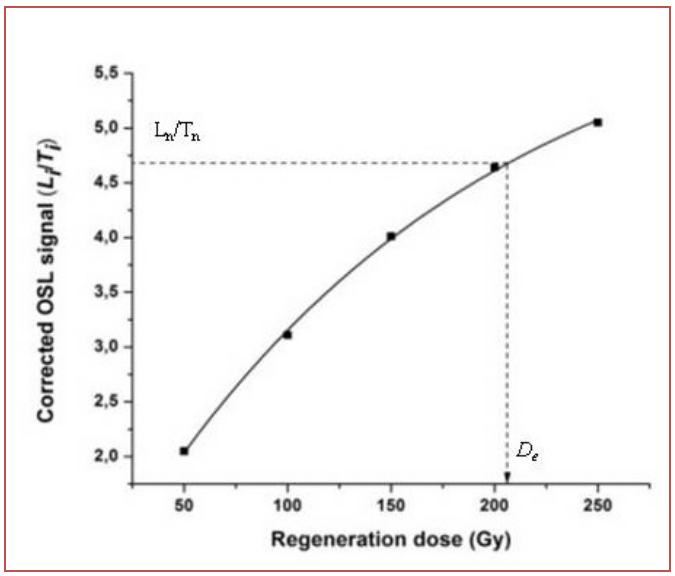

Fig. 4 - Regenerated growth curve for sample TA using the sequence of Table 2. The solid line represents the best fit curve obtained from experimental data. The intersection of the natural response (L_n/T_n) and the regenerated growth curve is shown (dashed line) giving an equivalent dose D_e of 207±22 Gy.

The uncertainty associated to D_e value of each aliquot includes counting errors, the errors of the fit and the error of source calibration. It is used the central age model to calculate the weighted mean D_e (Galbraith et al., 1999).

About 20 g of each sediment, coming from the external part of the sampling tubes, is dried, homogenized, ground to a fine powder and stored for 4 weeks to allow for the establishment of a secular equilibrium between ^{226}Ra and ^{222}Rn and sent to Actlabs Laboratory for Inductively Coupled Plasma Mass Spectrometry (ICP/MS) measurements for determination of U, Th and K concentrations (Preusser and Kasper, 2001). In calculating beta (D_β) and gamma (D_γ) dose rates, annual dose conversion factors by Adamiec and Aitken (1998) were weighted by attenuation factors depending on grain size (Mejdahl, 1979). These dose rates are validated from a comparison with gamma dose measured in situ at the sampling points with a portable NaI(Tl) probe.

The contribution of cosmic radiation to the total dose-rate is calculated using present depth following Prescott and Hutton (1988; 1994) considering the density and the depth of the sample below the surface. The moisture-corrected dose-rates values are obtained considering the present-day water content from $W_{in\text{-}situ}$ values (Aitken, 1998) using the attenuation factors given by Zimmerman (1971). All data are reported in Table 4.

3.4 AGE RESULTS AND CORRELATIONS

The OSL ages measured on the sediments sampled on distinct coastal terraces of the Capo Vaticano peninsula, covering the Middle-Late Pleistocene time-span, are consistent with a normal evolutionary model of terrace sequences, moving from the highest to the lowest elevations (Westaway, 1993; Armijo et al., 1996; Bosi et al., 1996; Bianca et al., 1999). The age determinations on the six samples, characterized

by high internal consistency, yield new constraints useful in correlating the distinct sequence of sampled terraces with the last main Marine Isotope Stages of the global eustatic curve (see Tabs. 1, 2 and 4). In a more detail, the OSL ages of 184±20 ka and 94±8 ka obtained, respectively, for the samples PA (collected near Vibo Marina, see Fig. 2 for location) and TB (collected near Tropea) allow us to correlate Terraces III and V to MIS 7.1 (197 ka) and 5.3 (100 ka), respectively. The assignment of Terrace V to MIS 5.3 in the area of Vibo Marina is problematic because of the occurrence of *Strombus bubonius* (Pata, 1947; Dai Pra et al., 1993) in sediments that, filling karst hollows, we think could have been deposited during the previous transgressive stage. On the other hand, the proposed time-correlation for the terrace sequence is also confirmed for Terrace IV by the TL age estimates of 128±13 ka and 134±13 ka obtained by Balescu et al. (1997) for marine terrace sands outcropping in the Paradisoni and Sacco areas (samples SC21 and PA21, respectively; see Fig. 2 for location). These absolute age determinations, together with the paleontological data of Barrier et al. (1988) who assigned to the Tyrrhenian stage marine deposits with Senegalese fauna found at Coccorino (Fig. 2), allow assignment of Terrace IV to the MIS 5.5 (125 ka).

As regards the youngest end-member of the terrace sequence, represented by Terrace VII, age determinations have been obtained from the sample NA, collected on the Gioia Tauro Basin (quarry of Iannì, Fig. 2), in the hanging-wall of south-dipping normal fault segments bounding the Capo Vaticano peninsula. This sample is collected at an elevation of 70 m in a sequence of aeolic cross-laminated sands containing remnants of *Hippopotamus sp*. And *Homo sapiens neanderthalensi* (Bonfiglio et al., 1988), deposited in a transitional coastal dune environment. These sediments overlie alternating sequences of continental and marine deposits, these latter containing *Strombus bubonius* (Bonfiglio et al., 1988), related to previous

transgressive stages. OSL analyses of sample NA provided ages of 62±6 ka. Taking into account that the sampled sediments were deposited coevally with marine terrace deposits, we correlate this deposit to the MIS 3.3 (60 ka) of the eustatic curve. The correlation of Terrace VII to the MIS 3.3, together with the attribution of Terrace V to the MIS 5.3 (see above), allow us to correlate Terrace VI to the intervening marine interglacial high-stand, that is the MIS 5.1 (81 ka, see Table 1).

The age determination of the highest terraces is more problematic. In fact, the sample TC, collected near the village of Spilinga (Fig. 2) in coarse marine sands of Terrace II, yielded OSL age of 199±21 ka. This age determination allows us to correlate Terrace II with the MIS stage 7.3 (215 ka) of the eustatic curve or, alternatively, to the MIS 7.1 (197 ka). Taking into account that the MIS 7.1 has easily been correlated with Terrace III (see above), it is possible to correlate Terrace II to the previous Marine Isotopic Stage (MIS 7.3). As regards the age of marine sands of Terrace I, it has been determined by OSL analyses of two samples.

The sample VVA, collected near the village of S. Costantino (Fig. 2), yields ages of 214±25 ka. This age determination allows us to correlate the Terrace I with the MIS 7.5 (236 ka) of the eustatic curve. The OSL age of sample TA, collected near the village of Zaccanopoli (Fig. 2) has been calculated to be 207±22 ka. Considering a larger margin of incertitude, we can use also this age determination to correlate Terrace I with the MIS 7.5.

3.5 DISCUSSION

The age and morphological distribution of the marine terraces and palaeoshorelines suggest that the Capo Vaticano peninsula has been differentially uplifted during Late Quaternary times. The beginning of the uplift process could be confined between the formation of the top surface, whose age has not been

determined, and Terrace I, i.e. just before 236 ka. The measured palaeoshorelines of terraces I-VII show elevations strongly increasing to the SW (Fig. 2 and Table 1). In order to better define the deformation pattern of the area the traces of the palaeoshorelines are projected on a ENE-WSW striking vertical plane, parallel to the present shoreline (A-A' in Fig. 2), extending for about 30 km from Capo Vaticano to Pizzo. In this projection (Fig. 5), the palaeoshorelines of Terraces II to VII display increasing elevations from ENE to WSW, with a geometry suggesting tilting to the ENE.

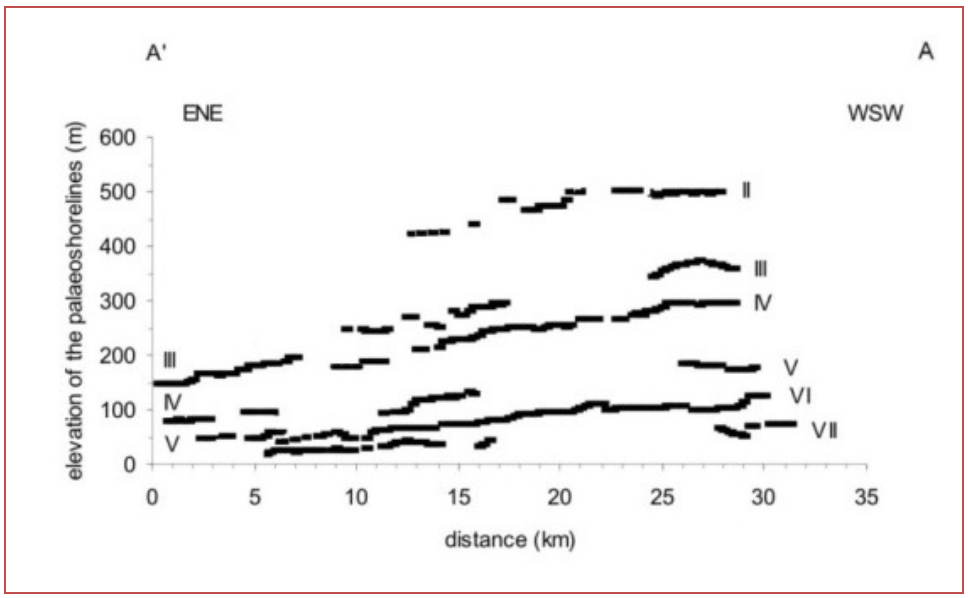

Fig. 5 - Vertically projected profiles, on ENE-WSW direction (A-A' in Fig. 2), of the palaeoshoreline elevations (from Tortorici et al., 2003, modified).

Taking into account the structural setting of the area, the north-eastward tilting of the Capo Vaticano peninsula (Fig. 1) can be related to its structural framework. In fact, it consists of a Late Quaternary relay ramp (Gawthorpe and Hurst, 1993), bounded to the south-east by the Vibo fault, to the north-west by the Tropea fault

and offshore faults, while to the south it is truncated by the Coccorino and Nicotera faults (Fig. 6). The geometry of the palaeoshorelines indicates that the uplift process has been characterized by uplift rates increasing towards the southwest.

For example, in the Vibo marina area, located on the hanging-wall of the Vibo Fault (Fig. 2), the palaeoshoreline of the Terrace III, IV and V are located at elevations of 150, 75 and 50 m a.s.l., respectively, indicating an average uplift rate (corrected for the palaeo-sea level, see Table 1) of 0.64 mm/yr in the last 200 ka.

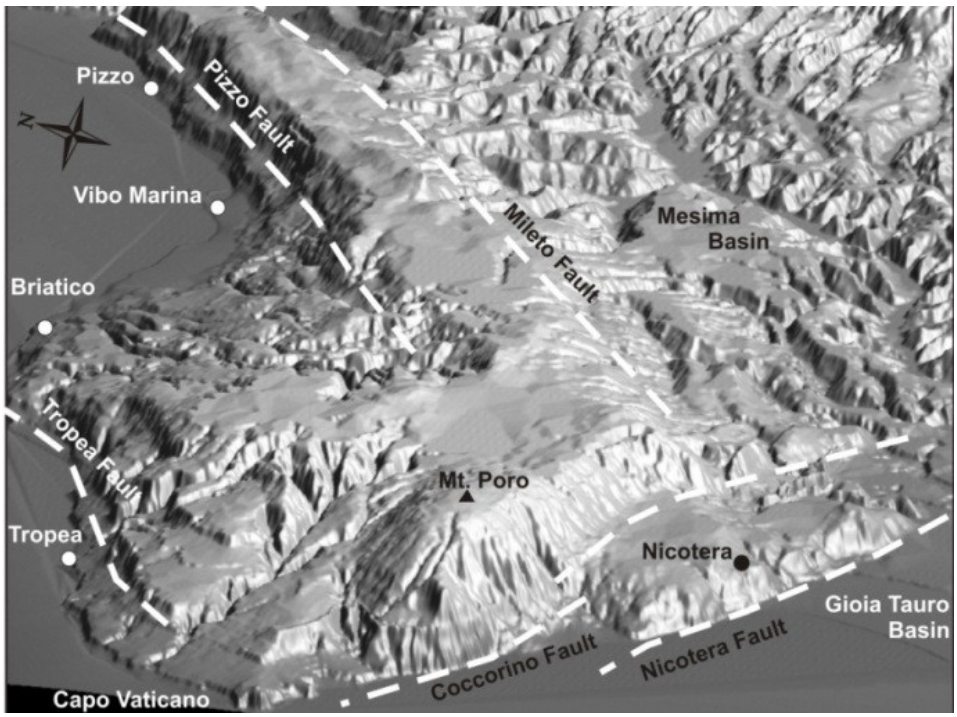

Fig. 6 - View from south-west of the Capo Vaticano Peninsula by a 3D prospective projection mode of DEM (ER –Mapper software elaboration); the area can be interpreted as a northeast-dipping relay ramp (Gawthorpe and Hurst, 1993) between the Pizzo and Tropea faults.

To the southwest, in the Capo Vaticano area at the footwall of the Coccorino Fault, the same palaeoshorelines are located at elevations of 370, 285 and 175 m

a.s.l., respectively, indicating an average uplift rate of ~2.0 mm/yr in the same period. The overall deformation pattern, also characterized by short-term accelerations and decelerations in uplift-rates (see Tortorici et al., 2003 for a more complete discussion), confirms the occurrence of an important tectonic component in the total amount of uplift, related to the Late Quaternary activity of the normal fault segments bounding the Capo Vaticano structural high that caused the tilting of the peninsula. On the other hand, the hanging-wall blocks affected by tectonic subsidence are certainly characterized by uplift-rates lower than the regional component of uplift in the overall amount of vertical movement. Actually, as regards the Calabrian Arc, several authors (Hearty et al., 1986; Westaway, 1993; Miyauchi et al., 1994) indicate a continuous, large-scale process of regional uplift since the Early Pleistocene at mean rates of ~1 mm/yr.

3.6 CONCLUSIONS

Absolute dating of Middle-Upper Pleistocene marine sediments by OSL methodology yielded new constraints for correlating the seven orders of coastal terraces exposed in the Capo Vaticano peninsula with the last Quaternary interglacial stages. In fact, the distinct coastal terraces can be correlated with the last seven major high-stands of the global eustatic curve (i.e. MIS 7.5, 7.3, 7.1, 5.5, 5.3, 5.1 and 3.3; see Table 1).

Present elevations of coastal terraces also suggest that this portion of the Calabrian Arc has been affected by a vigorous tectonic uplift during the last 236 ka, locally characterized by rates up to ~2 mm/yr, responsible for the preservation of all coastal terraces related to the entire series of the sea level high-stands. Moreover, the geometry of the palaeoshorelines indicates that the raising process was

characterized by uplift rates increasing toward the southwest, resulting in the tilting of the whole peninsula toward the northeast.

The coastal terracing on the Capo Vaticano peninsula is the result of raising processes of the area, which, as a whole, represents the footwall of both the SW-NE and the WNW-ESE striking offshore normal fault systems, the latter extending also on-land. Consequently, the uplift of the area, started just before 236 ka ago, is due to the combined activity of both regional uplift and faulting.

Table 1 - Elevations of the palaeoshorelines measured in five distinct sections of the Capo Vaticano area (for locations, see Fig. 2). The minimum and maximum elevations of each palaeoshoreline, attribution to distinct MIS and palaeo-sea level correction (from Waelbroek et al., 2002) are also indicated.

Order of terraces	**Palaeoshoreline elevation (m)**		**Palaeoshoreline elevation in different sections (m)**					**Marine Isotopic Stage (MIS)**	**Age (ka)**	**Sea level correction (m)**
	Min.	Max.	Vibo Marina	Briatico	Capo Vaticano	Nicotera	Gioia Tauro basin			
VII	30	75		30	75	40		3.3	60	+ 48
VI	45	135		45	135	75		5.1	81	+ 19
V	50	175	50	100	175	125		5.3	101	+ 21
IV	75	285	75	216	285	175	90	5.5	124	- 6
III	125	370	150	270	370	216	125	7.1	197	+10
II	250	500		440	500	260		7.3	215	+4
I	350	575			575	350		7.5	236	+9

Table 2 - Coordinates and elevations of sampling points.

Terrace	**Sample**	**Gauss-Boaga coordinates**		**Elevation (m)**
		East	**North**	
I	VVA	2613058	4275540	380
I	TA	2601942	4279620	560
II	TC	2599210	4275867	465
III	PA	2618118	4285182	125
V	TB	2599289	4281165	52
VII	NA	2606819	4263555	50

Table 3 - Single-aliquot regenerative-dose (SAR) protocol used in the study (adapted from Murray and Wintle, 2000).

Step	Treatment[a]	Observed[b]
1	Give dose, D_i	-
2	Preheat@220 °C for 10 sec	-
3	OSL@125 °C for 40 sec	L_i
4	Give test dose, D_t	-
5	Heat to 200°C	-
6	OSL@125 °C for 40 sec	T_i
7	Return to 1	-

[a]For the natural sample, i=0, and D_0=0 Gy with corresponding L_n and T_n values.
[b]Li and Ti were derived from the decay curve, taking the first 0.8 s minus a background estimated from the last 3.5 s integral of the OSL signal.

Table 4 - OSL age results of marine terrace sediments in Capo Vaticano area.

Terrace	Sample	K (%)	Th (ppm)	U (ppm)	W (%)	D_β[a] (Gy/ka)	$D_{\gamma+cosm}$[a] (Gy/ka)	AD[b] (Gy/ka)	D_e[c] (Gy)	n[c]	Age (ka) ± 1σ SE
I	VVA	0.27±0.01	1.11±0.05	0.78±0.01	15	0.32±0.02	0.41±0.03	0.63±0.06	136±8	16	214±25
I	TA	0.26±0.01	1.32±0.05	0.84±0.01	16	0.33±0.02	0.42±0.03	0.65±0.06	134±7	14	207±22
II	TC	0.35±0.01	1.27±0.05	0.76±0.01	14	0.38±0.02	0.43±0.03	0.71±0.06	142±9	18	199±21
III	PA	0.30±0.01	1.20±0.05	0.70±0.01	12	0.34±0.02	0.41±0.03	0.67±0.06	123±6	20	184±20
V	TB	0.84±0.01	1.92±0.05	1.12±0.01	10	0.80±0.02	0.62±0.03	1.29±0.06	122±6	15	94±8
VII	NA	0.61±0.01	1.33±0.05	0.73±0.01	11	0.57±0.02	0.50±0.03	0.96±0.06	59±4	16	62±6

[a]Data of radioactive content of K, Th and U obtained from ICP-MS were converted to infinite matrix dose using the conversion factors by Adamiec and Aitken (1998) and contributions from cosmic rays were included using the equations given by Prescott and Hutton (1988, 1994).
[b]The natural annual dose rate AD was calculated using the water content attenuation factor given by Zimmerman (1971) and size attenuation factors of Mejdahl (1979).
[c]D_e values are weighted mean values calculated using the central age model on data from the number n of measured aliquots (Galbraith et al., 1999).

Chapter 4

MIDDLE-LATE PLEISTOCENE MARINE TERRACES AND FAULT ACTIVITY IN THE SANT'AGATA DI MILITELLO COASTAL AREA (NORTH-EASTERN SICILY)

Published on Journal of Geodynamic (2012), Vol. 55, pp. 32-40 (v. Giunta et al., 2012).

4.1 INTRODUCTION

The coastal part of Sant'Agata di Militello (north-eastern Sicily; Fig. 1) is defined by a flight of raised Middle-Upper Pleistocene marine terraces being at different heights with regard to the present sea level. Although marine terraces in this area have been recognized by several authors since the beginning of the last century, their distribution both in space and time, mainly derived by morphological and palaeontological information, are still debated (Hugonie, 1982; Bonfiglio, 1991; Catalano and Di Stefano, 1997; Lentini et al., 2000; Bonfiglio et al., 2010).

References about the age of marine sediments are poor and not supported by numerical data. The only chronological information is related to continental sediments outcropping at Acquedolci (Fig. 2), which contain mammal bones (Hyppopotamus *Pentlandi*) that have been dated 200±40 ka BP by isoleucine epimerization method (Bada et al., 1991). Appropriate age constraints for marine terraces represent a basic tool for accurately evaluating vertical movements of regions affected by Quaternary tectonic uplift.

New absolute OSL age estimates of Pleistocene marine terrace deposits have been obtain. They are located along the Sant'Agata di Militello coastal area, where a complete series, characterized by marine deposits, occurs. In order to frame the sampled deposits within the sequence of marine terraces, a new detailed mapping of the distinct Quaternary terrace surfaces has been carried out on the entire coastal area between Acquedolci and Capo d'Orlando (Fig. 2). Terrace surfaces have been mapped by detailed field work on 1:25.000 and 10.000 scale topographic maps

integrated with analysis of 1:33.000 and 1:10.000 scale aerial photographs and LANDSAT and GOOGLE satellite imageries. Moreover, OSL dating of marine terrace deposits, together with detailed morphostructural analysis of tectonic structures, allowed to reconstruct the tectonic evolution of this coastal area and to constrain the relationships between marine terracing and normal faulting in a precise time range.

4.2 GEOLOGICAL SETTING

The Sant'Agata di Militello coastal area is located along the Tyrrhenian shore of north-eastern Sicily about 100 km west of the Messina town (Fig. 1). The area is part of the southernmost sector of the Calabrian arc. This prominent orogenic domain connects the Southern Apennines and the Sicilian-Maghrebian chain that developed during the Neogene-Quaternary Africa-Europe collision and Ionian slab roll-back (Malinverno and Ryan, 1986; Dewey et al., 1989; Boccaletti et al., 1990).

Since the Pliocene, the contractional processes in the most internal sector of the thrust belt are replaced by strike-slip and extensional faulting that produced a general stretching and the fragmentation into structural highs and marine sedimentary basins (Ghisetti and Vezzani, 1982).

The present-day structural pattern of northern Sicily is the result of the activation, during the Pliocene-Pleistocene, of a complex grid of fractures related to a W-E trending right-lateral regional shear zone which extends from the Pantelleria Rift to the Aeolian Islands (South Tyrrhenian System; Finetti and Del Ben, 1986; see also Boccaletti et al., 1984; Ghisetti and Vezzani, 1984; Giunta et al., 2000; 2002). This latter is characterized by a synthetic system, NW-SE to W-E oriented, characterized by right-lateral and oblique-slip faults, and an antithetic one, N-S to NE-SW oriented, characterized by left-lateral or normal faults. The shear zone

controls the hinge between northern Sicily and southern Tyrrhenian, corresponding to both emerged and submerged northern portion of the Sicilian-Maghrebian chain.

Some of these structures are still active and responsible for the shallow seismicity occurring both inland in northern Sicily and offshore in the Tyrrhenian Sea.

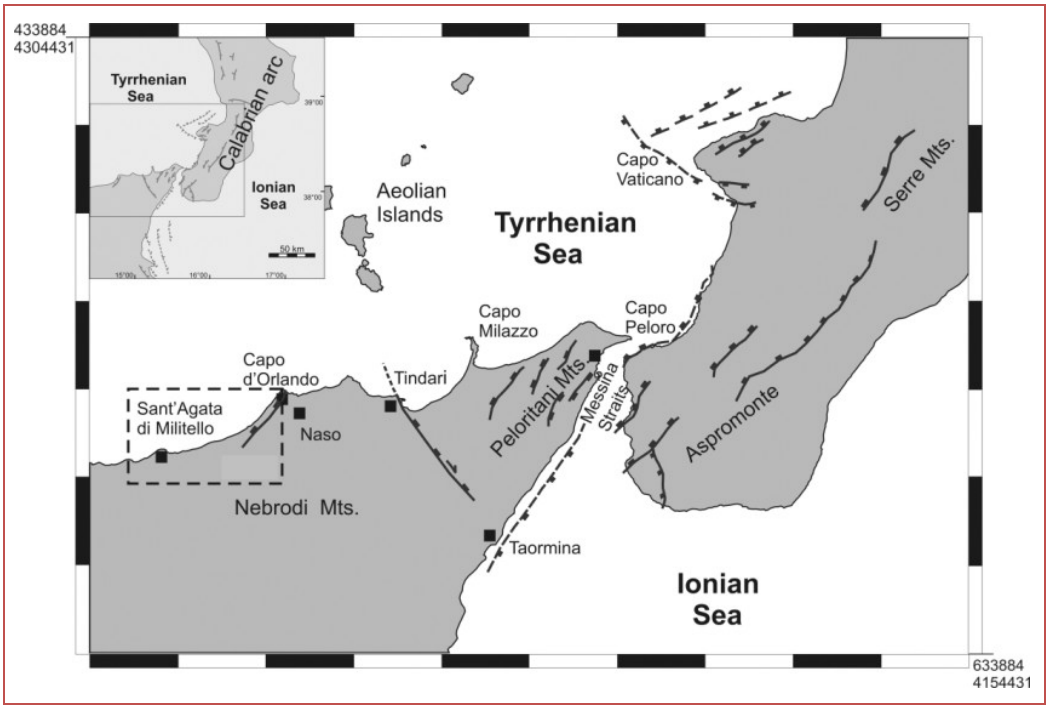

Fig. 1 - Simplified structural map of the southern part of the Calabrian Arc.

Focal mechanisms are mostly characterized by strike-slip and oblique kinematics compatible with low-dip NW-SE to NNW-SSE trending P-axes (Frepoli and Amato, 2000; Pondrelli, et al., 2002, 2004, 2006; Neri et al., 2005; Giunta et al., 2009), roughly consistent with the general convergence direction between the

European and the African plates (Hollenstein et al., 2003; Pepe et al., 2005; Billi et al., 2006; Lavecchia et al., 2007; Ferranti et al., 2008; Mattia et al., 2008).

In north-eastern Sicily and Calabria, the compressive processes along the thrust system and the collapse at the rear of the wedge have been followed by a strong uplift as recorded by flights of Quaternary marine terraces (Dumas et al., 1982; Ghisetti, 1984; Valensise and Pantosti, 1992; Westaway, 1993; Miyauchi et al., 1994; Bianca et al., 1999; Catalano and De Guidi, 2003; Ferranti et al., 2006). In particular, north-eastern Sicily is characterized by a prominent geomorphological marker (Hugonie, 1979; Bonfiglio, 1991; Bonfiglio et al., 2010), represented by a wide polycyclic marine platform located at altitudes between 150-135 m and 60 m a.s.l. and named "Grand Replat" (Hugonie, 1979). This marine feature extends along the Tyrrhenian coast from the Straits of Messina (Capo Peloro) to the west (Acquedolci) and along the Ionian coast to the south (Taormina), over a distance of about 100 km (Fig. 1). The elevation of marine terraces and their offset across the main faults has been used to establish the relative contribution of regional and fault-related sources to uplift. According to Westaway (1993), 1.7 mm/yr of post-Middle Pleistocene uplift of southern Calabria was partitioned into ~1 mm/yr due to regional processes and the remaining to the displacement of major faults.

Different uplift rates have been previously determined by morphological and palaeontological markers. Stratigraphic and morphological correlations with the MIS 5.5 terrace (Gliozzi and Malatesta, 1982) suggest an uplift rate of 0.65 mm/yr in the Tindari promontory, 35 km to the east (Fig. 1) whereas the bones of dated continental mammals found at Acquedolci (Fig. 2), near Sant'Agata di Militello (Bada et al., 1991), and geomorphological correlations allowed to determine lower rates in the Capo d'Orlando area (0.30-0.45 during the last 125 ka; Scicchitano et al., 2011). Longer-term uplift rates are obtained by 0.5-1.0 Ma-old marine deposits

outcropping at about 500 m a.s.l. in the Naso village (Catalano and Di Stefano, 1997), 5 km south-east from the coastline on the footwall of the Capo d'Orlando fault (Fig. 1).

The analysed terrace sequence lies at the hanging-wall and footwall of the Capo d'Orlando fault (Scicchitano et al., 2011). This is a NW-dipping, SW-NE trending, Pleistocene fault, characterized by dip slip normal motion (see inset in Fig. 2).

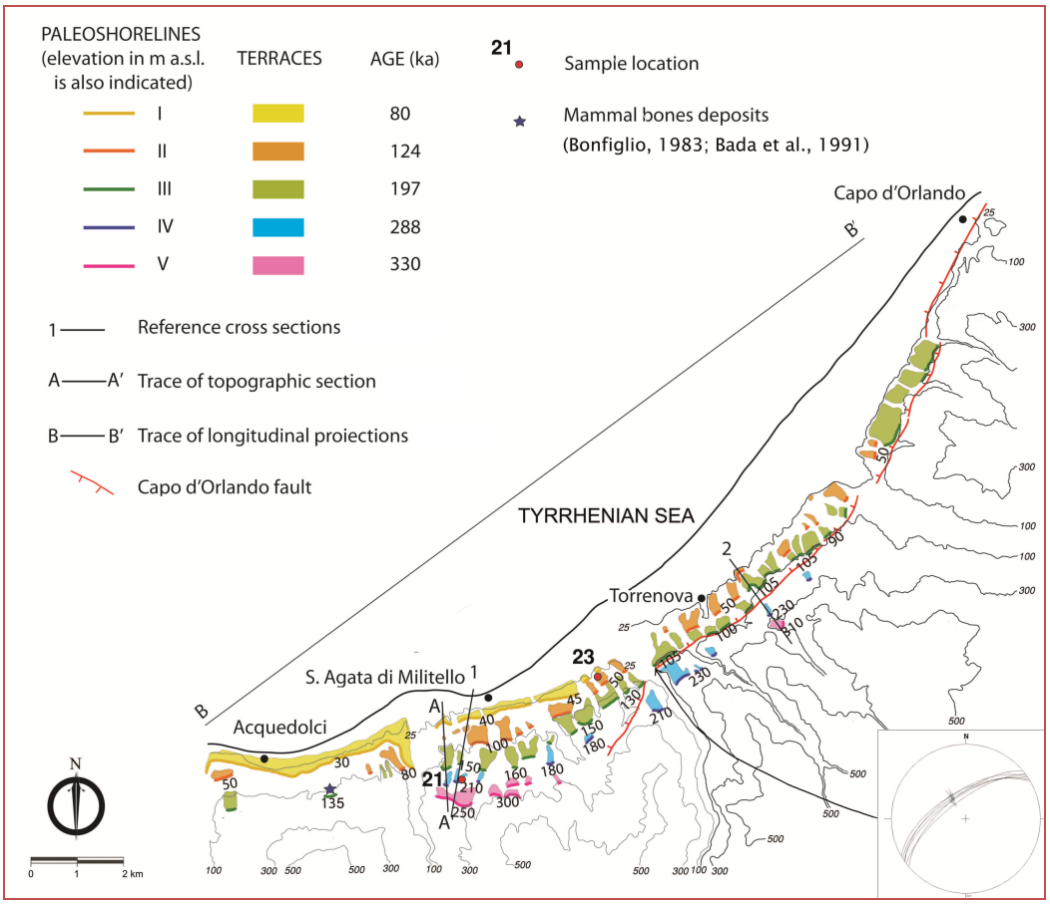

Fig. 2 - Morphotectonic map of the Sant'Agata di Militello coastal area. Lower-hemisphere Schmidt diagram in the inset show projections of Capo d'Orlando fault kinematic data. Arrows on fault planes indicate motion of the hanging-wall block.

This structure, belonging to the South Tyrrhenian System (Finetti and Del Ben, 1986), controlled the geomorphological evolution of the coast between Sant'Agata di Militello and Capo d'Orlando. As a whole, the Capo d'Orlando fault separates the coastal sector, where Pleistocene deltaic marine gravels and sands (the Ghiaie di Messina Fm) overlaid by terraced marine deposits extensively outcrop, from a 400-500 m high mountain front constituted by Mesozoic carbonate successions and/or their Palaeozoic metamorphic basement (Carbone et al., 1998). The footwall is entrenched by large river valleys ("fiumare"), while the hanging-wall is characterized by a shallow drainage network. The cumulative height of the major fault escarpment varies along strike reaching values of 400 m in its central sector.

No morphotectonic evidence of recent activity has been observed along the fault.

In fact, normal faults with Holocene postglacial activity are usually recognizable when affecting hard-rocks because they offset uniform mountain slopes regularized by intense Late Pleistocene cryogenetic processes (see Caputo et al., 2006 and references therein). Such morphological features, that have been commonly used to recognize the latest Quaternary tectonic activity along different fault segments in the Mediterranean area, are missing at the base of the Capo d'Orlando fault scarp.

Nevertheless, poor historical seismicity has been documented, showing a SW-NE alignment of major epicentres (I = VII-IX) on its footwall (Working Group CPTI, 2004).

4.3 MARINE TERRACES ALONG THE SANT'AGATA DI MILITELLO

Along the Sant'Agata di Militello coastal area five orders of marine terraces, showing good overall morphological continuity, have been recognized at elevations between 10 and 300 m a.s.l. (Fig. 2). Their number and distribution are nearly consistent with that recognized in this area by Robillard (1975), Hugonie (1979;

1982) and Scicchitano et al. (2011). They are characterized by wave-cut surfaces carved on Middle Pleistocene deltaic marine gravels and sandy deposits (the Ghiaie di Messina Fm), Mesozoic carbonate successions and/or their Palaeozoic metamorphic basement (Carbone et al., 1998). The marine platforms are overlain by littoral sediments made up of yellow littoral sand and gravels in a sandy matrix, passing upwards to continental alluvial and/or colluvial deposits.

In the following, the distinct terraces will be described from the highest to the lowest. They are bounded landwards by inner edges, sometimes accompanied by *Lithodomus* hole bands and/or other biological sea level markers, that have been mapped with an error margin in elevation of ±5 m depending on erosional and depositional processes following their emergence. This error is negligible in estimating the long-term Quaternary uplift-rates involving time spans of tens to hundreds of thousands of years (Caputo et al., 2010). However, it implies that the elevations of the palaeoshorelines reported in this paper are to be considered as mean values, useful for estimating long-term late Quaternary uplift rates (Table 1).

It is worth noting that the elevation of inner edges changes parallel to the coastline, due to the interaction between regional and local tectonic processes.

Terrace V, the highest and the oldest order of the Middle-Upper Pleistocene marine terraced sequence, mainly outcrops in the south-western sector. It is carved on deltaic marine gravels and sandy deposits (the Ghiaie di Messina Fm.) and bordered by an inner edge extending at elevations ranging from 250 to 300 m a.s.l. in the Sant'Agata Militello area (Fig. 2). The widest surface is located south-west of Sant'Agata di Militello. Downslope, in this area, an order of terraces (Terrace IV) additional to those reported by Scicchitano et al. (2011) has been recognized. It is represented by remnants of a narrow platform bounded landward by an inner edge extending at elevations ranging from 180 to 210 m a.s.l., carved on the Ghiaie di

Messina Fm. And on Mesozoic carbonate successions and/or their Palaeozoic metamorphic basement (Fig. 2). To the north-east, on the footwall block of the Capo d'Orlando fault, remnants of platforms related to Terraces V and IV are bounded landward by inner edges reaching elevations of 310 m and 230 m a.s.l., respectively.

Terrace III shows a good morphological continuity, following the present coastline and ranging in elevation from 110 to 160 m a.s.l. in the Acquedolci and Sant'Agata Militello area (Fig. 2). In the north-eastern sector, that is located on the hanging-wall of the Capo d'Orlando fault, the elevation of the inner edges of Terrace III ranges from 90 to 105 m a.s.l., decreasing with respect to the south-western sectors. In the Acquedolci area, the inner margin of this terrace has been recognized at ~135 m a.s.l. at the foot of an ancient calcareous cliff characterized by an alignment of marine caves and of *Lithodomus* holes. Here, a talus deposit accumulated on the edge of an ancient lacustrine basin (Bonfiglio, 1991; Bonfiglio et al., 2010), overlying marine gravels and sands, contains mammal bones (*Hyppopotamus Pentlandi*) that have been previously dated 200±40 ka BP by isoleucine epimerization method (Bada et al., 1991). Assuming that the marine-continental sequence formed during the same marine high-stand (Lajoie, 1986; Bosi et al., 1996), we can reasonably relate this terrace to the MIS 7 (197-236 ka, see Waelbroeck et al., 2002).

Terrace II is a discontinuous and narrow surface, rising in elevation from 50 to 100 m a.s.l. in the south-western sector, where it is carved on the Ghiaie di Messina Fm. (Fig. 2). In the north-eastern sector this surface is carved also on Mesozoic carbonate successions and it is bounded landward by an inner edge occurring at elevations from 50 to 75 m a.s.l. At Rocca Scodonì, near Torrenova, the inner margin of this terrace has been recognized at ~50 m a.s.l. at the foot of an ancient

calcareous cliff characterized by a band of *Lithodomus* holes and other biological remains (see Scicchitano et al., 2011).

Terrace I, the youngest and lowest order of the marine terraced sequence, is represented by a weakly tilted surface visible only in the Acquedolci and Sant'Agata di Militello villages, bordered by an inner edge extending at elevations between 30 and 45 m a.s.l. (Fig. 2). It is carved on the Ghiaie di Messina Fm.

4.4 LUMINESCENCE DATING

4.4.1 SAMPLE COLLECTION AND PREPARATION

In order to obtain new experimental data on the age of the studied terraces, OSL dating methodology is applied to sedimentary deposits. For this purpose, it is possible to collect only two samples (21 and 23, see Fig. 2) from unconsolidated marine sands. OSL dating is applicable to single crystals occurring in sedimentary deposits for which the light-sensitive signal has been removed (zeroed) by sunlight during erosion and transportation of the grain. The OSL measurements thus provide the time since the mineral grains extracted from a sedimentary unit were last exposed to daylight. In our geological context, this time sets the formation of the marine terrace. In particular, sample 21 is collected from sandy levels belonging to the distal portion of the clastic wedge of Terrace IV at elevation of 200 m a.s.l., while sample 23 is collected from yellow shore sands cropping out immediately above the major marine platform of the Terrace II at an elevation of 50 m a.s.l. (for samples location see Fig. 2). Other terraces are inaccessible, because of extensive and intensive coastal building.

For sampling, after cleaning the wall of the exposed terrace, a PVC tube with a diameter of 10 cm and length of 60 cm is pushed horizontally into the sediments.

Immediately after coring, the sampling tubes are sealed at both ends and stored so as to avoid any accidental light exposure and possible mixing of collected materials. Under controlled lighting, aliquots of coarse grained (200-212 µm) fraction are obtained (section 2.6).

Luminescence measurements are performed, for each sample, on 35 small aliquots of diameter equal to 9.7 mm (Duller, 2008) composed of quartz grains within the selected size range, deposited in a monolayer onto stainless-steel discs, coated with silicon spray using standard protocol of the PH3DRA laboratory.

4.4.2 MEASUREMENTS AND RESULTS

All measurements are made using a semi-automated Risø reader TL-DA-15 with EMI 9235QA photomultiplier (Bøtter-Jensen, 1997; Bøtter-Jensen et al., 2000); for detailed parameters see Appendix A).

The feldspar contamination was checked using IR stimulation choosing randomly some aliquots of each sample (Choi et al., 2009). Considering that no contamination was detected, the remaining aliquots are used for further experiments and dating. The natural dose (or rather its equivalent in the laboratory - the equivalent dose D_e) of each sample is determined using the SAR protocol of Murray and Wintle (2000; 2003), using a preheat of 10 s at 220°C and a cut heat at 200°C.

Preheat temperature is based on the results of preheat plateau test which shows the D_e to be independent of preheat temperature in the range 200-240 °C (Wintle and Murray, 2000). The parameters of SAR are shown in Table 2. The cycle of SAR protocol is repeated 5 times from step 1 using regeneration doses D_i increasing from 125 to 225 Gy in 25 Gy intervals for sample 21, and from 25 to 125 Gy in 25 Gy intervals for sample 23. The value of dose test D_t is respectively of 20 Gy for the first sample and 10 Gy for the second one. The integral signal of the first 0.8 s is

used as OSL intensity, after subtraction of the background calculated from the last 4 s. An example of OSL emission curves, for sample 23, is shown in Fig. 3a.

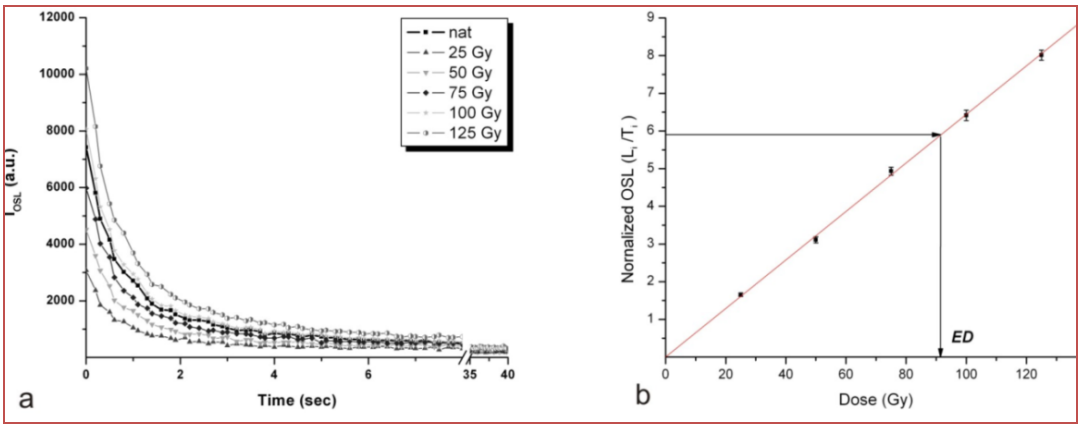

Fig. 3 - a) OSL decay curves of sample 23 for different regenerative doses. b) Regenerated growth curve for quartz extracted from sample 23. OSL was corrected for sensitivity changes and D_e was obtained from interpolation.

The D_e is estimated by interpolation of the ratio L_n/T_n, derived from the luminescence natural curve and associated test, onto the sensitivity corrected growth curve (Fig. 3b). The uncertainty associated to D_e value of each aliquot includes counting errors, the fit and the source calibration errors. We used the central age model (Fig. 4) to calculate the weighted mean D_e (Galbraith et al., 1999; Bøtter-Jensen et al., 2003). In a radial plot, each D_e value of each aliquot is plotted as an individual point on the graph. The position on the x-axis is a measure of the precision with which D_e is known. This axis can also be expressed in terms of the relative error (expressed as a percentage). The value plotted on the y-axis is the number of standard deviations that D_e value lies away from the reference value.

This last value, as shown in Fig. 4, is chosen to be the known given mean D_e of 94±5 Gy. The results obtained from 27 (white circles) of 30 measured aliquots fall within the ±2σ band.

The external part of each sediment was dried, homogenised, ground to a fine powder and sent to Actlabs Laboratory for Inductively Coupled Plasma Mass Spectrometry (ICP/MS) measurements for determination of U, Th, K and Rb concentrations (Preusser and Kasper, 2001). For determination of annual dose are used conversion factors by Adamiec and Aitken (1998).

Beta (D_β) dose rate was weighted by attenuation factors depending on grain size (Mejdahl, 1979). The contribution of cosmic radiation to the total dose-rate was calculated following Prescott and Hutton (1988, 1994) considering the density and the present depth of the sample below the surface.

The values of moisture-corrected dose-rates were obtained considering the water content at the moment of sampling using the attenuation factors given by Zimmerman and Huxtable (1971). A summary of average equivalent doses, dose rates and resulting OSL luminescence ages is reported in Table 3.

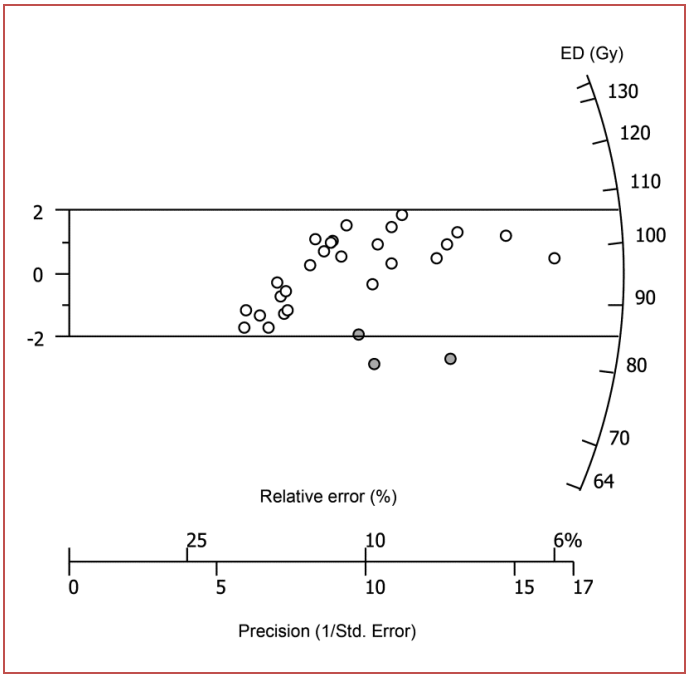

Fig. 4 - Radial plot for the same values obtained by applying SAR to aliquots of multiple grains of sand from sample 23.

4.5 AGE RESULTS, CORRELATIONS AND DEFORMATION PATTERN

The OSL ages measured on the marine sediments sampled along the Sant'Agata Militello coastal area are consistent with the normal evolutionary model of a terraced sequence, moving from the highest to the lowest elevations (Westaway, 1993; Armijo et al., 1996; Bosi et al., 1996; Bianca et al., 1999; Caputo et al., 2010). These determinations provide some new chronological constraints useful to correlate the sequence of sampled terraces with the last main MIS of the global eustatic curve. In particular, the OSL ages of 283±22 ka and 118±7 ka, respectively, obtained for samples 21 and 23, suggest the correlation of Terrace IV and II to MIS 8.5 (288 ka) and 5.5 (124 ka) respectively (Tabs. 1, 3). It is worth noting that the OSL dating of Terrace II is in perfect agreement with the attribution of this terrace

to MIS 5.5 suggested by Scicchitano et al. (2011), based on geomorphological correlation.

Taking into account that the altimetric position of terraces change along the coastal area in correspondence of the Capo d'Orlando fault, different values of uplift rates can be obtained. In the south-western sector, where the fault does not occur (see topographic section A-A' in Fig. 2), quasi-constant values of uplift rate can be estimated for the last 288 ka: taking into account the inner edge elevation of the terraces IV and II and the sea level correction for the MIS 8.5 and 5.5 (Table 1; Waelbroeck et al., 2002), the correlation suggest an uplift rate of ~0.8 mm/year. By modifying the eustatic curve for this value, a good correlation between the sequence of terraces and the global eustatic curve can be reasonably proposed (see Fig. 5).

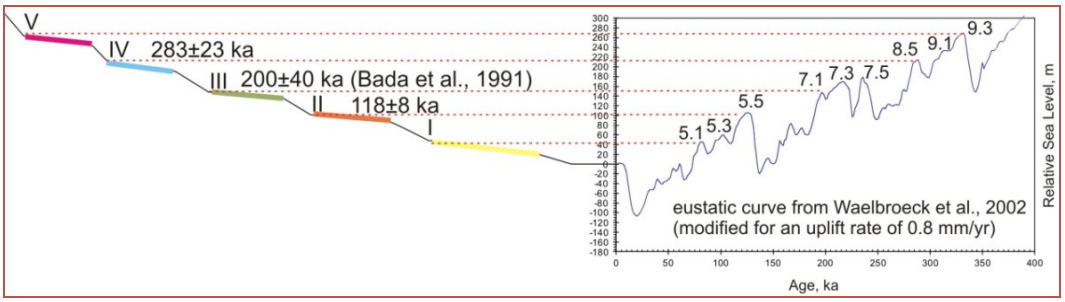

Fig. 5 - Correlation between the different sequences of sampled terraces (topographic section A-A' in Fig. 2) and the last major MIS of the global eustatic curve, obtained by modifying the eustatic curve with an uplift rate of 0.8 mm/yr.

Terrace I can be correlated to MIS 5.1 (80 ka), Terrace III to MIS 7.1 (197 ka), refining the palaeontologically-based age of Bada et al. (1991), and Terrace V to MIS 9.3 (330 ka). It is worth noting the lack of MIS 5.3, 7.3 and 7.5 terraces: depending on low uplift rates and on the clastic lithology of the substratum, they are probably removed by coastal erosion during the subsequent MIS 5.1 and 7.1,

respectively, since the relative sea level reached similar elevations (see Fig. 5). The occurrence of marine terraces both on the hanging-wall and the footwall of the northwest-dipping Capo d'Orlando fault, and the variability of the altimetric distribution of the marine terraces and palaeoshorelines suggest an important tectonic component in the uplifting of the area that is mainly related to Middle-Upper Pleistocene deformation. Actually, the complete sequence of marine terraces outcrops only in the area of Sant'Agata di Militello where the fault disappears.

Towards the north-east, the terraced sequence is incomplete and the elevation of the inner edges changes probably due to the fault activity. In order to better understand the deformation pattern of the area, a SW-NE longitudinal profile, parallel to the present shoreline (B-B' in Fig.2) and extending for about 20 km from Acquedolci to Capo d'Orlando, has been drawn. This profile (Fig. 6) shows an elevation decrease of the of the inner edges of Terraces II and III (the youngest terraces) from SW to NE. This geometry suggests a tilting toward the north-eastern sector, that is located on the hanging-wall of the fault. On the contrary, the elevation of the inner edges of Terraces IV and V (the oldest terraces) increases from the south-western to the north-eastern sector, that is located on the footwall of the fault, with a geometry suggesting a tilting toward the south-west. As a matter of fact, from the SW to the NE, the palaeoshorelines are characterized by convergent geometry on the hanging-wall and a divergent geometry on the footwall of the Capo d'Orlando fault. This pattern indicates that the eustatic and the local tectonic processes were coeval, suggesting that the Capo d'Orlando fault was active during the Middle-Late Pleistocene.

In order to quantify the uplift rates along the coast and to define their short-term variations, the velocity diagrams along two sections have been carried out. The elevation of the inner edges of the terraces I-V have been corrected for the original

sea level of the corresponding high-stands defined by the reference eustatic curve (Waelbroeck et al., 2002). In the south-western sector (between Acquedolci and Sant'Agata di Militello), which is not affected by faulting, a quasi-constant value of uplift-rate (0.74-0.81 mm/yr) during the last 330 ka can be estimated (see section 1 in Fig. 7).

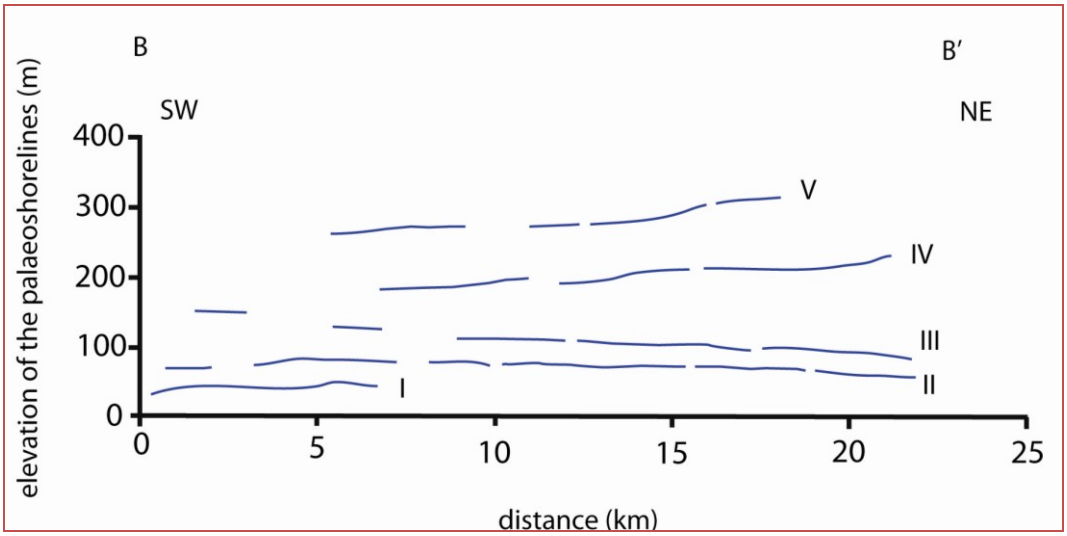

Fig. 6 - Vertically projected profiles of the palaeoshoreline elevations, on SW-NE direction (B-B' in Fig. 2).

In the north-eastern sector (between Sant'Agata di Militello and Capo d'Orlando) the uplift-rate is not constant, probably due to the fault activity. By comparing the uplift rates along the section 2 (Fig. 7), crossing the Capo d'Orlando fault, and the section 1, it is possible to observe that Terraces II and III, laying on the hanging-wall of the Capo d'Orlando fault, raised at a slower rate (0.35 and 0.58 mm/yr, respectively) than the same terraces located in the south-western sector. In the same way, the terraces IV and V, laying on the footwall, raised at a faster rate (0.86 and 0.92 mm/yr, respectively) than the same terraces to the south-west.

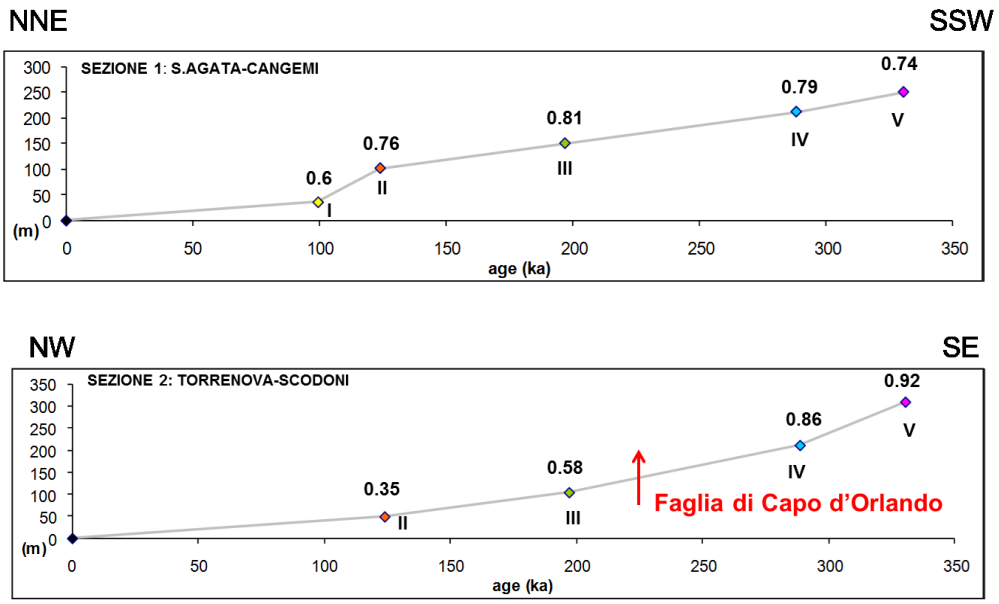

Fig. 7 - Uplift rates (mm/yr) along the Sant'Agata di Militello and Torrenova sections (1 and 2 in Fig. 2), located in the sector where the Capo d'Orlando fault does not occur, and where the fault occurs, respectively. Uplift rates have been calculated for the last 330 ka by fitting the elevations of the distinct palaeoshorelines corrected for sea-level changes according to the curve proposed by Waelbroek et al. (2002).

Assuming that i) the fault was active at least since 288 ka ago, ii) the footwall raised at constant rates of 0.86 mm/yr since that period and iii) the hanging-wall raised at rates ranging between 0.58 and 0.35 mm/yr since 197 ka ago, we can tentatively estimate the vertical throw-rate of the fault during the last 197 ka that is 0.28-0.51 mm/yr. Moreover, the estimated uplift rates are consistent with data from literature which suggest values of 0.30-0.45 during the last 125 ka for the area located at the hanging-wall of the Capo d'Orlando fault (Scicchitano et al., 2011) and values of about 1.0 mm/yr during the last million years for the area located at the footwall (Catalano and Di Stefano, 1997).

The morphological analysis of the marine terraces and the deformation pattern confirm the occurrence of an important tectonic component in the total amount of

uplift, which is related to the Middle-Upper Pleistocene activity of the Capo d'Orlando fault. The absence of fresh scarps at the base of the major escarpment and the poor historical seismicity indicate that the fault was probably not active during the Holocene. This is also confirmed by the short-term uplift rate estimated by an archaeological marker recently found in the harbour of Capo d'Orlando, located at the footwall of the fault (~0.3 mm/yr, Scicchitano et al., 2011).

4.6 CONCLUSIONS

The morphotectonic analysis of the Sant'Agata di Militello coastal area allowed us to recognize at least five main orders of well-preserved Quaternary surfaces and relative deposits, partially affected by a Pleistocene northwest-dipping normal fault, named Capo d'Orlando fault, that controlled the geomorphologic evolution of the north-eastern sector of the analysed coastal area. OSL age determinations of Pleistocene marine terrace deposits provided new constraints for correlating the five orders of marine terrace with five of the last major high-stands of the global eustatic curve (i.e. MIS 9.1, 8.5, 7.1, 5.5, 5.1). The analysis highlights a mean uplift rate of 0.8 mm/yr during the last 330 ka in the south-western sector; on the contrary, in the north-eastern sector, the uplift was characterized by larger rates for the oldest orders (up to 0.92 mm/yr) and lower ones for the youngest orders (down to 0.35 mm/yr), due to the fault activity.

The geometry of the palaeoshorelines and the uplift rates indicate that the eustatic and the local tectonic processes were coeval, suggesting the activity of the Capo d'Orlando fault during the Middle-Late Pleistocene. The morphological features and the historical seismicity suggest that the fault is probably inactive.

However, new OSL age determinations have been scheduled to better constrain the terrace stratigraphy and morphotectonic investigations to better verify the activity of the fault during the Holocene.

Table 1 - Mean elevation of the palaeoshorelines, their possible correlation to distinct MIS, age, and palaeo-sea level correction.

Order of terraces	Elevation of inner edge (m) in the SW sector	Elevation of inner edge (m) in the NE sector	MIS	ka	Sea level correction (m)
V	250-300	310	9.3	330	+4.6
IV	180-210	230	8.5	288	-16.8
III	110-160	90-105	7.1	197	-9.6
II	50-100	50-75	5.5	124	+6.3
I	30-45		5.1	80	-19.7

Table 2 - Parameters of SAR sequence used in the study (adapted from Murray and Wintle, 2000).

Step	Treatment [a]	Observed [b]
1	Give dose, D_i	-
2	Preheat@220 °C for 10 sec	-
3	OSL@125 °C for 40 sec	L_i
4	Give test dose, D_t	-
5	Heat to 200°C	-
6	OSL@125 °C for 40 sec	T_i
7	Return to 1	-

[a] For the natural sample, i=0, and D_0=0 Gy with corresponding L_n and T_n values.
[b] L_i and Ti were derived from the decay curve, taking the first 0.8 s minus a background estimated from the last 4 s integral of the OSL signal.

Table 3 - Summary of average equivalent doses, dose rates and resulting OSL luminescence ages for samples 21 and 23.

Sample	**U (ppm)**	**Th (ppm)**	**K (%)**	***D_e*** **(Gy)**	**D_β, (Gy/ka)**	**D_γ, (Gy/ka)**	**Total dose-rate (Gy/ka)**	**Age (ka)**
21	0,78±0,02	1,11±0,03	0,43±0,01	176±13	0,30±0,01	0,32±0,01	0,62±0,02	283±22
23	0,84±0,02	1,33±0,04	0,75±0,02	94±5	0,44±0,01	0,36±0,01	0,80±0,02	118±7

DETAILS..

Chapter 5

OSL CHRONOLOGY OF QUATERNARY TERRACED DEPOSITS OUTCROPPING BETWEEN MT. ETNA VOLCANO AND THE CATANIA PLAIN (SICILY, SOUTHERN ITALY)

Submitted to Physics and Chemistry of the Earth, in review (v. Ristuccia et al., submitted)

5.1 INTRODUCTION

The Ionian coastal sector of central-eastern Sicily (southern Italy), due to its peculiar geodynamic setting, is affected by tectonic uplift, with long-term rates in the order of 0.5-1.0 mm/yr (Bianca et al., 1999; Monaco et al., 2002; Di Stefano and Branca, 2002). Geometry and distribution of terraces, in relation to the age of their formation, provides useful information concerning regional and local tectonic processes coupled with sea-level changes.

In this area, distinct orders of fluvial-coastal terraces have been surveyed, distributed within an altitude range comprised between 330 and 25 m above sea level (a.s.l.), which testify as many relative sea-level stands (Monaco, 1997; Monaco et al., 2002; Catalano et al., 2004). Moreover, Monaco (1997) and Monaco et al. (2002) tried an indirect dating of the distinct terraces through the chronological attribution of volcanic clasts included in conglomeratic levels, whose petrologic features depends on the volcanic stage, previously dated through potassium-argon method by Gillot et al. (1994), after which they were involved in the sedimentary processes.

In this chapter, it is preliminarily tested the applicability of the Optically Stimulated Luminescence (OSL) technique (Aitken, 1998) through Single-Aliquot Regenerative-dose (SAR) protocol (Murray and Wintle, 2003) on single grain quartz extracted from alluvial-coastal sediments (Olley et al., 1999, 2004), collected from the area of interest. The optimum conditions for measuring equivalent dose (D_e) values of the samples are then examined and, lastly, OSL ages are presented.

The correlation of the terraces, mapped through field work and aerial photographs analysis (1:33.000 and 1:10.000 scales) and dated by OSL methodology, with the different MIS has allowed to carry out a detailed reconstruction of the tectonic process affecting the area and its evolution through time.

5.2 GEOLOGICAL SETTING

The study has been focused on a sector falling between the southern edge of the M. Etna volcanic edifice and the Catania Plain (eastern Sicily), known as the "Terreforti Hills", a belt of up to 325 m high hills constituted by an Upper Pliocene to Quaternary sedimentary succession with volcanic intercalations. The study area (Fig. 1) represents the external-most termination of the Sicilian orogenic front ("Apenninic-Maghrebian Chain" Auct.) overthrusting the Hyblean foreland domain, as response to the continental collision between the African and the European margins (Lentini, 1982; Labaume et al., 1990). In such a geodynamic context, the Catania Plain represents a foredeep sector, filled by Pliocene-Pleistocene sediments and volcanics, and by the Holocene alluvial-coastal deposits of the Simeto River (Longhitano and Colella, 2003). The sedimentary succession of the Terreforti Hills forms an asymmetric south-facing anticline, about 10 km long and ~E-W trending (the Terreforti anticline). It has been interpreted as a thrust propagation fold at the front of the orogenic system (Monaco et al.,1997; Labaume et al., 1990), related to the lately migration of the orogenic thrust front, as a response to the regional N-S compressive tectonic regime (Mattia et al., 2011; Palano et al., 2012). Contractional structures coexist with extensional tectonics, as suggested by the occurrence of a NNW-SSE striking oblique (normal-dextral) fault system running offshore, parallel to the Ionian coast, where it has reactivated the Malta Escarpment since the Middle

Pleistocene (Bianca et al. 1999; Monaco and Tortorici 2000, 2007; Palano et al., 2012).

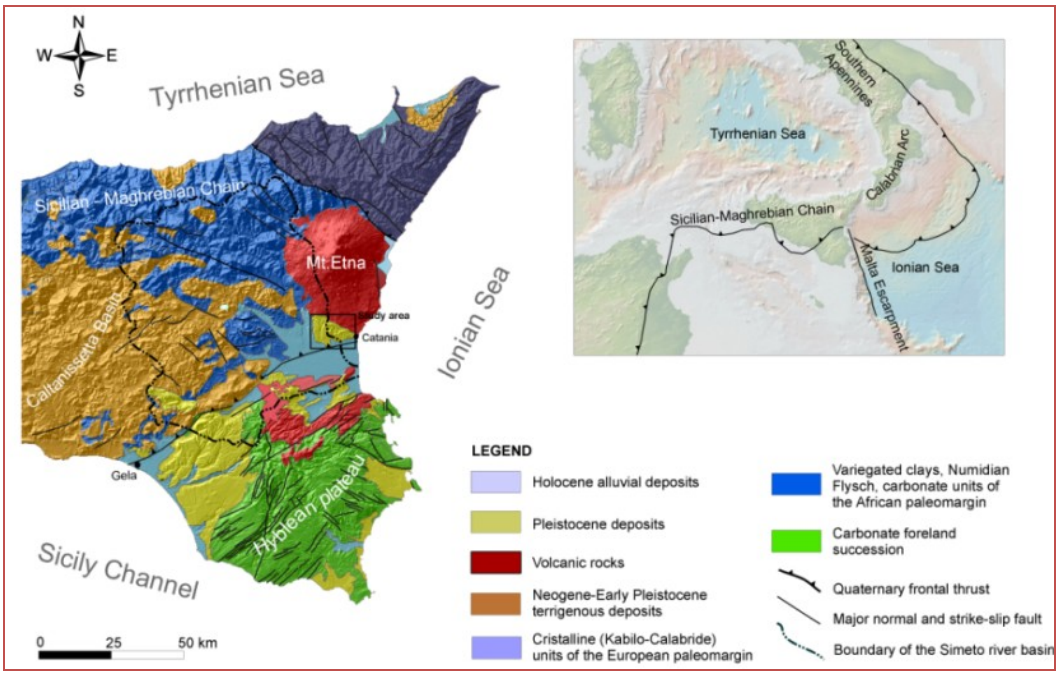

Fig. 1 – Location of the study area in the framework of the Central Mediterranean and Eastern Sicily.

Since the Middle Pleistocene rifting processes have gave rise to a vigorous tectonic uplift affecting the overall orogenic belt of eastern Sicily with rates, progressively decreasing southwards, where values of about 0.5 mm/yr have been detected (Bordoni and Valensise, 1999; Ferranti et al., 2006). Recently, a Holocene regional uplift, with rates of about 1 mm/yr, has been estimated in the Catania Plain area (Spampinato et al., 2012). Uplift process, combined with relative sea-level change, has caused the terracing of fluvial and coastal deposits of the Catania Plain (Monaco, 1997; Monaco et al., 2002). Current tectonic activity is also responsible

for destructive historical earthquakes (M≥7) which characterize this area (e.g. 1169 AD, 1693 AD events, Baratta, 1901; Postpischl, 1985; Boschi et al., 1995).

5.3 STRATIGRAPHICAL AND GEOMORPHOLOGICAL FEATURES

The present study focuses on the dating of terraced deposits outcropping in the area between Mt. Etna volcano and the Catania Plain (Fig. 2a). The outcropping sedimentary succession is represented by a coarsening upward sequence, evolving from open-sea to transitional and continental environment. According to a recent subdivision (Longhitano and Colella, 2003) these sediments represents four depositional sequences (D1-D4), bounded by regional unconformities. We partially followed that subdivision, because, in our opinion, each described depositional sequence is not exactly the result of a single relative sea-level oscillation. In particular, deposits of the third depositional sequence (D3) gather terraced alluvial to shallow water sediments belonging to several orders and relatable to distinct sea-level stands. For this reason, awaiting for a revision of the stratigraphic features of the Catania Plain, we prefer to indicate the distinct sedimentary intervals as generic "Units", adding the acronym CtF for "Catania Foredeep" (CtF_U1 to CtF_U4) (Fig. 2).

The oldest unit (CtF_U1) is represented by marly clays ("pre-Etnean clays", Wezel, 1967) of Early Pleistocene age (Lanzafame et al., 1999; Di Stefano and Branca, 2002), up to 600 m thick, interpreted as the result of steady sedimentation in a pre-Etnean relatively shallow marine gulf (Wezel, 1967; Labaume et al., 1990; Longhitano and Colella, 2003). The marly clays are overlain by gravelly sands (CtF_U2 = "Ghiaie e Sabbie di San Giorgio" Auct.), up to 45 m thick, traditionally

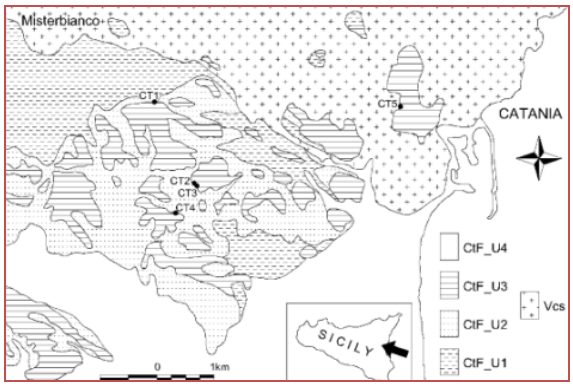

a

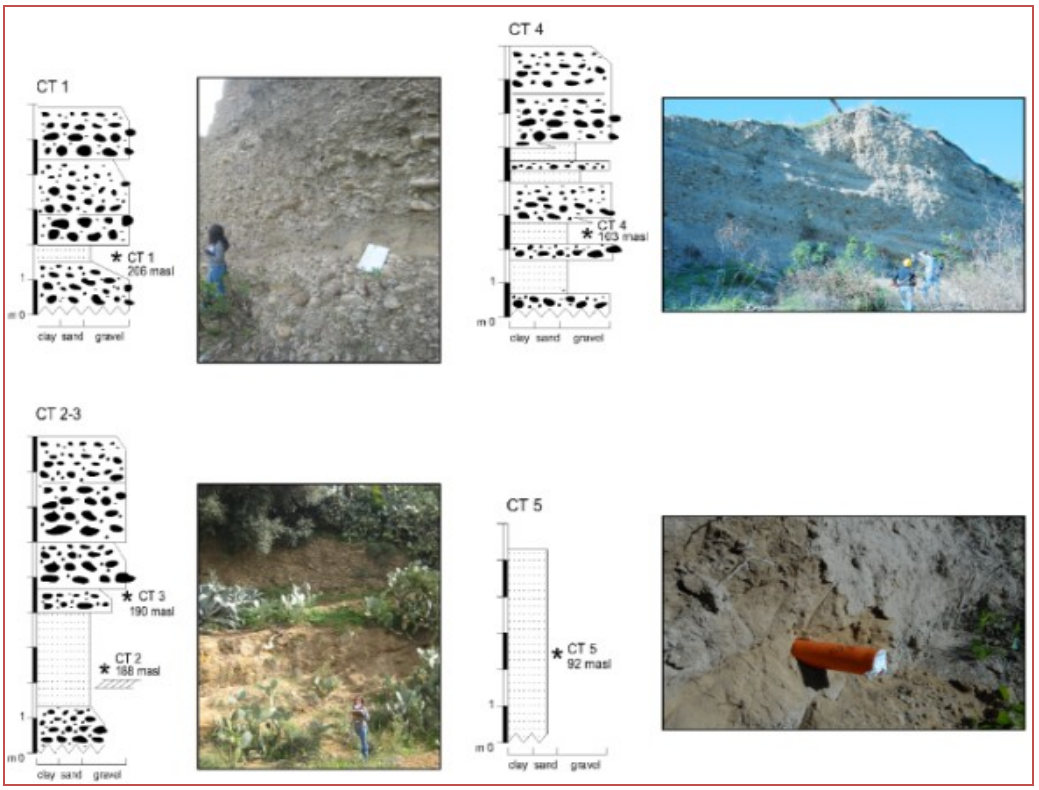

b

Fig. 2 - a) Geological sketch map of the sampled sites. CtF_U1: marly clays (Early Pleistocene); CtF_U2: gravelly sands (Middle Pleistocene); CtF_U3: alluvial to shallow-water polygenic conglomerates and coarse sands (Middle-Late Pleistocene); CtF_U4: alluvial of the Simeto River (Holocene); Vcs: volcanics of the Etna Mt. (Middle Pleistocene-Holocene). b) Location of the collected samples and stratigraphical logs of the sampled outcrops with photographs of the sampled sites.

attributed to Middle Pleistocene, interpreted as the product of coastal shallow marine sedimentation (Longhitano and Colella, 2003). In this area there is evidences of the Etnean fissural early activity (Romano, 1982) represented by products of tholeiitic-transitional affinity (pre-Etnean volcanism). These products, coeval or following the deposition of the CtF_U1 and CtF_U2 are mostly represented by the 320-250 ka old (Gillot et al., 1994) lava plateau outcropping east of Paternò (Fig. 3a). The third depositional sequence (CtF_U3 = "Ghiaie e Conglomerati di Mt. Tiritì" Auct.) includes the sediments object of our research. It is represented by Middle-Late Pleistocene marine shallow-water to alluvial polygenic conglomerates and coarse sands, organized in massive or poorly stratified bodies, up to few tens of meters thick. Sediments of CtF_U3 have been mapped as terraced deposits belonging to seven orders, widespread from Paternò to Catania cities (Fig. 3a). The uplifted marine terraces show a good physical continuity along the west-east direction, especially for the lowest ones (1st to 4th orders), with their corresponding, genetically correlated and coeval fluvial terraces, which are discontinuously preserved in the western sector, along the lower valley slopes of the Simeto river. It is noteworthy the limited extension of the 5th order terraces, restricted to the western sector. The terraces generally show a sub-planar, slightly southward sloping geometry (3°-5°), except for the highest (6th and 7th orders) that seem to be folded (see topographic profiles of Fig. 3b-3c). In particular, the 6th order terrace surface depicts a large anticline displaying an axis coincident with that of the main frontal fold (the Terreforti anticline, Fig. 3a-3d) (see also Monaco, 1997; Monaco et al., 2002). The terrace surfaces are bounded uphill by the inner edge, downhill by the outer edge and laterally by fluvial incisions. The inner edges have been mapped with an error margin in elevation of ±5 m depending on erosional and depositional processes following their emergence.

This error is negligible in estimating the long-term Quaternary uplift-rates involving time spans of tens to hundreds of thousands of years. However, it implies that the elevations of the palaeoshorelines reported in this paper (Table 1) are to be considered as mean values, useful for estimating long-term late Quaternary uplift rates. The inner edge of the 7th order terrace is completely hidden by the 320-250 ka old lava plateau outcropping east of Paternò (Fig. 3a).

The inner edges of the 6th and 5th order terraces can be mapped only in the western sector, the former south-east of Paternò at altitude of 270 m a.s.l., the latter between Paternò and Motta S.A. at altitudes decreasing from 230 to 205 m a.s.l. The inner edges of the 4th , 3rd and 2nd order terraces have been mapped in the whole area at altitudes decreasing from the west to the east, that are 190-150 m, 150-120 m and 95-85 m a.s.l., respectively. Finally, the 1st order surface outcrops both in the western sector, along the Simeto river valley, where it forms a fluvial terrace with inner edges at altitudes decreasing from 150 m to 40 m a.s.l., and along the Ionian onshore, in the Catania urban area, where its inner edge has been mapped at altitudes of 30 m a.s.l.

The younger depositional sequence (CtF_U4) is represented by the Holocene alluvial deposits of the Simeto River, up to 60 m thick, interpreted as the result of Holocene-to Present high-stand sedimentation (Longhitano and Colella, 2003).

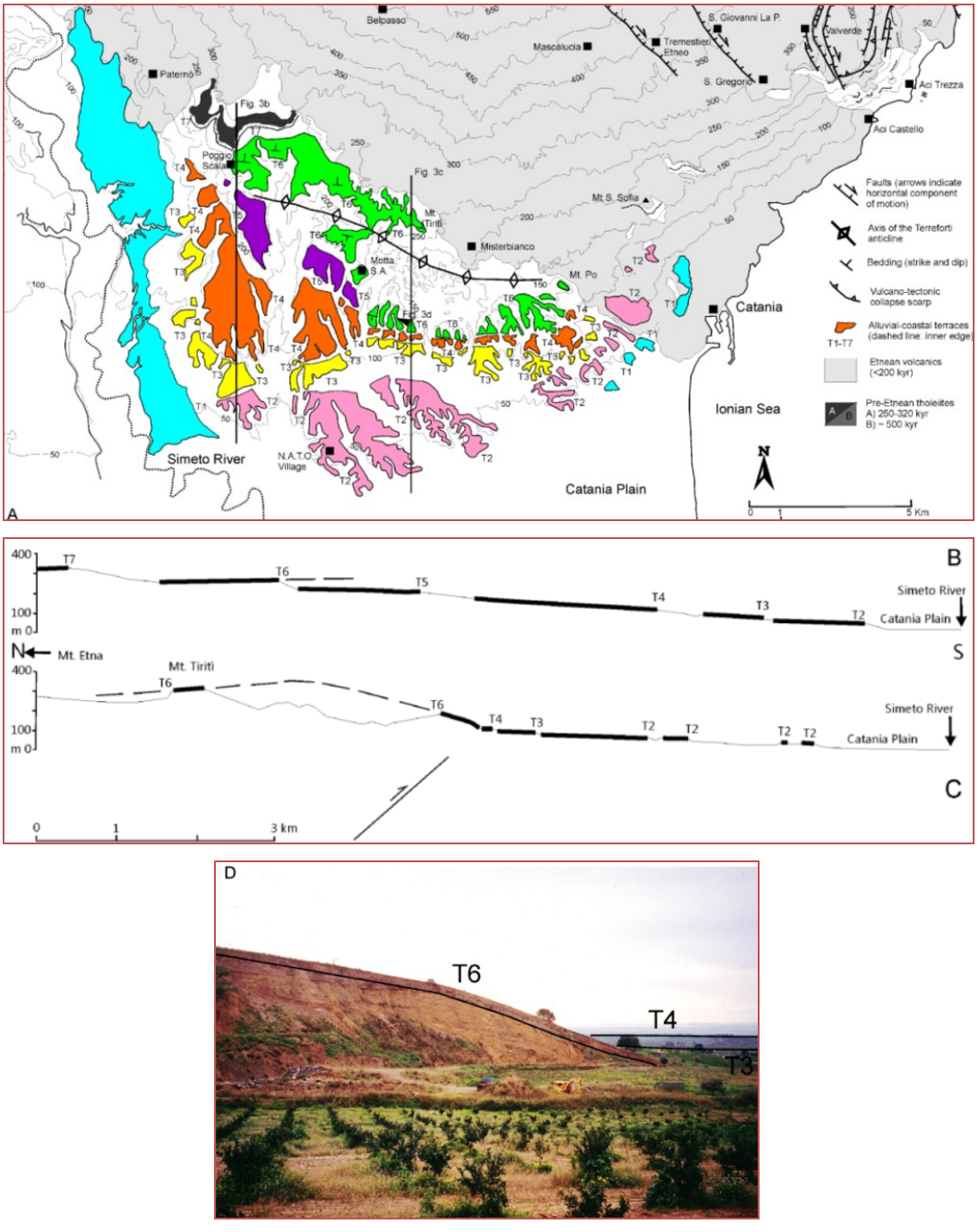

Fig. 3 - a) Map of the terraced deposits. b-c) Profiles across the different orders terraced surfaces. d) Particular of deformed terrace T6.

5.4 OSL DATING

5.4.1 EXPERIMENTAL DETAILS

The horizontal sampling is obtained by hammering opaque PVC pipes (60 cm long cylinder with a diameter of 10 cm; see Fig. 2b), into freshly cleaned vertical geological sections. To prevent light exposure, the tubes are covered and sealed on-site. Five samples (Table 2) have been collected for the OSL analysis located within four different sites (Fig. 2a). Sample CT1, representative of the 6th order terrace, comes from a sandy layer few dm thick, interbedded within massive polygenic conglomerates, poorly graded, up to 6 m thick (Fig. 2b). The stratigraphic succession along which samples CT2 and CT3 are collected (Fig. 2b), is characterized by a lower interval, 1.3 m thick, made up of gravelly sands passing to coarse sands, 2.7 m thick, showing parallel and crossed lamination (CT2), abruptly passing upward to massive conglomerates with rare thin coarse sandy intercalations (CT3) up to 5 meters thick. Both samples are representative of the 4th order terraces.

Samples CT4, representing the 3rd order terraces, is collected from an outcrop about 7 m thick, made up of polygenic conglomerates, interdigitized by coarse sandy layers (Fig. 2b). The last sample (CT5) is representative of the 2nd order terraces, about 4 m thick, made up by homogeneous unstratified thin sands (Fig. 2b).

The preparation of the coarse grain (sand-size) OSL samples is carried out under subdued red light, following standard methodologies. The light-un-exposed sand grains from middle part of the tube are used both for equivalent dose (D_e) estimation and annual dose (AD) measurements. After the preparation at laboratory (see section 2.6), the samples with 180<Ø<212 μm are ready for OSL measurements. It is important to ensure that the feldspar contamination has been

efficiently removed in order to avoid age underestimation (Roberts, 2007). On small aliquots of each sample the purity of quartz is checked by IR diode stimulation (830 nm) method (Mauz and Lang, 2004), and no obvious IRSL (Duller, 2003) is observed from any sample.

The single grains quartz are mounted on discs drilled with a 10×10 array (300 μm wide and 300 μm deep) and for each sample are prepared four discs. In total are middly filled the 60% of the holes of each disc. All the luminescence measurements, beta irradiation and preheat treatments are carried out on a semi-automated Risø TL-DA-15 reader equipped with a calibrated $^{90}Sr/^{90}Y$ beta source, and a single-grains OSL attachment system (Duller, 2003; *in press*). The single-grain quartz is stimulated using a green (532 nm) laser delivering ~45 W/cm^2 (90% power) and stimulated luminescence signal detected in the 280-380 nm region, using an Hoya U-340 optical filter (for parameters see Appendix A).

The modified SAR protocol (Murray and Wintle, 2003) is employed for D_e determination for each grain. In Table 3 the experimental parameters for D_e determination are reported.

Six regenerative beta doses (including a zero dose and a repeated test dose) are used and the corresponding sensitivity-corrected OSL (regenerated OSL signal divided by the subsequent test-dose OSL signal) is used to construct a growth curve.

The value of D_e is estimated by interpolating the sensitivity-corrected natural OSL onto the growth curve. All the OSL signals are measured for 1 sec at a sample temperature of 125°C.

The OSL signals are evaluated taking the first 0.2 sec minus a background estimated from the last 0.3 sec integral of the whole signal to avoid a contribution of the medium and the slow component.

At the end of each measurements cycle, the grains are optically stimulated at 280°C for 1 sec to bleach the remaining OSL signal as much as possible (Wintle and Murray, 2000; Choi et al., 2003; Murray and Wintle, 2003; Kiyak and Canel, 2006), hence to check if there is any thermally transferred charge from light-insensitive traps to the OSL traps. A the end of SAR sequence, the same regeneration dose as the first point of beta irradiation given (50 Gy), is repeated to check whether the sensitivity corrected OSL $(L_R/T_R)/(L_1/T_1)$ is reproducible (recycling ratio R). This value, moreover, identifies the presence of a possible systematic error in the interpolation of L_n/T_n onto the dose-response curves (Roberts, 2006).

On the same grains a recovery test is done. In such a test, a SAR measurement is applied to grains that have been given a laboratory dose after optical bleaching. We expect that the ratio is closed around the unit. For D_e calculation, data are accepted if the recovery test and recycling ratio were within ±10% of unity (Murray and Wintle, 2000; 2003).

The concentrations of uranium, thorium, potassium and rubidium are measured by the Inductively Coupled Plasma mass spectrometry (ICP/MS), performed at Actlabs Laboratory (Ontario, Canada). These radioisotope concentrations are converted to dose rates using the factors of Adamiec and Aitken (1998). Beta (D_β) dose rate is weighted by attenuation factors depending on grain size (Mejdahl, 1979). Considering the assumption of infinite matrix, the gamma dose rate by radioisotope concentrations is compared with in situ gamma measurements by Canberra InSpector 1000 spectrometer, performed with a probe inside the hole of sampling, showing a good agreement.

Cosmic ray contributions are estimated for each sample from the altitude and latitude of the section as well as the thickness and density of the overburden

(Prescott and Hutton, 1988, 1994). The values of moisture-corrected dose-rates are obtained considering the water content at the moment of sampling using the attenuation factors given by Zimmerman and Huxtable (1971).

The OSL ages (Table 4) of the sampled fluvial-coastal sediments are obtained by dividing each D_e (expressed in Gy) with the sample AD (expressed in Gy/ka).

5.4.2 SINGLE GRAIN D_e DISTRIBUTION AND BLEACHING

The shape of the D_e distribution as a histogram (Murray and Olley, 1995; Goedicke, 2003; Saini and Mujtaba, 2010) is the simplest method of displaying the obtained data to evaluate if the sample is well-beached or partial-bleached and the local dosimetry influences. Fig. 4a shows the results obtained for each sample. The individual D_e value is entered into bins of 10 Gy and so the frequency distribution is obtained. In all investigated samples, the scattering of D_e values are rather narrow and symmetrical, displaying approximately normal distribution. In addition, no sample shows a long "tail" towards the upper end of the distribution histogram, indicating sufficient bleaching for the investigated sediments (Fuchs and Owen, 2008).

Considering that histograms take no account of differences in precision associated with individual dose values, the inclusion of relatively imprecise estimates may distort the plot. This could produce incorrect assumption about the true pattern of the dose distribution (Lian et. Al., 2006). A radial plot (Galbraith, 1990; Galbraith et al., 1999) is a more informative graphical means of displaying data with differing precisions, because each dose estimate is plotted together with its measurement uncertainty (expressed as the standard error, found by extending a line vertically to intersect the x-axis; see Fig. 4a). The latter is displayed as both "relative error" and as its reciprocal ("precision"), so that the dose estimates measured with the highest

precision plot farthest to the right. We calculated "true" D_e using the "central age model" (CAM, see Galbraith et al., 1999; 2005). It estimates the weighted-mean equivalent dose for a set of single grains estimates, taking into account the extra spread above and beyond that associated with the measurement uncertainties.

In Fig. 4b all samples showed similar degrees of dispersion within the 15%, except for CT4, which has a higher overdispersion. Most data points cluster around the 2σ-region which is centered at the mean, but a rather low proportion of the grains fall out of this region. This distribution confirms the data obtained by radial plot; is typically present in well-bleached sediments that have not been disturbed since burial (Galbraith, 2005; Bailey et al., 2006; Arnold and Roberts, 2009; Jacobs et al., 2006; Murray et al., 2012). The D_e values obtained are considered for the calculation of OSL ages (Table 4).

5.5 AGE RESULTS, CORRELATIONS AND GEODYNAMIC IMPLICATIONS

Table 4 shows the radionuclide concentrations, dose rates, equivalent doses and OSL ages for all samples. The ages are consistent with the normal evolutionary model of a terraced sequence, moving from the highest to the lowest elevations (Westaway, 1993; Armijo et al., 1996; Bosi et al., 1996; Bianca et al., 1999; Caputo et al., 2010). These determinations provide some new chronological constraints useful to correlate the sequence of sampled terraces (Tables 1, 2, 4) with the last main MIS of the global eustatic curve of Waelbroeck et al. (2002). In particular, the OSL age of 240±12 ka obtained for the sample CT1 suggests the correlation of the 6th order terraces to MIS 7.5 (236 ka); the OSL age of 116±6 and 127±7 ka obtained for samples CT2 and CT3, respectively, suggest the correlation of the 4th order terraces to MIS 5.5 (124 ka); the OSL age of 105±6 ka obtained for the sample CT4 suggests the correlation of the 3rd order terraces to MIS 5.3 (100 ka); finally, the

OSL age of 80±4 ka obtained for the sample CT5 suggests the correlation of the 2nd order terraces to MIS 5.1 (80 ka).

a b

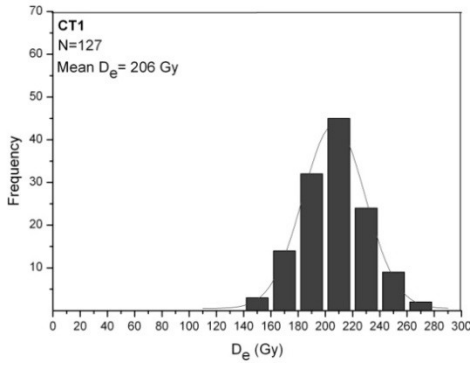

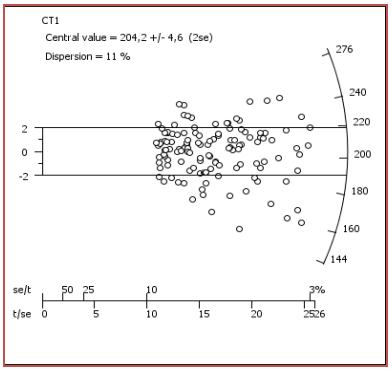

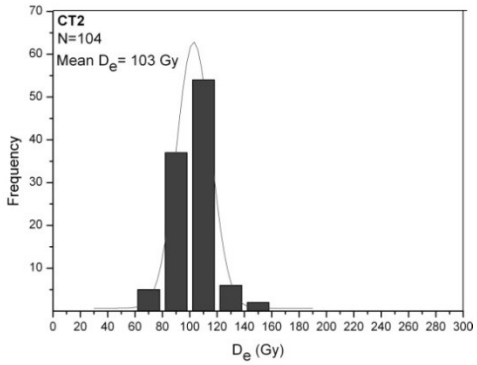

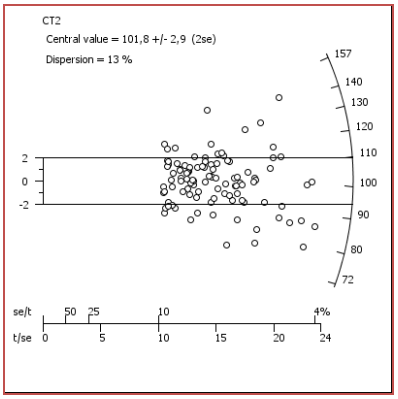

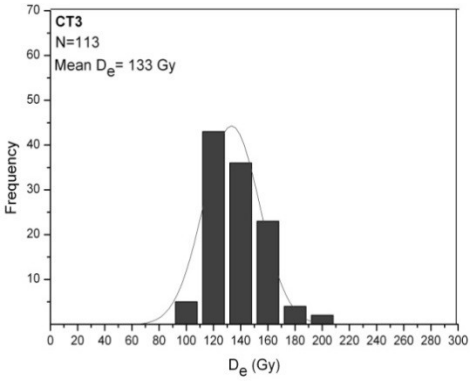

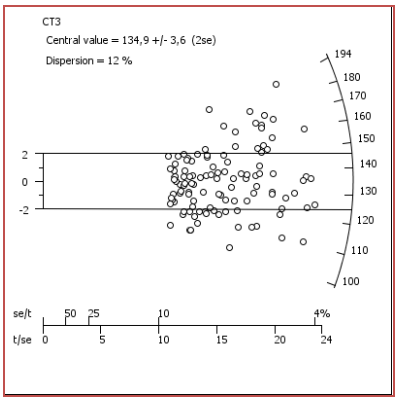

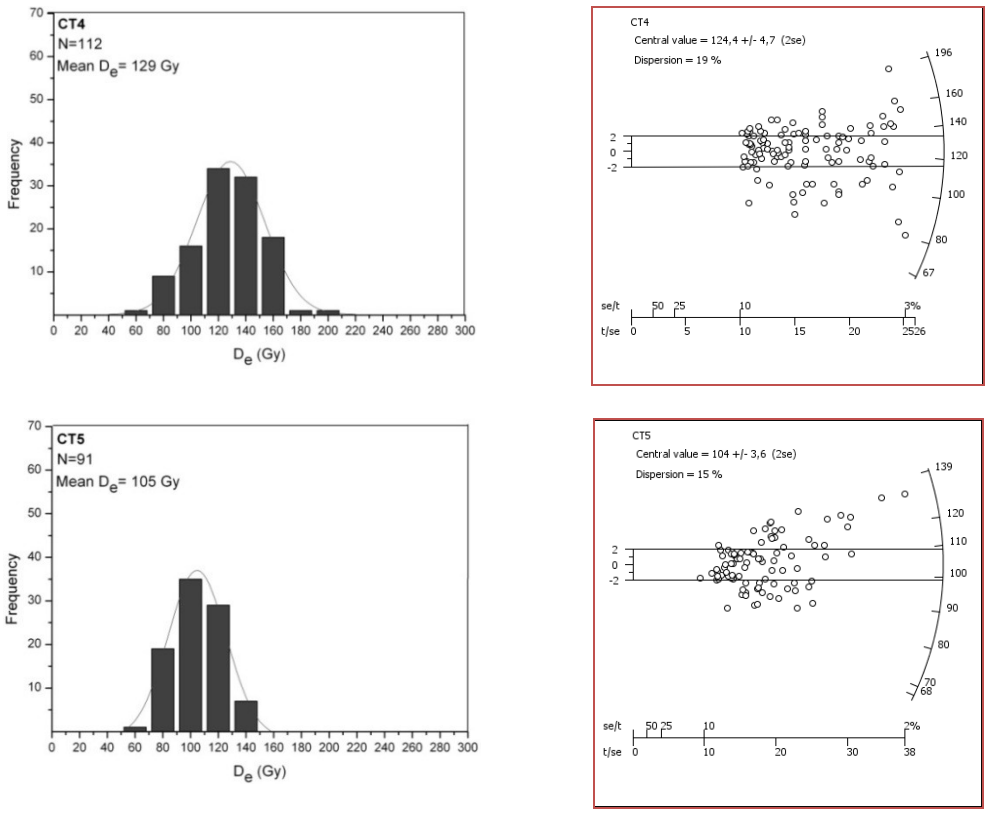

Fig. 4 - Results of the OSL dating on the 180<Ø<212 µm quartz grains. a) Distribution of D_e values in histograms. N represents the total grains number of each sample. b) Radial plots of the measured doses following Galbraith et al. (1990, 1999). Note that more than 80% of single-grain equivalent-dose estimates agrees with the value adopted for age calculation (within 2σ), indicating that the OSL signal of the vast majority of quartz is reset at the time of deposition and burial.

Taking into account that the 7th order terrace should be attributed to the MIS 9.3 (330 ka), being covered by a 320-250 ka old lava plateau (see also Kieffer, 1971 and Monaco et al., 2002), a good correlation between the whole sequence of terraces and the last main MIS of the global eustatic curve can be reasonably achieved (Table 1). In particular, the 5th order terrace could be attributed to the MIS 7.1 (197 ka) and the 1st order terrace to the MIS 3.3 (60 ka).

It is worth noting that the OSL dating of these sediments is in agreement with the attribution suggested by Monaco et al. (2002), based on indirect dating of the distinct terraces through the chronological attribution of volcanic clasts included in conglomeratic levels.

OSL chronology of terraced deposits confirms that central-eastern Sicily has undergone uplifting during the Late Quaternary (see also Di Stefano and Branca, 2002; Monaco et al., 2002, 2004). To better quantify the uplift rates and to define their short-term variations, a velocity diagram has been carried out (Fig. 5).

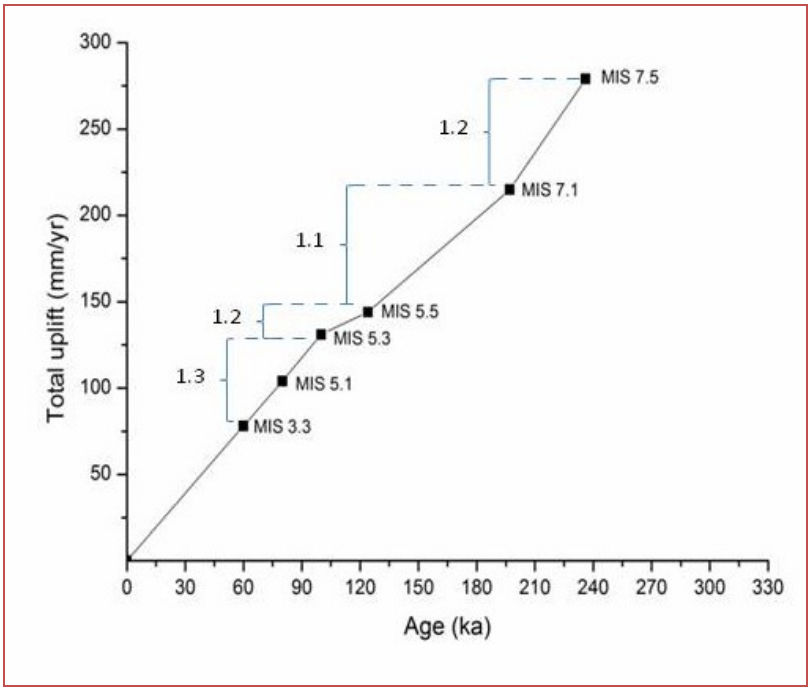

Fig. 5 - Velocity diagram showing the short-term variations of the uplift rates (mm/yr) along the area of interest. The uplift rates (see Table 1) have been calculated for the last 330 ka by fitting the elevations of the distinct palaeoshorelines corrected for sea-level changes.

For this purpose, for the most recent terraces (1st to 4th orders), the elevation of inner edges measured in the eastern coastal sector has been used (Table 1), in order to prevent interference with fluvial processes. The elevation has been corrected for the original sea level of the corresponding high-stands defined by the reference eustatic curve (Table 1; Waelbroeck et al., 2002). Taking into account the observed inner edge elevation of the dated terraces and the sea level correction for the implicated MIS, an average uplift rate value of ~1.2 mm/yr can be estimated for the last 240 ka, even though a slight acceleration has occurred in the last 100 ka. This value is consistent with the short-term uplift rates estimated through the analysis of Holocene deposits drilled in the coastal area of the Catania Plain (Spampinato et al., 2012). The morphological analysis of the terraces and the deformation pattern also suggest the occurrence of an important tectonic component in the uplifting of the oldest terraces (6th and 7th orders) which is related to Middle-Upper Pleistocene contractional processes at the front of the Sicilian chain. Even though the inner edge of 6th order terraces is located at 270 m a.s.l., along the axial zone of the Terreforti anticline this surface reaches an elevation of 325 m a.s.l. (Mt. Tiritì, Fig. 3a).

Taking into account that this terrace formed between 236 ka and 197 ka (this latter is the age of the first unfolded terrace next), a fold growth rate of 1.4 mm/yr along the hinge can be estimated. It is worth noting the limited extension of the MIS 7.1 terraces (5th order), restricted to the westernmost sector of the area, that can be related to the fold geometry whose axis is oblique with respect to the terrace trend. Moreover, the lack of MIS 7.3 terraces could depend on the clastic lithology of the substratum, as they were probably removed by coastal erosion during the subsequent MIS 7.1, when the relative sea level reached similar elevations.

5.6 CONCLUSIONS

OSL age determinations of Pleistocene alluvial-coastal terrace deposits outcropping between Mt. Etna volcano and the Catania Plain provided new constraints for correlating the seven orders of terraces with seven of the last major high-stands of the global eustatic curve (i.e. MIS 9.3, 7.5, 7.1, 5.5, 5.3, 5.1, 3.3).

The performance of applied test in this study (recycling ratio, recuperation and the dose recovery test) has shown that the SAR protocol for determination of the equivalent dose (D_e) is successfully used for all samples and before burial the grains were well-bleached. The chronological data of this study confirm the accurate geochronology investigations of the coastal-alluvial environment.

The analysis highlights a mean uplift rate of 1.2 mm/yr during the last 330 ka, probably related to regional processes (Bianca et al., 1999). Moreover, the geometry of terraces indicates that local tectonic processes, related to the migration of the front of the Sicilian chain, are coeval to the sea-level changes during the Middle Pleistocene. The two highest terraces are in fact folded, as a response of thrust propagation. The OSL age determinations suggests that the activity of the frontal thrust occurred between 236 and 197 ka. Moreover, OSL chronology and topographic data allowed us to determine for the Terreforti anticline a growth rate of 1.4 mm/yr along its hinge. However, GPS velocity fields (Ferranti et al., 2008; Mattia et al., 2011), seismological (Lavecchia et al., 2007) and interferometric synthetic aperture radar data (Lundgren et al., 2004; Bonforte et al., 2011) suggest that contractional processes are still active, even though current thrusting and folding has migrated slightly to the north, to the back of the Middle Pleistocene anticline.

Table 1 - Elevations of inner edge, MIS, sea level correction and uplift rate of each terrace.

Order of terraces	Elevation of inner edge (m) in the western sector	Elevation of inner edge (m) in the eastern sector	MIS	ka	Sea level correction (m)	Uplift (m)	Rate (mm/yr)
7th			9.3	330	+4.7		
6th	270		7.5	236	-9.4	279.4	1.2
5th	230-205		7.1	197	-9.7	214.7	1.1
4th	190	150	5.5	124	+6.3	143.7	1.2
3rd	150	110	5.3	100	-21	131	1.3
2nd	95	85	5.1	80	-18.7	103.7	1.3
1st	150-40	30	3.3	60	-48	78	1.3

Table 2 - List of samples with elevation and coordinates.

Sample	Elevation (m)	Position
CT1	210	37° 30’ 18.57’’ N 15° 01’ 50.63’’ E
CT2	138	37° 29’ 33.75’’ N 15° 02’ 22.05’’ E
CT3	140	37° 29’ 33.75’’ N 15° 02’ 22.05’’ E
CT4	110	37° 29’ 13.47’’ N 15° 02’ 12.22’’ E
CT5	82	37° 30’ 11.79’’ N 15° 03’ 09.64’’ E

Table 3 - Experimental parameters of SAR (adapted from Murray and Wintle, 2003) sequence used for D_e determination.

Step	Treatment[a]	Observed[b]
1	Give dose, D_i	-
2	Preheat for 10 sec at 240 °C	-
3	Stimulate with green laser for 1 sec at 125 °C	L_i
4	Test dose, D_t	-
5	Cut-heat at to 200°C	-
6	Stimulate with green laser for 1 sec at 125 °C	T_i
7	Stimulate with green laser for 1 sec at 280 °C[c]	R
8	Return to 1	-

[a]For the natural dose i=0.
[b]L_i and T_i are derived from the initial 0.2 s OSL signal minus a background estimated from the last part of the stimulation curve (in this experiment, the last 0.3 s is used as a background).
[c]R is recuperation(at the end of each run the grains are optically stimulated at 280°C for 1 sec to bleach the remaining OSL signal as possible to minimize the thermal transfer of charges possible; Wintle and Murray, 2000; Choi et al., 2003; Murray and Wintle, 2003; Kiyak and Canel, 2006).

Table 4 - Contents of radioactive elements of each sample.

Sample	**U (ppm)**	**Th (ppm)**	**Rb (ppm)**	**K (%)**
CT1	0.97±0.04	2.72±0.13	18±0.36	0.47±0.01
CT2	0.73±0.03	1.54±0.08	24±0.48	0.66±0.02
CT3	1.14±0.04	4.14±0.20	32±0.64	0.71±0.02
CT4	1.35±0.05	3.95±0.19	28±0.56	0.76±0.02
CT5	1.91±0.07	4.51±0.22	25±0.50	0.61±0.02

Table 5 - Radionuclide concentrations, dose rates, equivalent doses, OSL ages and corresponding MIS of our terraces.

Sample	[1],[2]D_β (Gy/ka)	[2]D_γ (Gy/ka)	*AD* (Gy/ka)	[3]SG (#)	D_e-Mean (Gy)	D_e CAM (Gy) (2se)	Age CAM (ka) (2se)	MIS (ka)
CT1	0.41±0.01	0.44±0.01	0.85±0.04	127	206±46	204±5	240±12	7.5 (236)
CT2	0.47±0.02	0.42±0.01	0.88±0.04	104	103±25	102±3	116±6	5.5 (124)
CT3	0.54±0.02	0.53±0.01	1.07±0.05	113	133±41	135±4	127±7	5.5 (124)
CT4	0.61±0.02	0.58±0.01	1.19±0.05	112	129±50	124±5	105±6	5.3 (100)
CT5	0.63±0.02	0.66±0.01	1.29±0.05	91	105±42	104±4	80±4	5.1 (80)

[1]For D_β by quartz (180<Ø<212 µm) were used following f correction factor: f_U = 0.86; f_{Th} = 0.81; f_K = 0.94; f_{Rb} = 0.75 (Mejdahl, 1979; Adamiec and Aitken, 1998).
[2]D_β and D_γ are corrected for moisture content.
[3]# Is the number of accepted grains (Murray and Wintle, 2003).

DETAILS..

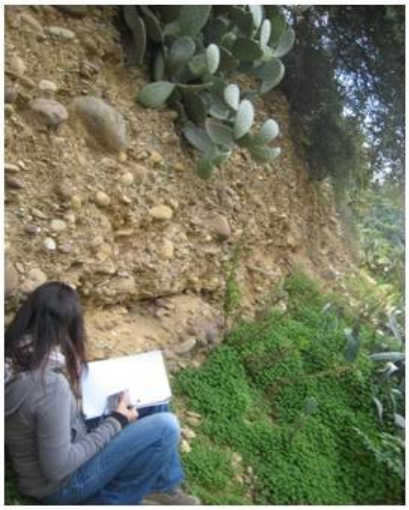

CONCLUSION

This thesis is the result of interdisciplinary work aimed at accurately dating Pleistocene terraced sequences of Calabrian Arc and Eastern Sicily, in order to determinate uplift rates and to discriminate, where possible, the regional component of uplift from local tectonic activity. In order to obtain the best results, the choice of dating method was of primary importance. In the geochronological field there are few direct dating methods capable of accurately determining the time of sediment deposition. This is because most techniques require a specific material that is not always present in the studied areas. Moreover, many dating methods are only useful over short time scales, the calculated age does not directly date the selected event, and/or complex age calibration may be necessary which can significantly increase the uncertainty in the final result. The choice of using an independent dating technique, such as the Optically Stimulated Luminescence (OSL) method (Huntley et al., 1985; Aitken, 1998), primarily depends on its applicability to the detrital minerals of the terraced sediment (i.e. quartz and feldspars) and on its accuracy. So, the research project was developed in cooperation with PH3DRA (Physics for Dating Diagnostic Dosimetry Research and Applications) laboratories of the Department of Physics and Astronomy of the Catania University, Italy.

Since Middle Pleistocene times, a strong regional uplift with values of ~1 mm/yr occurred along the Calabrian Arc, gradually decreasing to the north and to the south (Westaway, 1993; Bordoni and Valensise, 1999; Ferranti et al., 2006). This process has been accompanied by extensional tectonics along the Tyrrhenian side of the Arc and by contractional and/or transcurrent deformation along the northern and southern margin. The Quaternary period was also characterized by climatic fluctuations that resulted in sea-level changes. Coastal terraces are the product of

the combination of tectonic uplift and sea-level changes and their formation is mostly related to interglacial maxima (high sea-level stands) By combining ages and elevations of inner edges with the OIT stages of high sea-level stands, it has been possible to accurately evaluate the uplift rates of the studied areas (Westaway 1993; Armijo et al. 1996; Bosi et al. 1996) and to discriminate between regional and local components.

Firstly, the distribution of interested coastal terraced surfaces with their relative inner and outer edges were mapped over the whole interested area using the 1:25,000 scale topographic maps of the Istituto Geografico Militare, 1:10,000 scale regional topographic maps, SPOT satellite images and 1:33.000 and 1:10.000 scale aerial photographs.

Secondly, for each site the structural and geomorphological issues were dealt with and then samples of sands were collected from the key areas. Successively, geological samples preparation, measurements and analysis of results were optimized in order to reduce the uncertain of the final OSL age. Finally, tectonic implication were considered, discriminating, where possible, the regional and local components of uplift. In the following, the results obtained in each area, published in various ISI journals, are briefly shown.

The marine terracing on the **Capo Vaticano peninsula** (western Calabria) is the result of raising processes of the area, which, as a whole, represents the footwall of both the SW-NE and the WNW-ESE striking offshore normal fault systems, the latter extending also on-land. These form a flight of distinct levels distributed between about 600 m and 30 m of altitude. New OSL age determinations have been scheduled to better constrain the terrace stratigraphical and morphotectonic investigations to better verify the activity of the fault during the Pleistocene. Six samples collected from unconsolidated sediments associated with the major marine

terraces were analysed by OSL technique, whose results gave reliable absolute ages, showing a range between 214±25 ka and 62±6 ka. Absolute dating of Middle-Upper Pleistocene marine sediments yielded new constraints for correlating the seven orders of marine terraces exposed in the Capo Vaticano peninsula with the last Quaternary interglacial stages. In fact, the distinct marine terraces can be correlated with the last seven major high-stands of the global eustatic curve (i.e. MIS 7.5, 7.3, 7.1, 5.5, 5.3, 5.1 and 3.3). The overall deformation pattern, also characterized by short-term accelerations and decelerations in uplift-rates (see Tortorici et al., 2003 for a more complete discussion), confirms the occurrence of an important tectonic component in the total amount of uplift, related to the Late Quaternary activity of the normal fault segments bounding the Capo Vaticano structural high that caused the tilting of the whole peninsula toward the northeast and an uplift rates increasing toward the southwest. On the other hand, the hanging-wall blocks affected by tectonic subsidence are certainly characterized by uplift-rates lower than the regional component of uplift in the overall amount of vertical movement. Present elevations of coastal terraces also suggest that this portion of the Calabrian Arc has been affected by a vigorous tectonic uplift during the last 236 ka, locally characterized by rates up to ~2 mm/yr, responsible for the preservation of all coastal terraces related to the entire series of the sea level high-stands. Consequently, the uplift of the area, started just before 236 ka ago, is due to the combined activity of both regional uplift and faulting.

The coastal sector of **Sant'Agata di Militello** (north-eastern Sicily) is characterized by a flight of raised Middle-Upper Pleistocene marine terraces with an overall good morphological continuity, formed by marine platforms overlain by littoral deposits made up of yellow littoral sand and gravels in a sandy matrix. In particular, at least five main orders of well-preserved Quaternary surfaces and

relative deposits, mostly located at the hanging-wall and at the footwall of the Pleistocene northwest-dipping Capo d'Orlando normal fault are recognized. In order to better define the whole terrace chronology, deposited samples were analysed by OSL methodology, and the modified SAR protocol (Murray and Wintle, 2000, 2003) used with sand-sized quartz. OSL age determinations of Pleistocene marine terrace deposits provided new constraints for correlating the five orders of marine terrace with five of the last major high-stands of the global eustatic curve (i.e. MIS 9.1, 8.5, 7.1, 5.5, 5.1). The continental sedimentary cover of the 3rd order terrace contains mammal-bearing deposits that were previously dated 200±40 ka BP by the isoleucine epimerization method (Bada et al., 1991), allowing their relation to MIS 7.1 high-stand. The analysis highlights a mean uplift rate of 0.8 mm/yr during the last 330 ka in the south-western sector; on the contrary, in the north-eastern sector, the uplift was characterized by larger rates for the oldest orders (up to 0.92 mm/yr) and lower ones for the youngest orders (down to 0.35 mm/yr), due to the fault activity. The geometry of the palaeoshorelines and the uplift rates indicate that the eustatic and the local tectonic processes were coeval, suggesting the activity of the Capo d'Orlando fault during the Middle-Late Pleistocene. The morphological features and the historical seismicity suggest that the fault is probably inactive.

The study has been also focused on the sector falling between the southern edge of the Mt. Etna volcanic edifice and the Catania Plain (eastern Sicily), known as the "**Terreforti Hills**", a belt of hills up to 325 m high constituted by an Upper Pliocene to Quaternary sedimentary succession with volcanic intercalations, at the front of the Sicilian fold and thrust system. Five samples were collected from deposits belonging to a flight of seven orders of coastal-alluvial terraces. The applicability of the OSL technique through modified SAR protocol (Murray and Wintle, 2000, 2003) on single grain quartz extracted from alluvial-coastal sediments

was tested. The performance of applied tests (i.e. recycling ratio, recuperation and dose recovery) in this study has shown that the SAR protocol for determination of the equivalent dose (D_e) can be successfully used for all samples and before burial the grains were well-bleached. The chronological data of this study confirm the accurate geochronology investigations of the coastal-alluvial environment. In fact, OSL ages ranging between 240±12 and 80±4 ka were obtained, providing new constraints for correlating the seven orders of terraces with seven of the last major high-stands of the global eustatic curve (i.e. MIS 9.3, 7.5, 7.1, 5.5, 5.3, 5.1, 3.3).

The analysis highlights a mean uplift rate of 1.2 mm/yr during the last 330 ka, probably related to regional processes (Bianca et al., 1999). Moreover, the geometry of terraces indicates that local tectonic processes, related to the migration of the front of the Sicilian chain, are coeval to the sea-level changes during the Middle Pleistocene. The two highest terraces are in fact folded, suggesting the activity of a frontal thrust propagation fold between 236 and 197 ka. OSL age determinations and topographic data allowed us to determine for the Terreforti anticline a growth rate of 1.4 mm/yr along its hinge. However, GPS velocity fields (Ferranti et al., 2008; Mattia et al., 2011), seismological (Lavecchia et al., 2007) and interferometric synthetic aperture radar data (Lundgren et al., 2004; Bonforte et al., 2011) suggest that contractional processes are still active, even though current thrusting and folding has migrated slightly to the north, to the back of the Middle Pleistocene anticline.

Dating attempts were executed on marine terraces occurring in the **Amendolara area** (northern-eastern Calabria), at the north-eastern margin of the Calabrian Arc.

Unfortunately, the quartz physical behavior from six collected samples, did not allow its use as dosimeter with the purpose of dating the formation of the terraces.

The future perspective will be the employment of feldspars in order to better understand the limits and the possible application of the OSL dating method in this area.

In conclusion, the OSL dating method has proved to be suitable to date coastal terraced deposits occurring in various geological domains and to be an excellent tool for determining vertical tectonic deformation. In particular, it allowed the discrimination of the regional and local component of Quaternary vertical deformation of key areas of the Calabrian Arc, pointing out the occurrence of tectonic structures whose activity could contribute to the assessment of the geological risk of the area.

APPENDIX A - INSTRUMENTATION

The measurement equipment used is a Risø TL/OSL reader (model TL/OSL-DA-15, see Fig. 1) equipped with a single grain OSL attachment (Bøtter-Jensen et al., 2000). Indispensable components of an OSL measurement facility are i) a stimulation light source, ii) a light detection system, iii) an irradiation source and iv) a heater for heating the samples. The Risø system enables measurement of both thermoluminescence and optically stimulated luminescence. The system allows up to 48 samples to be individually heated to any temperature between room temperature and 700 °C, to be individually irradiated by a beta source ($^{90}Sr/^{90}Y$) mounted on the reader and to be optically stimulated by various light sources in situ.

The emitted luminescence is measured by a light detection system comprised of a photomultiplier tube and suitable detection filters. A schematic drawing of the system is shown in Fig. 2.

1.1 The Risø TL/OSL system

Samples are either mounted on 9.7 mm diameter aluminium or stainless steel discs using silicone oil. Samples are loaded onto an exchangeable sample carousel that can accommodate up to 48 samples. The sample carousel is then located in the sample chamber which can be programmed to be evacuated or have a nitrogen atmosphere maintained by a nitrogen flow.

The sample carousel rests on a motor driven turntable, which enables rotation (in steps) of the sample carousel. An infrared light emitting diode (LED) is positioned underneath the turntable, which is switched on during rotation.

The measurement is initiated by moving a given sample to the measurement position located directly underneath the light detection system.

Fig. 1 - The Risø TL/OSL-DA-15 system.

The sample is then lifted through slots in the sample carousel into the measurement position by a lift, which also functions as the heating element.

In the measurement position the sample can be stimulated optically and/or thermally. Thermal stimulation is obtained by linearly increasing the temperature of the heater strip and optical stimulation is provided by different light sources focused onto the sample position. The emitted luminescence is measured by the light detection system (see Fig. 2).

1.2 Light detection system

The essential components of the light detection system are i) a photomultiplier tube (PMT) and ii) suitable detection filters. The detection filters serve both to shield the PMT from scattered stimulation light and to define the spectral detection window.

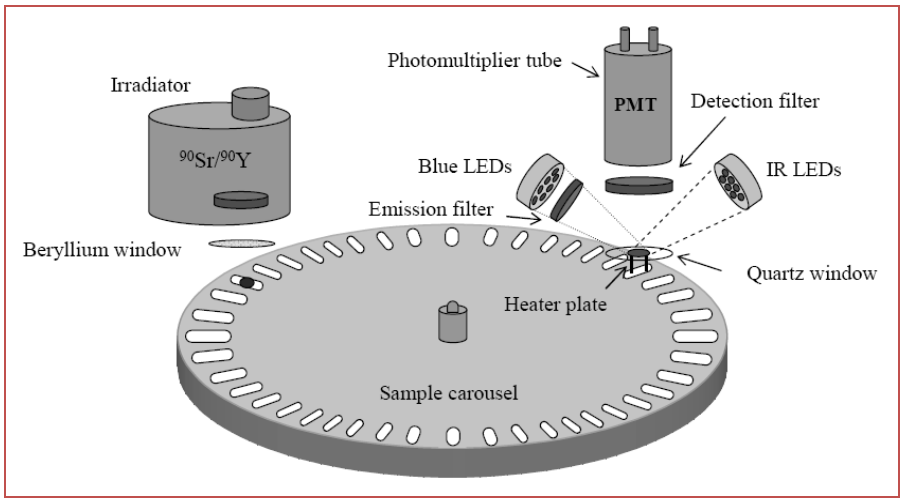

Fig. 2 - Schematic illustration of the Risø TL/OSL luminescence reader (Thomsen, 2004).

1.2.1 Photomultiplier tube

The emitted luminescence is detected by a photomultiplier tube (PMT). The light sensitive component in the PMT is the cathode. This is coated with a photo-emissive substance; CsSb and other bialkali compounds are commonly used for this material. Electrons emitted from the photocathode are accelerated towards a series of dynodes maintained at a positive voltage relative to the photocathode. Electrons with sufficient velocity striking the dynode will eject several secondary electrons from the surface. The standard PMT in the Risø TL/OSL luminescence reader is a bialkali EMI 9235QA PMT, which has maximum detection efficiency at approximately 400 nm, making it suitable for detection of luminescence from both quartz and feldspar (see emission spectra in Fig. 3). Fig. 4 displays the quantum efficiency (i.e. sensitivity) as a function of incident photon wave-length for EMI 9235QA. The PMT is operated in "photon counting" mode, where each pulse of charge arising at the anode is counted. Many samples are only weakly luminescent making optimization of light collection important. Thus, it is critical that the

distance between the PMT and the sample is as small as possible. As the stimulation sources have to be placed between the sample and the PMT the sample-to-PMT cathode distance in the Risø TL/OSL luminescence reader is 55 mm.

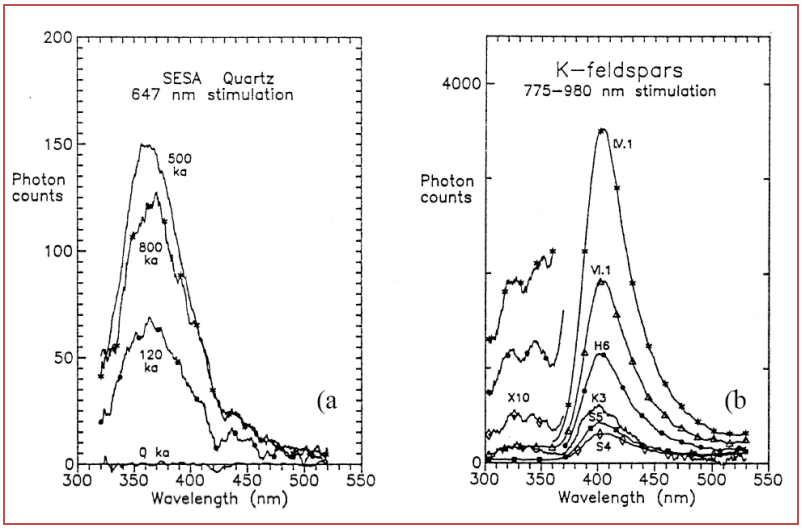

Fig. 3 - Emission spectra of sedimentary quartz and K feldspars (from Huntley et al., 1991). a) Emission spectra of several sedimentary quartz samples from South Australia obtained for stimulation using the 647 nm line from a Krypton laser. b) Emission spectra of several sedimentary K feldspars using IR diode stimulation.

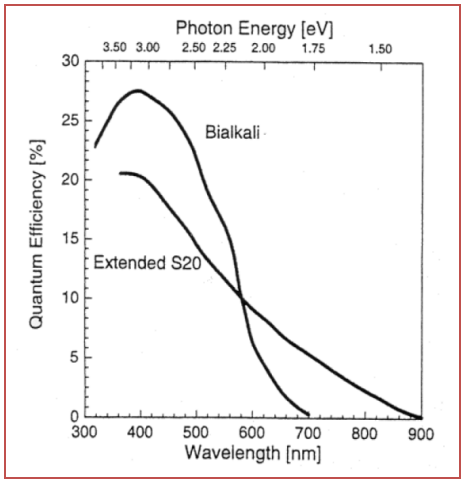

Fig. 4 - The quantum efficiency of the photomultiplier tubes EMI 9235QA PMT (Bialkali) and EMI 9658R PMT (Extended S20) as a function of photon wavelength and energy (from Bøtter-Jensen, 1997).

1.2.2 Detection filters

The intensity of the stimulation light is ~10^{18} orders of magnitude larger than the emitted luminescence. In order to be able to measure the emitted luminescence, detection filters must be used to prevent scattered stimulation light from reaching the PMT, and the spectral stimulation and detection windows must be well separated. Quartz has a strong emission centred on 365 nm (near UV) and many types of feldspars have a strong emission centred on 410 nm (violet). In Fig. 3 emission spectra from several samples of sedimentary quartz and K feldspars are shown. A commonly used detection filter is Hoya U-340 (see Fig. 5), which has a peak transmission around 340 nm (FWHM = 80 nm).

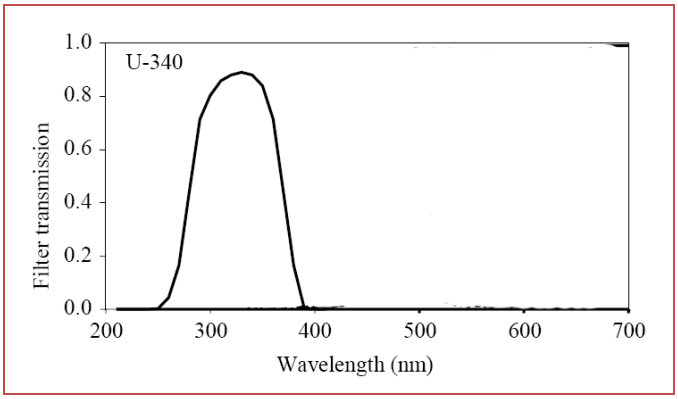

Fig. 5 - The transmission curves of the Hoya U-340 filter (detection filter in front of the PMT); after Bøtter-Jensen et al. (1999).

1.3 Luminescence stimulation system

1.3.1 Heating system

The heating element and lift mechanism is located directly underneath the photomultiplier tube. The heating element has two functions: i) it heats the sample

and ii) it lifts the sample into the measurement position. The heating system is able to heat samples to 700 °C.

1.3.2 Optical stimulation system

In OSL, the probability of eviction depends on the rate at which photons arrive at the trap and the sensitivity of that particular trap to photo-eviction. The sensitivity of the trap depends strongly on the wavelength of the stimulating light, generally the shorter the wavelength the greater the chance of eviction. However the wavelength of the stimulation light is not the only factor to take into consideration.

The wavelength of the emitted luminescence must also be considered. The intensity of the emitted luminescence is many orders of magnitude smaller than the intensity of the stimulation light, so in order to effectively prevent stimulation light from reaching the PMT, the wavelengths of the stimulation light and the luminescence must be well separated or appropriate filters used. In the standard Risø TL/OSL luminescence reader (Bøtter-Jensen et al., 2000) a choice of two stimulation sources exists: i) infrared (IR) light emitting diodes (LEDs) and ii) blue LEDs (see Fig. 6).

LEDs are inexpensive, compact, have short response times and the illumination power density can be controlled electronically. The latter offers the possibility of stimulation at different intensities and varying the stimulation intensity as a function of stimulation time.

Infrared LEDs

Infrared (IR) stimulation in the region 800-900 nm can stimulate luminescence from most feldspars (but not from quartz at room temperature) probably by a

thermal assistance mechanism (Hütt et al., 1988). This has the important advantage that a wider range of wavelengths for the detection window becomes available.

The IR LEDs used here emit at 875 nm, which is close to the IR resonance wavelength at 870 nm found in most feldspars (Bøtter-Jensen et al., 2003).

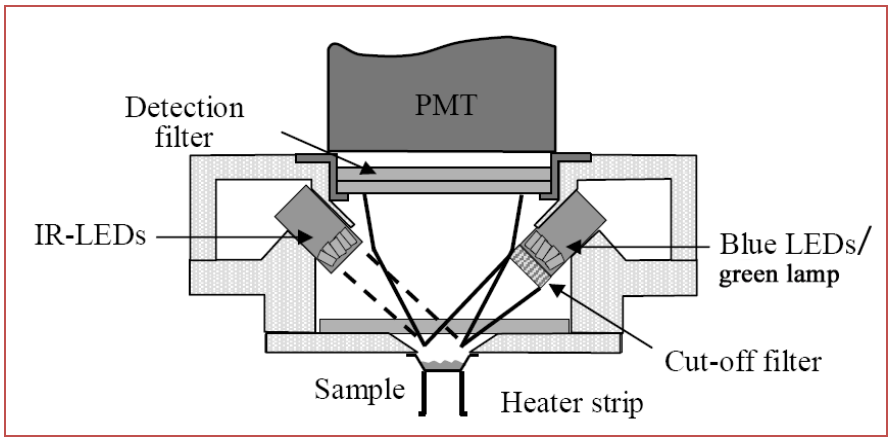

Fig. 6 - Schematic diagram of the combined blue and IR LED OSL unit.

Blue LEDs

The Risø reader is equipped with blue LEDs with a peak emission at 470 nm (FWHM = 20 nm). The advantage of using the stimulation spectrum from the blue LEDs is that the OSL decay will be rapid because of the short wavelength, but the disadvantage is that the spectrum has a significant tail into the detection window (centred on 365 nm).

1.4 Beta irradiator

A detachable beta irradiator is located above the sample carousel. Artificial irradiation are performed with the $^{90}Sr/^{90}Y$ calibrated beta source with a maximum energy of 2.27 MeV, integrated in the system delivering 6 Gy/min. The source is

mounted into a rotating, stainless steel wheel, which is pneumatically activated; it takes the source 0.11 s to rotate from the closed position to the open position (Markey et al., 1997). The distance between the source and the sample is 5 mm.

1.5 Single grain laser OSL system

The Risø single grain OSL attachment enables routine measurements of sand-sized single grains (Duller et al., 1999). The sample is loaded into special aluminium discs, each containing 100 grains in holes of known position on the disc surface. The sample discs designed for mounting single grains are 1 mm thick and have a diameter of 9.7 mm (i.e. same surface area as the conventional sample discs).

The individual grains are placed in 100 holes drilled into the surface of the sample disc. These holes are 300 µm deep by 300 µm in diameter and drilled on a 10 by 10 grid with 600 µm spacing between centres (see Fig. 7). Three further holes are drilled at the periphery of the disc. These holes (called location holes) have a diameter of 500 µm and are drilled all the way through the disc. The relative positions between the location holes and the grain holes are well-known, but the relative distance between the holes and the circumference of the disc may vary slightly from disc to disc. Irradiation and heating can thus be performed simultaneously on all 100 grains, whereas the OSL signal can be measured separately from individual grains by using a focused a green (532 nm) laser delivering ~45 W/cm^2 (90% power), (beam diameter on the sample disc is < 20 µm). This laser spot is steered to each of the grain holes in turn and switched on. The focused laser enables a high energy fluence rate and reduces the risk of optical cross-talk by ensuring that the entire spot enters the 300 µm diameter hole. Only a small part of the grain will be stimulated directly by the laser beam, but internal reflection within the grain hole is assumed to provide a uniform illumination of the

grain. The OSL is detected by an EMI 9635QA photomultiplier tube that is shielded from the stimulation light by 4 mm of Hoya U-340 filter. A schematic diagram of the single grain OSL attachment is shown in Fig. 8.

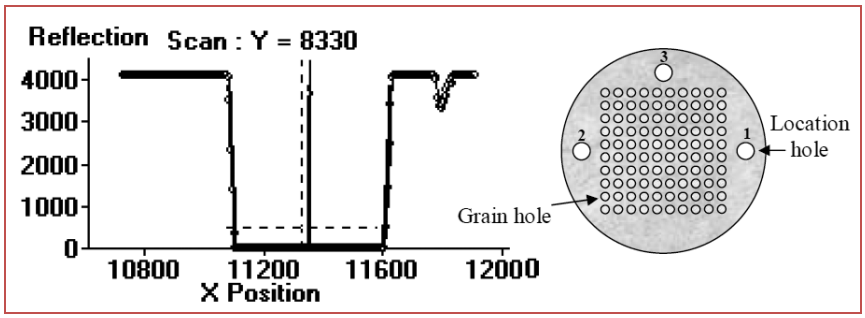

Fig.7 - Example of a location hole scan. The change in reflectivity as the laser passes over the location hole is clearly seen. The diameter of the location hole is 500 µm as expected. Also shown is a schematic drawing of a single grain disc.

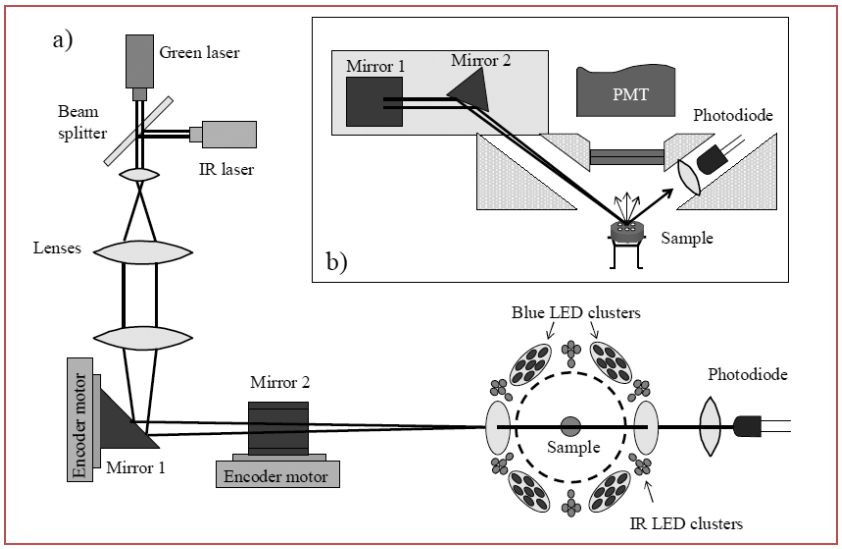

Fig. 8 - Schematic diagram of the single grain OSL attachment (redrawn from Bøtter-Jensen et al., 2000). Optical stimulation is achieved using a laser beam focused by three lenses. The position of the laser spot on the sample is controlled by moving the two mirrors. a) Single grain OSL attachment seen from above. b) Cross-section of the single grain OSL attachment.

REFERENCES

Adamiec, G., Aitken, M.J., 1998. Dose-rate conversion factors: update. Ancient TL 16 (2), 37-50.

Aitken, M.J., 1985. Thermoluminescence dating. Academic Press, London., 359 pp.

Aitken, M.J., 1998. An Introduction to Optical Dating. The Dating of Quaternary Sediments by the Use of Photon-stimulated Luminescence. Oxford Science Publications, 267 pp.

Aitken, M.J., Smith, B.W., 1988. Optical dating: Recuperation after bleaching. Quaternary Science Reviews 7 (3-4), 387-393.

Amato, A., Alessndrini, B., Cimini, B., Frepoli, A., Selvaggi, G., 1993. Active and remnant subducted slabs beneath Italy: evidence from seismic tomography and seismicity. Ann. Geofis. 36 (2), 201-214.

Argnani, A., Serpelloni, E., Bonazzi, C., 2007. Pattern of deformation around the central Aeolian Islands: evidence from multichannel seismics and GPS data. Terra Nova 19, 317-323.

Argnani, A., Trincardi, F., 1988. Paola Slope Basin: evidence of regional contraction on the eastern Tyrrhenian margin. Memorie della Società Geologica Italiana 44, 93-105.

Armijo, R., Meyer, B., King, G.C.P., Rigo, A., Papanastassiou, D., 1996. Quaternary evolution of the Corinth Rift and its implications for the Late Cenozoic evolution of the Aegean. Geophysical Journal International 126, 11-53.

Arnold, L.J., Bailey, R.M., Tucker, G.E., 2007. Statistical treatment of fluvial dose distributions from southern Colorado arroyo deposits. Quaternary Geochronology 2 (1-4), 162-167.

Arnold, L.J., Roberts, R.G., 2009. Stochastic modelling of multi-grain equivalent dose (De) distributions: Implications for OSL dating of sediment mixtures. Quaternary Geochronology 4, 204-230.

Bada, J. L., Belluomini, G., Bonfiglio, L., Branca, M., Burgio, E., Delitala, L., 1991. Isoleucine epimerization ages of Quaternary mammals from Sicily. Il Quaternario 4 (1a), 49-54.

Bailey, R.M., Smith, B.W., Rhodes, E.J., 1997. Partial bleaching and the decay form characteristics of quartz OSL. Radiation Measurements 27 (2), 123-136.

Bailey, R.M., 2000. The slow component of quartz optically stimulated luminescence. Radiation Measurements 32, 233-246.

Bailey, R.M., Singarayer, J.S., Ward, S., Stokes, S., 2003. Identification of partial resetting using De as a function of illumination time. Radiation Measurements 37 (4-5), 511-518.

Bailey, R.M., Arnold, L.J., 2006. Statistical modelling of single grain quartz De distributions and an assessment of procedures for estimating burial dose. Quaternary Science Reviews 25, 2475-2502.

Balescu, S., Dumas, B., Guérémy, P., Lamothe, M., Lhénaff, R., Raffy, J., 1997. Thermoluminescence dating tests of Pleistocene sediments from uplifted marine shorelines along the southwest coastline of the Calabrian Peninsula (southern Italy). Palaeogeography, Palaeoclimatology, Palaeoecology 130, 25-41.

Banerjee, D., Bùtter-Jensen, L., Murray, A.S., 2000. Retrospective dosimetry: estimation of the dose to quartz using the single aliquot regenerative-dose protocol. Applied Radiation Isotopes 52, 831-844.

Baratta M.; 1901: I terremoti d'Italia. Arnaldo Forni Editore, Bologna, 951 pp.

Barrier, P., Di Geronimo, S., Zibrowius, H., Raisson, F., 1988. Faune Sénégalienne du paléoescarpment du Capo Vaticano (Calabre Méridionale). Implications néotectoniques. Proceedings of the Fourth Symposium on Ecology and Paleoecology of Benthic Communities (E. Robba, ed.), pp. 511-526. Museo Regionale Scienze Naturali, Torino.

Bassinot, F.C., Labeyrie, L.D., Vincent, E., Quidelleur, X., Shackleton, N.J., Lancelot, Y., 1994. The astronomical theory of climate and the age of the Brunhes-Matuyama magnetic reversal, Earth and Planetary Science Letters 126, 91-108.

Bianca, M., Monaco, C., Tortorici, L., Cernobori, L., 1999. Quaternary normal faulting in southeastern Sicily (Italy): a seismic source for the 1693 large earthquake. Geophysical Journal International 139, 370-394.

Bianca, M., Catalano, S., De Guidi, G., Gueli, A.M., Monaco, C., Ristuccia, G.M., Stella, G., Tortorici, G., Tortorici, L., Troja, S.O., 2011. Luminescence chronology of Pleistocene marine terraces of Capo Vaticano peninsula (Calabria, Southern Italy). Quaternary International 232, 121-144.

Billi, A., Barberi, G., Faccenna, C., Neri, G., Pepe, F., Sulli, A., 2006. Tectonics and seismicity of the Tindari Fault System, southern Italy: crustal deformations at the transition between ongoing contractional and extensional domains located above the edge of a subducting slab. Tectonics 25 (2), 1-20.

Billi, A., Presti, D., Faccenna, C., Neri, G., Orecchio, B., 2007. Seismotectonics of the Nubia plate compressive margin in the south Tyrrhenian region, Italy: Clues for subduction inception. Journal of Geophysical Research 112, 13 pp.

Bloom, A.L., Broecker, W.S., Chappell, J., Matthews, R.K., Mesolella, K.J., 1974. Quaternary sea level fluctuations on a tectonic coast; new 230Th/234U dates from the Huon Peninsula, New Guinea. Quaternary Research 4, 185-205.

Boccaletti, M., Nicolich, R., Tortorici, L., 1984. The Calabrian Arc and the Ionian Sea in the dynamic evolution of the Central Mediterranean. Marine Geology 55, 219-245.

Boccaletti, M., Nicolich, R., Tortorici, L., 1990. New data and hypothesis on the development of the Tyrrhenian basin. Palaeogeography, Palaeoclimatology, Palaeoecology 77, 15-40.

Bonfiglio, L., 1991. Correlazioni tra depositi a mammiferi, depositi marini, linee di costa e terrazzi medio e tardo-pleistocenici nella Sicilia orientale. Il Quaternario 4 (1b), 205-214.

Bonfiglio, L., Bellomo, E., Bellomo, G., Bonaduce, G., Violanti, D., 1988. Analisi biostratigrafica e paleoambientale dei depositi marini e salmastri del Pleistocene di Contrada Iannì di S. Calogero (Catanzaro, Calabria; Italia). Proceedings of the Fourth Symposium on Ecology and Paleoecology of Benthic Communities (E. Robba, ed.), pp. 527-574. Museo Regionale Scienze Naturali, Torino.

Bonfiglio, L., Mangano, G., Pino, P., 2010. The contribution of mammal-bearing deposits to timing Late Pleistocene tectonics of Cape Tindari (north-eastern Sicily). Rivista Italiana di Paleontologia e Stratigrafia 116 (1), 103-118.

Bonforte, A., Guglielmino, F., Coltelli, M., Ferretti, A., Puglisi, G., 2011. Structural assessment of Mount Etna volcano from Permanent Scatterers analysis. Geochemistry Geophysics Geosystems 12, 19 pp. Q02002, doi:10.1029/2010GC003213.

Bordoni, P., Valensise G., 1999. Deformation of the 125 ka marine terrace in Italy: tectonic implications. Geological Society, London, Special Publications 146, 71-110.

Boschi, E., Ferrari, G., Gasperini, P., Guidoboni, E., Smeriglio, G., Valensise, G., 1995. Catalogo dei forti terremoti in Italia dal 461 a.C. al 1980. ING-SGA, Bologna, 973 pp.

Bosi, C., Carobene, L., Sposato, A., 1996. Il ruolo dell'eustatismo nella evoluzione geologica nell'area mediterranea. Memorie della Società Geologica Italiana 51, 363-382.

Bøtter-Jensen, L., 1997. Luminescence techniques: instrumentation and methods. Radiation Measurements 27, 749-768.

Bøtter-Jensen, L., Banerjee, D., Jungner, H., Murray, A. S., 1999. Retrospective assessment of environmental dose rates using optically stimulated luminescence from Al2O3: C and quartz. Radiation Protection Dosimetry, 84, 537-542.

Bøtter-Jensen, L., Bulur, E., Duller, G.A.T., Murray, A.S., 2000. Advances in luminescence instrument system. Radiation Measurements 32, 523-528.

Bøtter-Jensen, L., Andersen, G.A., Duller, G.A.T., Murray, A.S., 2003. Developments in radiation, stimulation and observation facilities in luminescence measurements, Radiation Measurements 37, 535-541.

Bøtter-Jensen, L., McKeever, S.W.S., Wintle A.G., 2003. Optical stimulation luminescence dosimetry. Elsevier Sciences B.V., 302 pp.

Bulur, E., Bøtter-Jensen, L., Murray, A.S., 2000. Optically stimulated luminescence from quartz measured using linear modulation technique. Radiation Measurements 32, 407-411.

Burton, A.N., 1971. Relazione generale, carta geologica della Calabria Cassa per il Mezzogiorno, Roma 120 pp.

CPTI Working Group, 2004. INGV, Bologna. http://emidius.mi.ingv.it/CPTI04.

Caputo, R., Monaco, C., Tortorici, L., 2006. Multi-seismic cycle deformation rates from Holocene normal fault scarps on Crete (Greece). Terra Nova, 18, 181-190.

Caputo, R., 2007. Sea level curves: perplexities of an end-user in morphotectonic applications. Global and Planetary Change 57 (3-4), 417-423.

Caputo, R., Bianca, M., D'Onofrio, R., 2010. Ionian marine terraces of Southern Italy: insights into the Quaternary tectonic evolution of the area. Tectonics 29, 1-24.

Carbone, S., Lentini, F., Vinci, G., 1998. Carta geologica del settore occidentale dei Monti Peloritani (Sicilia Nord-Orientale), scala 1:25.000. S.EL.CA., Firenze.

Carobene, L., Dai Pra, G., 1991. Middle and Upper Pleistocene sea level high-stands along the Tyrrhenian coast of Basilicata (southern Italy). Il Quaternario 4, 173-202.

Catalano, S., Di Stefano, A., 1997. Sollevamenti e tettogenesi pleistocenica lungo il margine tirrenico dei Monti Peloritani: integrazione dei dati geomorfologici, strutturali e biostratigrafici. Il Quaternario 10, 337-342.

Catalano, S., De Guidi, G., 2003. Late Quaternary uplift of northeastern Sicily: relation with the active normal faulting deformation. Journal of Geodynamics 36, 445-467.

Catalano, S., De Guidi, G., Monaco, C., Tortorici, G., Tortorici, L., 2003. Long-term behaviour of the late Quaternary normal faults in the Straits of Messina area (Calabrian arc): structural and morphological constraints. Quaternary International 101-102, 81-91.

Catalano, S., Torrisi, S., Ferlito, C., 2004. The relationship between Late Quaternary deformation and volcanism of Mt. Etna (eastern Sicily): new evidence from the sedimentary substratum in the Catania region. Journal of Volcanology and Geothermal Research 132, 311-334.

Cello, G., Spadea, P., Tortorici, L., Turco, E., 1982. Plio-Pleistocene volcanoclastic deposits of southern Calabria. Bollettino della Società Geologica Italiana 102, 87-93.

Chappell, J., Shackleton, N.J., 1986. Oxygen isotopes and sea level. Nature 324, 137-140.

Chappell, J., Omura, A., Esat, T., McCulloch, M., Pandolfi, J., Ota, Y. and Pillans, B., 1996. Reconciliation of late Quaternary sea levels derived from coral terraces at Huon Peninsula with deep sea oxygen isotope records. Earth and Planetary Science Letters 141, 227-236.

Chiarabba, C., De Gori, P., Speranza, F., 2008. The southern Tyrrhenian subduction zone: Deep geometry, magmatism and Plio-Pleistocene evolution. Earth and Planetary Science Letters 268, 408-423.

Choi, J.H., Murray, A.S., Cheong, C.S., Hong, D.G., Chang, H.W., 2003. The resolution of stratigraphic inconsistency in the luminescence ages of marine terrace sediments from Korea. Quaternary Science Reviews 22, 1201-1206.

Choi, J.H., Kim, J.W., Murray, A.S., Hong, D.G., Chang, H.W., Cheong, C.-S., 2009. OSL dating of marine terrace sediments on the southeastern coast of Korea with implications for Quaternary tectonics. Quaternary International 199, 3-14.

Cinque, A., De Pippo, T., Romano, P., 1995. Coastal slope terracing and relative sea-level changes: deductions based on computer simulations. Earth Surface Processes and Landforms 20, 87-103.

Cocina, O., Neri, G., Privitera, E., Spampinato, S., 1997. Stress tensor computations in the Mount Etna area (Southern Italy) and tectonic implications. Journal of Geodynamics 23, 109-127.

Cucci, L., Tertulliani, A., 2006. I terrazzi marini nell'area di Capo Vaticano (Arco Calabro): solo un record di sollevamento regionale o anche di deformazione cosismica? Il Quaternario 19 (1), 89-101.

Cunningham, A.C., Wallinga, J., 2010. Selection of integration time intervals for quartz OSL decay curves Quaternary Geochronology 5 (6), 657-666.

Dai Pra, G., Miyauchi, T., Anselmi, B., Galletti, M., Paganin, G., 1993. Età dei depositi a Strombus bubonius di Vibo Valentia Marina (Italia meridionale). Il Quaternario 6, 139-144.

D'Agostino, N., Selvaggi, G., 2004. Crustal motion along the Eurasia-Nubia plate boundary in the Calabrian Arc and Sicily and active estension in the Messina Straits from GPS measurements. Journal of Geophysical Research 109, 16 pp.

Dewey, J.F., Helman, M.L., Turco, E., Hutton, D.H.W., Knott, S.D., 1989. Kinematics of the western Mediterranean. In: Coward, M.P., Dietrich, D., Park, R.G. (Eds.), Alpine Tectonics, Geological Society of London Special publication 45, 265-283.

Di Stefano, A., Branca, S., 2002. Long-term uplift rate of the Etna volcano basement (southern Italy) based on biochronological data from Pleistocene sediments. Terra Nova 14, 61-68.

Doglioni, C., 1991. A proposal of kinematic modelling for W-dipping subductions - possible applications to the Tyrrhenian-Apennines system. TerraNova 3, 423-434.

Doglioni, C., Innocenti, F., Mariotti, G., 2001. Why Mt Etna? Terra Nova, 13, 25-31.

Duller, G.A.T., Bøtter-Jensen, L., Murray, A.S., Truscott, A.J., 1999. Single grain laser luminescence (SGLL) measurements using a novel automated reader. Nuclear Instruments and Methods in Physics Research Section B 155, 506-514.

Duller, G.A.T., 2003. Distinguishing quartz and feldspar in single grain luminescence measurements. Radiation Measurements 37, 161-165.

Duller, G. A. T., 2008. Single-grain optical dating of Quaternary sediments: why aliquot size matters in luminescence dating. Boreas 37, 589-612.

Duller, G.A.T. Improving the accuracy and precision of equivalent doses determined using the optically stimulated luminescence signal from single grains of quartz. Radiation Measurements, *in press*.

Dumas, B., Guérémy, P., Lhénaff, R., Raffy, J., 1982. Le soulèvement quaternaire de la Calabre méridionale. Revue de Géographie Physique et de Géologie Dynamique 23, 27-40.

Dumas, B., Guérémy, P., Lhénaff, R., Raffy, J., 1987. Rates of uplift as shown by raised Quaternary shorelines in Southern Calabria (Italy). Z. Geomorphol. N.F., 63, 119-132.

Dumas, B., Guérémy, P., Haong, C. T., Lhénaff, R., Raffy, J., 1991. Gisement et rivages tyrrhéniens de Vibo Marina (Italie du Sud): datation 230Th/234U, soulèvement différentiel de la Calabre méridionale. C. R. Acad. Sci. Paris, 312, Série II, 785-791.

Faccenna, C., Becker, T. W., Lucente, F.P., Jolivet, L., Rossetti, F., 2001. History of subduction and back-arc extension in the Central Mediterranean. Geophysical Journal International 145 (3), 809-820.

Faccenna, C., Heuret, A., Funiciello, F., Lallemand, S., Becker, T.W., 2007. Predicting trench and platemotion from the dynamics of a strong slab. Earth and Planetary Science Letters 257 (1-2), 29-36.

Ferranti, L., Antonioli, F., Mauz, B., Amorosi, A., Dai Pra, G., Mastronuzzi, G., Monaco, C., Orrù, P., Pappalardo, M., Radtke, U., Renda, P., Romano, P., Sansò, P., Verrubbi, V., 2006. Markers of the last interglacial sea-level high stand along the coast of Italy: tectonic implications. Quaternary International 145-146, 30-54.

Ferranti, L., Oldow, J. S., D'Argenio, B., Catalano, R., Lewis, D., Marsella, E., Avellone, G., Maschio, L., Pappone, G., Pepe, F., Sulli, A., 2008. Active deformation in Southern Italy, Sicily and southern Sardinia from GPS velocities of the Peri-Tyrrhenian Geodetic Array (PTGA). Bollettino della Società Geologica Italiana 127, 299-316.

Ferranti, L., Santoro, E., Mazzella, M.E., Monaco, C., Morelli, D., 2009. Active transpression in the northern Calabria Apennines, southern Italy. Tectonophysics 476 (1-2), 226-251.

Finetti, I., Del Ben, A., 1986. Geophysical study of the Tyrrhenian opening. Bollettino di Geofisica Teorica e Applicata 28, 75-155.

Finetti, I.R., Lentini, F., Carbone, S., Den Ben, A., Di Stefano, A., Forlin, E., Guarnieri, P., Pipan, M., Prizzon, A., 2005. Geological outline of Sicily and lithospheric tectono-dynamics of its Tyrrhenian margin from new CROP seismic data. 2005. In: CROP Project. Deep Seismic Exploration of the Central Mediterranean and Italy. I.R. Finetti (Eds.), 319-375.

Franklin, A.D., Prescott, J.R., Scholefield, R.B., 1995. The mechanism of thermoluminescence in an Australian sedimentary quartz. Journal of Luminescence 63, 317-326.

Frepoli, A., Amato, A., 2000. Spatial variation in stresses in peninsular Italy and Sicily from background seismicity. Tectonophysics 317, 109-124.

Fuchs, M., Owen, L.A., 2008. Luminescence dating of glacial and associated sediments: reviews, recommendations and future directions. Boreas 37, 636-659.

Galbraith, R.F., 1988. Graphical display of estimates having differing standard errors. Technometrics 30, 271-81.

Galbraith, R.F., 1990. The radial plot: graphical assessment of spread in ages. Nuclear Tracks Radiation Measurements 17 (3), 207-214.

Galbraith, R.F., Roberts, R.G., Laslett, G.M., Yoshida, H., Olley, J.M., 1999. Optical dating of single and multiple grains of quartz from Jinmium rock shelter, northern Australia: part I, experimental design and statistical models. Archaeometry 41, 339-364.

Galbraith, R.F., 2005. Error variation in OSL palaeodose estimates from single aliquots of quartz: a factorial experiment. Radiation Measurements 39, 289-307.

Gasparini, C., Iannaccone, G., Scarpa, R., 1985. Fault plane solutions and seismicity of the Italian Peninsula. Tectonophysics 117, 59-78.

Gascoyne, M., 1992. The geochemistry of the actinides and their daughters. In: Ivanovich, M. and Harmon, R.S. (eds), Uranium-series Disequilibrium: Applications to Earth, Marine, and Environmental Sciences, 2nd Edn, pp. 3458. Clarendon Press, Oxford.

Gawthorpe, R.L., Hurst, J.M., 1993. Transfer zones in extensional basins: their structural style and influence on drainage development and stratigraphy. Journal of the Geological Society of London 150,1137-1152.

Ghisetti, F., Vezzani, L., 1982. The recent deformation mechanisms of the Calabrian Arc. Earth Evolution Sciences 3, 197-206.

Ghisetti, F., 1984. Recent deformations and the seismogenic source in the Messina Strait (Southern Italy). Tectonophysics 109 (3-4), 191-208.

Ghisetti F., 1992. Fault parameters in the Messina Straits (southern Italy) and relations with the seismogenic source. Tectonophysics 210, 117-133.

Ghisetti, F., Vezzani, L., 1984. Thin-skinned deformation of theWestern Sicily thrust belt and relationships with crustal shortening mesostructural data on the M. Kumeta-Alcantara fault zone and related structures. Bollettino della Società Geologica Italiana 103, 129-157.

Giardini, D., Velonà, M., 1991. The deep seismicity of the Tyrrhenian Sea. Terra Nova 3, 57-64.

Gillot, P.Y., Kieffer, G., Romano, R., 1994. Evolution of Mt. Etna volcano in the light of potassium-argon dating. Acta Vulcanologica 5, 81-87.

Giunta G., Gueli A.M., Monaco C., Orioli S., Ristuccia G.M., Stella G., Troja S.O., 2012. Middle-Late Pleistocene marine terraces and fault activity in the Sant'Agata di Militello coastal area (north-eastern Sicily). Journals of geodynamics 55, 32-40.

Giunta, G., Luzio, D., Agosta, F., Calò, M., Di Trapani, F., Giorgianni, A., Oliveti, E., Orioli, S., Perniciaro, M., Vitale, M., Chiodi, M., Adelfio, G., 2009. An integrated approach to investigate the seismotectonics of northern Sicily and southern Tyrrhenian. Tectonophysics 476, 13-21.

Giunta, G., Nigro, F., Renda, P., Giorgianni, A., 2000. The Sicilian-Maghrebides Tyrrhenian Margin: a neotectonic evolutionary model. Memorie della Società Geologica Italiana 119, 553-565.

Gliozzi, E., Malatesta, A., 1982. A Megacerine in the Pleistocene of Sicily. Geologica Romana 21, 311-395.

Godfrey-Smith, D.I., Huntley, D.J., Chen, W.H., 1988. Optical dating studies of quartz and feldspar sediment extracts. Quaternary Science Reviews 7, 373-380.

Goedicke, C., 2003. Dating historical calcite mortar by blue OSL: results from known age samples. Radiation Measurements 37, 409-415.

Goes, S., Giardini, D., Jenny, S., Hollenstein, C., Kahle, H.G., Geiger, A., 2004. A recent tectonic reorganization in the south-central Mediterranean. Earth and Planetary Science Letters 226 (3-4), 335-345.

Gueguen, E., Doglioni, C., Fernandez, M., 1998. On the post-25 Ma geodynamic evolution of the western Mediterranean. Tectonophysics 298 (1-3), 259-269.

Gvirtzman Z., Nur A., 1999. The formation of Mount Etna as the consequence of slab rollback. Nature, 401, 782-785.

Henshilwood, C.S., d'Errico, F., Yates, R., Jacobs, Z., Tribolo, C., Duller, G.A.T., Mercier, N., Sealy, J.C., Valladas, H., Watts, I., Wintle, A.G., 2002. Emergence of modern human behaviour: middle stone age engravings from South Africa. Science 295, 1278-1280.

Hearty, P.J., Bonfiglio, L., Violanti, D., Sazo, B.J., 1986. Age of late Quaternary marine deposits of Southern Italy determined by aminostratigraphy, faunal correlation and uranium-series dating. Rivista Italiana di Paleontologia e Stratigrafia 92, 149-164.

Hirn, A., Nicolich, R., Gallart, J., Laigle, M., Cernobori, L., ETNASEIS Scientific Group, 1997. Roots of Etna volcano in faults of great earthquakes. Earth and Planetary Science Letters 148, 171-191.

Hollenstein, C., Kahle, H.G., Geiger, A., Jenny, S., Goes, S., Giardini, D., 2003. New GPS constraints on the Africa-Eurasia plate boundary zone in southern Italy. Geophysical Research Letters 30, 1-4.

Hossain, S.M., 2003. A critical comparison and evaluation of methods for the annual radiation dose determination in the luminescence dating of sediments. PhD thesis.

Hugonie, G., 1979. L'èvolution gèomorphologique de la Sicilie septentrionale. Thèse de Doctorat en Lettres, Université de Paris Sorbonne, 949 pp.

Hugonie, G., 1982. Mouvements tectoniques et variations de la morphogenèse au Quaternarie en Sicilie septentrionale. Revue de Géographie Physique et Géologie Dynamique 23 (1), 3-14.

Huntley, D.J., Clague, J.J., 1996. Optical dating of tsunami-laid sands. Quaternary Research 46, 127-140.

Huntley, D. J., Godfrey-Smith, D. I., Haskell, E. H., 1991. Light-induced emission spectra from some quartz and feldspars. Nuclear Tracks and Radiation Measurements 18, 127-131.

Huntley, D.J., Godfrey-Smith, D.I., Thewalt, M.L.W., 1985. Optical dating of sediments. Nature 313 (105-107).

Hütt, G., Jaek, I., Tchonka, J., 1988. Optical dating: K - feldspars optical response stimulation spectra. Quaternary Science Reviews 7, 381-385.

Imbrie, J., Hays, J.D., Martinson, D.G., McIntyre, A., Mix, A.C, Morley, J.J., Pisias, N.G., Prell, W.L., Shackleton, N.J., 1984. The orbital theory of Pleistocene climate: Support from a revised chronology of the marine 18O record. In: Milankovitch and Climate, Part 1, (A. Berger, J. Imbrie, J. Hays, G. Kukla and G. Saltzman, eds), pp. 269-305, Plenum Reidel, Dordrecht.

Ivanovich, M., Harmon, R.S., 1982. Uranium Series Disequilibrium: Applications to Environmental Problems. Clarendon Press, Oxford.

Ivanovich, M., Harmon, R.S., 1992. Uranium-series Disequilibrium: Applications to Earth, Marine, and Environmental Sciences, 2nd Edn. Clarendon Press, Oxford.

Iyengar, M.A.R., 1990. The natural distribution of radium. In: The Environmental Behaviour of Radium, IAEA Technical Report Series 310 (1), 59-70.

Jacobs, Z., Duller, G.A.T., Wintle, A.G., 2003. Optical dating of dune sand from Blombos Cave, South Africa: II single grain data. Journal of Human Evolution 44, 611-623.

Jacobs, Z., Duller, G.A.T., Wintle, A.G., 2006. Interpretation of single grain De distributions and calculation of De. Radiation Measurements 41, 264-277.

Jacques, E., Monaco, C., Tapponnier, P., Tortorici, L., Winter, T., 2001. Faulting and earthquake triggering during the 1783 Calabria seismic sequence. Geophysical Journal International 147 (3), 499-516.

Jain, M., Murray, A.S., Bøtter-Jensen, L., 2003. Characterisation of blue-light stimulated luminescence components in different quartz samples: implications for dose measurement. Radiation Measurements 37 (4-5), 441-449.

Jain, M., Murray, A.S., Bøtter-Jensen, L., 2004. Optically stimulated luminescence dating: How significant is incomplete light exposure in fluvial environments? Quaternaire, 15, 143-157.

Jenny, S., Goes, S., Giardini, D., Kahle, H.G., 2006. Seismic potential of Southern Italy. Tectonophysics 415, 81-101.

Key, R.M., Guinasso, N.L., Schink D.R., 1979. Emanation of radon-222 from marine sediments. Marine Chemistry 7 (3), 221-250.

Kieffer, G., 1971. Dépôts et niveaux marins et fluviatiles de la région de Catane (Sicile). Leurs corrélations avec certains épisodes d'activité tectonique ou volcanique. Méditerranée 5-6, 591-626.

Kiyak, N.G., Canel, T., 2006. Equivalent dose in quartz from young samples using the SAR protocol and the effect of preheat temperature. Radiation Measurements 41, 917-922.

Labaume, P., Bousquet, J.C., Lanzafame, G., 1990. Early deformation at a submarine compressive front: the Quaternary Catania foredeep south of Mt. Etna, Sicily, Italy. Tectonophysics 177, 349-366.

Lajoie, K.R., 1986. Coastal tectonics. Geophysics Studies Committee, Commission on Physical Sciences, Mathematics and Resources, Active Tectonics, National Academy Press, Washington, 95-124.

Lanzafame, G., Leonardi, A., Neri, M., 1999. Middle Pleistocene back-thrust of Argille Scagliose at Serra San Biagio (eastern Sicily): stratigraphic and tectonic evidence. Rendiconti Lincei 10 (2), 63-80.

Lavecchia, G., Ferrarini, F., De Nardis, R., Visini, F., Barbano, M.S., 2007. Active thrusting as a possible seismogenic source in Sicily (Southern Italy): Some insights from integrated structural-kinematic and seismological data. Tectonophysics 445, 145-167.

Lentini, F., 1982. The geology of the Mt. Etna basement. Memorie della Società Geologica Italiana 23, 7-25.

Lentini, F., Catalano, S., Carbone, S., 2000. Note illustrative della Carta geologica della Provincia di Messina. S.El.Ca, Firenze.

Lepper, K., McKeever, S.W.S., 2002. An objective methodology for dose distribution analysis. Radiation Protection Dosimetry 101 (1-4), 349-352.

Lian, O.B., Roberts, R.G., 2006. Dating the Quaternary: progress in luminescence dating of sediments. Quaternary Science Reviews 25, 2449-2468.

Longhitano, S., Colella, A., 2003. Stratigraphy and basin-fill architecture of the Plio-Pleistocene Catania Plain foredeep basin (eastern Sicily): a preliminary synthesis. Geologica Acta 1, 75-89.

Lundgren, P., Casu, F., Manzo, M., Pepe, A., Berardino, P., Sansosti, E., Lanari. R., 2004. Gravity and magma induced spreading of Mount Etna volcano revealed by satellite radar interferometry. Geophysical Research Letters 31, 4 pp.

Malinverno, A., Ryan, W.B.F., 1986. Extension in the Tyrrhenian Sea and shortening in the Apennines as a result of arc migration driven by sinking of the lithosphere. Tectonics 5, 227-245.

Martinson, D.G., Pisias, N.G., Hays, J.D., Imbrie, J., Moore, T.C., Shakleton, N.J., 1987. Age dating and the orbital theory of ice ages: development of a high-resolution 0 to 300,000 years chronostratigraphy. Quaternary Research 27, 1-29.

Markey, B.G., Bøtter-Jensen, L., Duller, G.A.T. (1997). A new flexible system for measuring thermally and optically stimulated luminescence. Radiation Measurements, 27 (2), 83-89.

Mattia, M., Bruno, V., Cannavò, F., Palano, M., 2011. Evidences of a contractional pattern along the northern rim of the Hyblean Plateau (Sicily, Italy) from GPS data. Geologica Acta, *in press* (available at http://www.geologica-acta.com/pdf/vol1002a01).

Mattia, M., Palano, M., Bruno, V., Cannavò, F., Bonaccorso, B., Gresta, S., 2008. Tectonic features of the Lipari-Vulcano complex (Aeolian archipelago, Italy) from 10 years (1996–2006) of GPS data. Terra Nova 20 (5), 370-377.

Mattia, M., Palano, M., Bruno, V., Cannavò, F., 2009. Crustal motion along the Calabro-Peloritan Arc as imaged by twelve years of measurements on a dense GPS network. Tectonophysics 476, 528-537.

Mauz, B., 1999. Late Pleistocene records of littoral processes at the Tyrrhenian Coast (Central Italy): depositional environments and luminescence chronology. Quaternary Science Reviews 18, 1173-1184.

Mauz, B., Lang, A., 2004. Removal of the feldspar-derived luminescence component from polymineral fine silt samples for optical dating applications: evaluation of chemical treatment protocols and quality control procedures. Ancient TL 22, 1-8.

Mckeever, S.W.S., Chen, R., 1997. Theory of Thermoluminescence and Related Phenomena. World Scientific Publishing Co. Pte. Ltd. 561 pp.

Mejdahl, V., 1979. Thermoluminescence dating: beta-dose attenuation in quartz grains. Archaeometry 21, 61-72.

Mejdahl, V., 1985. Further comments on extrapolation methods of dating sediments. Nuclear Tracks and Radiation Measurements 10, 711-715.

Miyauchi, T., Dai Pra, G., Labini, S., 1994. Geochronology of Pleistocene marine terraces and regional tectonics in the Tyrrhenian coast of South Calabria, Italy. Il Quaternario 7 (1), 17-34.

Monaco, C., 1997. Tettonica Pleistocenica nell'area a sud dell'Etna (Sicilia Orientale). Italian Journal of Quaternary Sciences 10 (2), 395-400.

Monaco, C., Antonioli, F., De Guidi, G., Lambeck, K., Tortorici, L., Verrubbi, V., 2004. Sea-level change and tectonic uplift during the Holocene in the Catania Plain (eastern Sicily). Riassunto e guida alle escursioni.

Monaco, C., Bianca, M., Catalano, S., De Guidi, G., Tortorici, L., 2002. Sudden change in the late Quaternary tectonic regime in eastern Sicily: evidences from geological and geomorphological features. Bollettino Società Geologica Italiana 1, 901-913.

Monaco, C., Tapponier, P., Tortorici, L., Gillot, P.Y., 1997. Late Quaternary slip rates on the Acireale-Piedimonte normal faults and tectonic origin of Mt. Etna (Sicily). Earth and Planetary Science Letters 147, 125-139.

Monaco, C., Tortorici, L., 2000. Active faulting in the Calabrian arc and eastern Sicily. Journal of Geodynamics 29, 407-424.

Monaco, C., Tortorici, L., 2007. Active faulting and related tsunami in eastern Sicily and south-western Calabria. Bollettino di Geofisica Teorica e Applicata 48 (2), 163-184.

Murray, A.S., Olley, J.M., 1999. Determining sedimentation rates using luminescence dating. In: Bruns, P., Hass, H.C. (Eds.), Determination of Sediment Accumulation Rates. GeoResearch Forum 5, Trans Tech Publications, Switzerland 121-144.

Murray, A.S., Olley, J.M., 2002. Precision and accuracy in the optically stimulated luminescence dating of sedimentary quartz: a status review. Geochronometria 21, 1-16.

Murray, A.S., Olley, J.M., Caitcheon, G., 1995. Measurement of equivalent doses in quartz from contemporary water-lain sediments using optically stimulated luminescence. Quaternary Science Reviews 14, 365-371.

Murray, A.S., Roberts, R.G., 1998. Measurement of the equivalent dose in quartz using a regenerative-dose single-aliquot protocol. Radiation Measurements 29, 503-515.

Murray, A.S., Thomsen, K.J., Masuda, N., Buylaert, J.P., Jain, M., 2012. Identifying well-bleached quartz using the different bleaching rates of quartz and feldspar luminescence signals. Radiation Measurements xx, 1-8, *in press*.

Murray, A.S., Wintle, A.G., 1998. Factors controlling the shape of the OSL decay curve in quartz. Radiation Measurements 29, 65-79.

Murray, A.S., Wintle, A.G., 2000. Luminescence dating of quartz using an improved single-aliquot regenerative-dose protocol. Radiation Measurements 32, 57-73.

Murray, A.S., Wintle, A.G., 2003. The single aliquot regenerative dose protocol: potential for improvements in reliability. Radiation Measurements 37, 377-381.

Muhs, D.R., Rockwell, T.K., Kennedy, G.L., 1992. Late quaternary uplift rates of marine terraces on the Pacific coast of North America, southern Oregon to Baja California sur. Quaternary International 15-16, 121-133.

Neri, G., Caccamo, D., Cocina, O., Montalto, A., 1991. Shallow earthquake features in the Southern Tyrrhenian region: geostructural and tectonic implications. Boll. Geofis. Teor. Appl. XXXIII 129., 47-60.

Neri, G., Caccamo, D., Cocina, O., Montalto, A., 1996. Geodynamic implications of earthquake data in the Southern Tyrrhenian Sea. Tectonophysics 258, 233-249.

Neri, G., Barberi, G., Oliva, G., Orecchio, B., 2005. Spatial variation of seismogenic stress orientations in Sicily, South Italy. Physics of the Earth and Planetary Interiors 148, 175-191.

Neri, G., Oliva, G., Orecchio, B., Presti, D., 2006. A possible Seismic gap within a highly Seismogenic Belt crossing Calabria and eastern Sicily, Italy. B.S.S.A., 96, 1321-1331.

Neri, G., Orecchio, B., Totaro, C., Falcone, G., Presti, D., 2009. Subduction Beneath Southern Italy Close the Ending: Results from Seismic Tomography. Seismological Research Letters 80, 63-70.

Nicolich, R., Laigle, M., Hirn, A., Cernobori, L., Gallard, J., 2000. Crustal structure of the Ionian margin of Sicily: Etna volcano in the frame of regional evolution, Tectonophysics 329, 121-139.

Olley, J.M., Caitcheon, G., Murray, A.S., 1998. The distribution of apparent dose as determined by optically stimulated luminescence in small aliquots of fluvial quartz: implications for dating young sediments. Quaternary Geochronology 17, 1033-1040.

Olley, J.M., Caitcheon, G.G,. Roberts, R.G, 1999. The origin of dose distributions in fluvial sediments, and the prospect of dating single grains from fluvial deposits using optically stimulated luminescence. Radiation Measurements 30 (2), 207-217.

Olley, J.M., Pietsch, T., Roberts, R.G., 2004. Optical dating of Holocene sediments from a variety of geomorphic settings using single grains of quartz. Geomorphology 60, 337-358.

Olley, J.M., Roberts, R.G., Yoshida, H., Bowler, J.M., 2006. Single-grain optical dating of grave-infill associated with human burials at Lake Mungo, Australia. Quaternary Science Reviews Volume 25 (19-20), 2469-2474.

Osmond, J.K., Cowart, J.B., 1976. The theory and uses of natural uranium isotopic variations in hydrology. Atomic Energy Review 14, 621-678.

Osmond, J.K., Cowart, J.B., 1982. Groundwater. In: Ivanovich, M. and Harmon, R.S. (eds), Uranium Series Disequilibrium: Applications to Environmental Problems, 202-245 pp. Clarendon Press, Oxford.

Palano, M., Ferranti, L., Mattia, M., Monaco, C., Aloisi, M., Bruno, V., Cannavò, F., Siligato, G., 2012. GPS velocity and strain fields in Sicily and southern Calabria, Italy: updated geodetic constraints on tectonic block interaction in the central Mediterranean. Journal of Geophysical Research 117, 1-12.

Pata, O., 1947. Su di un nuovo giacimento a Strombus Bubonius Lmk. Presso Vibo Valentia Atti della Società Toscana di Scienze Naturali, 54 (1947), pp. 159-166.

Pawley, S.M., Toms, P., Armitage, S.J., Rose, J., 2010. Quartz luminescence dating of Anglian Stage (MIS 12) fluvial sediments: Comparison of SAR age estimates to the terrace chronology of the Middle Thames valley, UK. Quaternary Geochronology 5, 569-582.

Pepe, F., Sulli, A., Agate, M., Di Maio, D., Kok, A., Lo Iacono, C., Catalano, R., 2003. Plio-Pleistocene geological evolution of the northern Sicily continental margin (southern Tyrrhenian Sea): new insights from high-resolution, multi-electrode sparker profiles. Geo-Marine Letters 23, 53-63.

Pepe, F., Sulli, A., Bertotti, G., Catalano, R., 2005. Structural highs formation and their relationship to sedimentary basins in the north Sicily continental margin (southern Tyrrhenian Sea): implication for the Drepano Thrust Front. Tectonophysics 409 (1-4), 1-18.

Pirazzoli, P.A., 1991. World Atlas of Holocene sea-level changes. Elsevier, London, 1991.

Pirazzoli, P.A., Suter, J.R., 1986. Late Quaternary cea-level changes and coastal evolution. Journal Coastal Research 1, 1-98.

Polonia, A., Torelli, L., Mussoni, P., Gasperini, L., Artoni, A., Klaeschen, D., 2011. The Calabrian Arc subduction complex in the Ionian Sea: Regional architecture, active deformation, and seismic hazard. Tectonics 30, 28 pp.

Pondrelli, S., Morelli, A., Ekström, G., Mazza, S., Boschi, E., Dziewonski, A.M., 2002. European-Mediterranean regional centroid-moment tensors: 1997-2000. Physics of the Earth and Planetary Interiors 130, 71-101.

Pondrelli, S., Morelli, A., Ekström, G., 2004. European-Mediterranean regional centroid-moment tensor catalog: solutions for years 2001 and 2002. Physics of the Earth and Planetary Interiors 145, 127-147.

Pondrelli, S., Salimbeni, S., Ekström, G., Morelli, A., Gasperini, P., Vannucci, G., 2006. The Italian CMT dataset from 1977 to the present. Phys. Physics of the Earth and Planetary Interiors 159, 286-303.

Postpischl, D., 1985. Catalogo dei terremoti italiani dall'anno 1000 al 1980. CNR, P.F. Geodinamica, Graficcop Bologna, 239 pp.

Prescott, J.R., Hutton, J.T., 1988. Cosmic ray and gamma ray dosimetry for TL and ESR. International Journal of Radiation Applications and Instrumentation. Part D. Nuclear Tracks and Radiation Measurements 14 (1-2), 223-227.

Prescott, J.R., Hutton, J.T., 1994. Cosmic ray contributions to dose rates for luminescence and ESR dating: large depths and long-term time variations. Radiation measurements 23 (2-3), 497-500.

Preusser, F., Kasper, H.U., 2001. Comparison of dose rate determination using high-resolution gamma spectrometry and inductively coupled plasma- mass spectrometry. Ancient TL 19 (1), 19-23.

Reimann, T., Naumann, M., Tsukamoto, S., Frechen, M., 2010. Luminescence dating of coastal sediments from the Baltic Sea coastal barrier-spit Darss-Zingst, NE Germany. Geomorphology 122, 264-273.

Roberts, H.M., 2006. Optical dating of coarse-silt sized quartz from loess: Evaluation of equivalent dose determinations and SAR procedural checks. Radiation Measurements 41, 923-929.

Roberts, H.M., 2007. Assessing the effectiveness of the double-SAR protocol in isolating a luminescence signal dominated by quartz. Radiation Measurements 42 (10), 1627-1636.

Roberts, R. G., Galbraith, R. F., Olley, J. M., Yoshida, H., Laslett, G. M., 1999. Optical dating of single and multiple grains of quartz from Jinmium rock shelter, northern Australia: Part II, results and implications. Archaeomety 41 (2), 365-395.

Roberts, R., Yoshida, H., Galbraith, R., Laslett, G., Jones, R., Smith, M., 1998. Single-aliquot and single-grain optical dating confirm thermoluminescence age estimates at Malakunanja II rock shelter in northern Australia. Ancient TL 16, 19-24.

Robillard, D., 1975. Les dépôts quaternaires du versant tyrrhènien de la Sicile (secteur d'Aquedolci-Capo d'Orlando): stratigraphie et tectonique. D. E. A. Universitè des Sciences et Techniques de Lille.

Rodnight, H., Duller, G.A.T., Tooth, S., Wintle, A.G., 2005. Optical dating of a scroll-bar sequence on the Klip River, South Africa, to derive the lateral migration rate of a meander bend. The Holocene 15, 802-811.

Romano, R., 1982. Succession of the volcanic activity in the Etnean area. Memorie della Società Geologica Italiana 23, 75-97.

Rosenbaum, G., Lister, G.S., 2004. Neogene and Quaternary rollback evolution of the Tyrrhenian Sea, the Apennines, and the Sicilian Maghrebides. Tectonics 23, 17 pp.

Saini, H.S., Mujtaba, S.A.I., 2010. Luminescence Dating of the Sediments from a Buried Channel Loop in Fatehabad Area, Haryana: Insight into Vedic Saraswati River and its Environment. Geochronometria 37, 29-35.

Santoro, E., Mazzella, M.E., Ferranti, L., Randisi, A., Napolitano, E., Rittner, S., Radtke, U., 2009. Raised coastal terraces along the Ionian Sea coast of northern Calabria, Italy, suggest space and time variability of tectonic uplift rates. Quaternary International 206, 78-101.

Scicchitano, G., Antonioli, F., Castagnino, Berlinghieri, E.F., Dutton, A., Monaco, C., 2008. Submerged archaeological sites along the Ionian coast of south-eastern Sicily and implications for the Holocene relative sea level change. Quaternary Research 70, 26-39.

Scicchitano, G., Lo Presti, V., Spampinato, C.R., Gasparo Morticelli, M., Antonioli, F., Auriemma, R., Ferranti, L., Monaco, C., 2011. Millstones as indicators of relative sea-level changes in northern Sicily and southern Calabria coastlines, Italy. Quaternary International 232, 92-104.

Selvaggi, G., Chiarabba, C., 1995. Seismicity and P-wave velocity image of the Southern Tyrrhenian subduction zone. Geophysical of Journal International 121, 818-826.

Shackleton, N.J., Opdyke, N.D., 1973. Oxygen isotope and palaeomagnetic stratigraphy of Equatorial Pacific core V28-238: Oxygen isotope temperature and ice volumes on a 105 year and 106 year time scale. Quaternary Research 3, 39-55.

Singarayer, J.S., Bailey, R.M., 2003. Component-resolved bleaching spectra of quartz optically stimulated luminescence: preliminary results and implications for dating. Radiation Measurements 37 (4 -5), 451-458.

Sivia, D. S., Burbidge, C., Roberts, R.G., Bailey, R.M., 2004. A Bayesian Approach to the Evaluation of Equivalent Doses in Sediment Mixtures for Luminescence Dating. AIP Conference Proceedings 735, 305-311.

Smith, B.W., Rhodes, E.J., 1994. Charge movements in quartz and their relevance to optical dating. Radiation Measurements 23, 329-333.

Spampinato, C., Scicchitano, G., Ferranti, L., Monaco, C., 2012. Raised Holocene paleo-shorelines along the Capo Schisò coast, Taormina: New evidence of recent co-seismic deformation in northeastern Sicily (Italy). Journal of Geodynamics 55, 18-31.

Stewart, I., Cundy, A., Kershaw, S., Firth, C., 1997. Holocene coastal uplift in the Taormina area, northeastern Sicily: implications for the southern prolongation of the Calabrian seismogenic belt. Journal of Geodynamics 24, 37-50.

Stokes, S., Bray, H.E., Blum, M.D., 2001. Optical resetting in large drainage basins: tests of zeroing assumptions using single-aliquot procedures. Quaternary Science Reviews 20, 879-885.

Taylor, J.R., 1990. Introduzione all'analisi degli errori. Lo studio delle incertezze nelle misure fisiche. Zanichelli, Bologna, 223 pp.

Thomsen, K.J., 2004. Optically Stimulated Luminescence Techniques in Retrospective Dosimetry using Single Grains of Quartz extracted from Unheated Materials. PhD thesis.

Tortorici, G., Bianca, M., De Guidi, G., Monaco, C., Tortorici, L., 2003. Fault activity and marine terracing in the Capo Vaticano area (southern Calabria) during the Middle-Late Quaternary. Quaternary International 101-102, 269-278.

Tortorici, L., Monaco, C., Tansi, C., Cocina, O., 1995. Recent and active tectonics in the Calabrian Arc (Southern Italy). Tectonophysics 243, 37-55.

Trincardi, F., Cipolli, M., Ferretti, P., La Morgia, J., Ligi, M., Marozzi, G., Palumbo, V., Taviani, M., Zitellini, N., 1987. Slope basin evolution on the Eastern Tyrrhenian margin: preliminary report. Giornale di Geologia 49, 1-9.

Tsukamoto, S., Rink, W.J., Watanuki, T., 2003. OSL of tephric loess and volcanic quartz in Japan and an alternative procedure for estimating De from a fast OSL component. Radiation Measurements 37, 459-465.

Valensise, G., Pantosti, D., 1992. A 125 kyr-long of geological record of seismic source repeatability: the M.S.s (southern Italy) and the 1908 earthquake (MS 7 ½). Terra Nova 4, 472-483.

Van Dijk, J.P., Bello, M., Brancaleoni, G.P., Cantarella, G., Costa, V., Frixa, A., Golfetto, F., Merlini, S., Riva, M., Torricelli, S., Toscano, C., Zerilli, A., 2000. A regional structural model for the northern sector of the Calabrian Arc (southern Italy). Tectonophysics 324, 267-320.

Ventura, G., Vilardo, G., Milano, G., Pino, N.A., 1999. Relationships among crustal structure, volcanism and strike-slip tectonics in the Lipari-Vulcano Volcanic Complex (Aeolian Islands, Southern Tyrrhenian Sea, Italy). Physics of the Earth and Planetary Interiors 116 (1-4), 31-52.

Waelbroeck, C., Labeyrie, L., Michel, E., Duplessy, J.C., McManus, J.F., Lambeck, K., Balbon, E., Labracherie, M., 2002. Sea-level and deep water temperature changes derived from benthic foraminifera isotopic records. Quaternary Science Reviews 21, 295-305.

Westaway, R., 1993. Quaternary uplift of southern Italy. Journal of Geophysical Research 98, 21741-21772.

Westaway, R., Bridgland, D., 2007. Late Cenozoic uplift of southern Italy deduced from fluvial and marine sediments: Coupling between surface processes and lower-crustal flow. Quaternary International 175, 86-124.

Wezel, F.C., 1967. I terreni quaternari del substrato dell'Etna. Atti della Accademia Gioenia di Scienze Naturali, Catania, 6, 279-293.

Wintle, A.G., Murray, A.S., 2000. Quartz OSL: Effects of thermal treatment and their relevance to laboratory dating procedures. Radiation Measurements 32, 387-400.

Wintle, A.G., Murray, A.S., 2006. A review of quartz optically stimulated luminescence characteristics and their relevance in single-aliquot regeneration dating protocols. Radiation Measurements 41, 369-391.

Working Group CPTI, 2004. Catalogo Parametrico dei Terremoti Italiani, versione 2004 (CPTI04), INGV, Bologna available at: http://emidius.mi.ingv.it/CPTI04.

Wortel, M.J.R., Spakman, W., 2000. Subduction and slab detachment in the Mediterranean-Carpathian region. Science 290, 1910-1917.

Zimmerman, D.W., Huxtable, J., 1971. Thermoluminescent dating of upper palaeolithic fired clay from Dolnì Věstonice. Archaeometry 13, 53-57.

Zoback, M.L., 1992. First- and second-order patterns of stress in the lithosphere: The World Stress Map Project, Journal of Geophysical Research 97 (B8), 703-728.